

DEVELOPMENT OF
A HIGH SPEED PLANING TRIMARAN
WITH HYDROFOIL SUPPORT

Thesis presented in partial fulfillment of
the requirements for the degree

MASTER OF SCIENCE IN ENGINEERING

By



Barend Grobler

Supervisor

Prof. T.M. Harms

Department of Mechanical Engineering
University of Stellenbosch

Co-supervisor

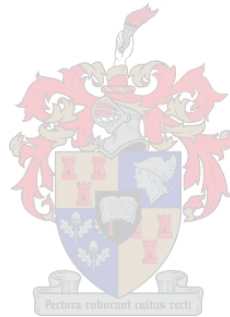
Dr. G. Migeotte

December 2007

Declaration

I, the undersigned, declare that the work contained in this thesis is my own original work and has not previously, in its entirety or in part, been submitted at any University for a degree.

Signature of Candidate



Date

Copyright ©2007 Stellenbosch University
All rights reserved

Abstract

The successful use of hydrofoil systems on catamarans, such as the Hysucat, led to the development of a similar foil system for a high speed trimaran.

Firstly a mathematical model was developed to calculate the equilibrium planing conditions of a planing trimaran. This was then used in the hydrodynamic design of a fully planing trimaran with a design speed of 65 kn. The mathematical model was then modified to include the effects of added hydrofoils. This model was then used to design a hydrofoil support system for the planing trimaran.

Towing tank tests were then performed on a scale model of the boat, with and without the supporting hydrofoil system. This was done to verify the theoretical design and to gather resistance data, which could then be compared to other boats.

The results showed a notable improvement in efficiency of the boat with the addition of foils. The conclusion was made that with the addition of a well-designed foil system, hull efficiencies similar to that expected for the Hysucat, can be attained when the foil system is added to the trimaran.

As this work was focused mainly on the high-speed performance of the boat, it is not certain how the boat will perform through the speed-range. It is therefore recommended that further testing be done, to determine the performance of the boat at lower speeds.

Opsomming

Die suksesvolle gebruik van waterfleuls op dubbelromp bote soos die Hysucat, het gelei na die ontwikkeling van 'n soortgelyke fleul stelsel op 'n hoë spoed, drierompboot.

Eerstens is 'n wiskundige model ontwikkel om die bestendegde-vaart omstandighede te bereken vir 'n hoë spoed drierompboot. Dië model is toe gebruik in die ontwerp van 'n hoë spoed drierompboot met 'n ontwerpspoed van 65 kn. Die wiskundige model is toe aangepas om die effek van aangehegde waterfleuls in ag te kan neem. Hierdie model is toe gebruik om 'n waterfleul steunstelsel te ontwerp vir die hoë spoed drierompboot.

Sleeptenk toetse was gedoen met 'n skaalmodel van die boot, met en sonder die waterfleul steunstelsel. Die toetse is gedoen om die ondersoek te kan instel of die wiskundige model die ware boot akkuraat modeleer. Hefkrag en sleurkrag is ook gemeet en kon dus met ander soortgelyke bote vergelyk word.

Die toets resultate het 'n beduidende effektiwiteits verbetering getoon met die byvoeging van die waterfleul steunstelsel. Dit het gelei tot die gevolgtrekking dat met 'n goed ontwerpte waterfleul steunstelsel kan soortgelykte effektiwiteits verbeteringe verwag word vir die drierompboot as vir die Hysucat.

Siende dat die werk gefokus was op die hoë spoed werking van die boot, is dit nie seker hoe die boot sal werk teen 'n laer spoed nie. Dit word dus voorgestel dat daar in toekomstige werk verdere navorsing gedoen word om vas te stel hoe die boot teen 'n laer spoed werk.

Table of Contents

	<i>Page no.</i>
Declaration	i
Abstract	ii
Opsomming	iii
Table of Contents	iv
Nomenclature	vi
List of Figures	x
List of Tables	xiii
1 Introduction	1
1.1 Background.....	1
1.2 Objectives.....	2
2 Planing Hulls	4
2.1 Planing Hull Theory.....	4
2.2 Planing Hull Mathematical Model.....	12
2.3 Program Verification.....	20
2.4 Hull Design Process.....	21
2.5 CAD Model.....	26
3 Trimaran Design	28
3.1 Trimaran Theory.....	28
3.1.1 Wave interference.....	29
3.1.2 Spay interference.....	31
3.1.3 Hull proximity effect.....	32
3.2 Mathematical Model.....	32
3.3 Trimaran Design Process.....	34
4 Hydrofoils	38
4.1 Hydrofoil Theory.....	38
4.1.1 Hydrofoil configurations.....	39
4.1.2 Hydrofoil-craft size limit.....	41
4.1.3 Resistance and powering.....	41
4.1.4 Sea-keeping and manoeuvring.....	42
4.2 Hydrofoil Performance Prediction.....	43

4.2.1 Super-cavitating foils.....	44
4.2.2 Sub-cavitating foils.....	44
4.3 Hydrofoil Calculations.....	51
5 Planing Trimaran with Hydrofoil Support.....	53
5.1 Hydrofoil Design.....	53
5.1.1 Foil configuration.....	53
5.1.2 Foil profile.....	55
5.1.3 Dihedral and sweep angle.....	58
5.1.4 Angle of attack.....	58
5.2 Hull Configuration.....	59
5.3 Mathematical Model.....	60
5.4 Optimization Analysis.....	61
5.5 Final Hull-Foil Configuration.....	66
6 Model Testing.....	68
6.1 Testing Facilities.....	68
6.2 Model Production.....	69
6.2.1 Model scaling.....	69
6.2.2 Final model.....	69
6.3 Test Procedure.....	71
6.3.1 Test set-up.....	71
6.3.2 Test procedure.....	72
7 Test Results.....	74
7.1 Hull Configurations and Appendages.....	74
7.2 Design Theory Verification.....	75
7.3 Trimaran With and Without Foils.....	77
7.4 Comparison to Other Craft.....	78
8 Conclusions and Recommendations.....	81
References.....	82
Appendix A Matlab Code.....	87
Appendix B Model Production.....	114
Appendix C Limits of Tank Testing.....	116
Appendix D Scaling Procedure.....	118

Nomenclature

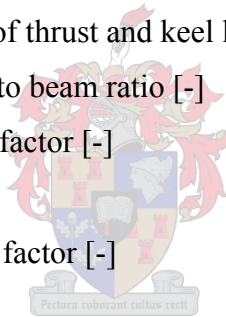
A	Cross sectional area [m ²]
a	Perpendicular distance between D_f and CG [m]
AR	Aspect ratio [-]
b	Beam of planing hull [m]
C	Ratio of lateral distance between planing surfaces divided by b [-]
c	Chord length [m]
C_D	Hydrofoil total drag coefficient [-]
C_{Di}	Hydrofoil induced drag coefficient [-]
C_{Dint}	Hydrofoil interference drag coefficient [-]
C_{DP}	Hydrofoil profile drag coefficient [-]
C_{DS}	Strut drag coefficient [-]
C_{Dsep}	Separation drag coefficient [-]
C_{Dspr}	Spray drag coefficient [-]
C_{DSP}	Strut profile drag coefficient [-]
C_{DSw}	Strut wave drag coefficient [-]
C_{Dw}	Hydrofoil wave drag coefficient [-]
C_F	Frictional drag coefficient [-]
C_L	Hydrofoil lift coefficient [-]
$C_{L\alpha}$	Hydrofoil lift curve slope [-]
$C_{L\beta}$	Lift coefficient of deadrise planing surface [-]
C_{L0}	Lift coefficient of flat plate [-]
C_{Ld}	Dynamic lift of planing surface [-]
C_{Ls}	Static lift of planing surface [-]
C_{Ls}	Static lift coefficient [-]
C_P	Ratio of distance from transom to the centre of pressure divided by λb [-]
C_R	Residuary resistance coefficient [-]
C_v	Speed coefficient [-]
ΔC	Correlation coefficient [-]

c_N	perpendicular distance between N and CG [ft]
D	Total resistance [lb]
D_f	Component of resistance force parallel to keel line [lb]
D_{foil}	Foil drag [N]
D_P	Component of resistance due to pressure forces [lb]
d	Depth at transom [ft]
Fn	Froude number $[V/\sqrt{gL}]$
Fn_{Δ}	Volumetric Froude number $[V/\sqrt{g\Delta^{1/3}}]$
fh	Perpendicular distance from foil drag centre to CG [m]
fl	Perpendicular distance from foil lift centre to CG [m]
f	Foil camber [m]
g	Gravitational constant [ft/s ²]
h	Submerged depth of foil quarter chord [m]
I	Second moment of Area [m ⁴]
I_i	Iteration coefficient [-]
k_{ϕ}	Lift curve slope correction factor [-]
L	Length of vessel [ft]
L_c	Wetted chine length [ft]
L_{foil}	Foil lift [N]
L_k	Wetted keel length [ft]
M	Bending moment [Nm]
m_p	Correction factor [-]
N	Component of resistance force normal to bottom [lb]
P	Free surface effect correlation factor [-]
P_a	Atmospheric pressure [Pa]
Rn	Reynolds number $[VL/\nu]$
R_T	Total resistance [N]
R_O	Total resistance for outriggers [N]
S	Foil span [m]
SW_{mh}	Wetted surface area main-hull [m ²]

T	Thrust [lb]
t	Maximum foil thickness [m]
V	Velocity [kn]
V_m	Mean bottom velocity [ft/s]
V_L	Fluid flow speed over foil surface [m/s]

Greek Symbols

α	Angle-of-attack [rad]
α_0	Zero lift angle-of-attack [rad]
$\Delta\alpha_0$	Zero lift angle-of-attack correction [rad]
β	Deadrise angle [deg]
ε	Angle between line of thrust and keel line [deg]
λ	Mean wetted length to beam ratio [-]
ξ	Planform correction factor [-]
ρ	Density [kg/m ³]
σ	Munk's interference factor [-]
τ	Trim angle [deg]
τ_c	Foil closure angle [deg]
φ	Free surface correction factor [-]
∇	Boat displacement [m ³]
Γ	Dihedral angle [rad]
Λ	Sweep angle [rad]



Superscripts

* Denotes any factor referring to the scale model

Subscripts

1 Centre hull
2 Outriggers
c Normalised by chord

Abbreviations and Acronyms

CAD	Computer aided design
CG	Centre of gravity
HP	Horsepower
ITTC	International towing tank conference
LCG	Longitudinal centre of gravity
LOA	Length over all
NACA	National advisory committee for aeronautics
VCG	Vertical centre of gravity

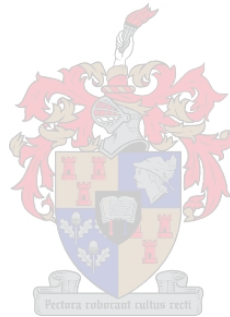


List of Figures

	P.
Figure 1: ICE Marine BladeRunner	2
Figure 2.1: Wave-making at various speed/length ratios	5
Figure 2.2: Operating regimes of different hull-forms	6
Figure 2.3: Flat-bottomed planing hull	7
Figure 2.4: Vee-bottomed planing hull	7
Figure 2.5: Wetted area of flat-bottomed vs deep-vee hull	9
Figure 2.6: Pitching lever for flat-bottomed vs deep-vee hull	10
Figure 2.7: Transverse sections of planing hulls	11
Figure 2.8: General spray-rail arrangement	12
Figure 2.9: Waterline intersection for constant deadrise surface	13
Figure 2.10: Wave rise on flat planing surface	14
Figure 2.11: Typical pressure distribution on flat planing surface	14
Figure 2.12: Resistance components of a planing surface	16
Figure 2.13: Force and moment equilibrium diagram	17
Figure 2.14: Solution of trim-angle	19
Figure 2.15: Solution of required horsepower	19
Figure 2.16: Beam vs. lift to drag ratio	22
Figure 2.17: Beam vs. trim angle	22
Figure 2.18: Deadrise angle vs. lift to drag ratio	24
Figure 2.19: Final spray-rail arrangement	25
Figure 2.20: Hull lines from CAD model of center hull	27
Figure 3.1: Outrigger terminology for a trimaran	29
Figure 3.2: Destructive wave interference	30
Figure 3.3 Forces acting on trimaran	33
Figure 3.4: Keel height difference vs. trim angle	36
Figure 4.1: Hydrofoil variables and typical pressure distribution	38
Figure 4.2: Most common hydrofoil configurations	39

Figure 4.3: Hysucat configuration	40
Figure 4.4: Surface piercing vs. fully submerged hydrofoils	40
Figure 4.5: Required sizes of hydrofoils for various boat sizes and various speeds	41
Figure 4.6: Comparison of hydrofoil supported craft vs. planning craft	42
Figure 4.7: Typical hydrofoil supported craft operation in various sea-states	43
Figure 4.8: Super-cavitating sections	44
Figure 4.9: Drag of wing fuselage configuration as a function of the angle along the wing roots	50
Figure 4.10: Prediction of hydrofoil lift compared with experimental results for various submergence ratios	51
Figure 4.11: Prediction of hydrofoil drag compared with experimental results for various submergence ratios	52
Figure 5.1: Hydrofoil configuration	54
Figure 5.2: Circular arc segment foil profile	55
Figure 5.3: Simple beam theory for clamped in beam	56
Figure 5.4: Integration across foil profile	57
Figure 5.5: Forces acting on hydrofoil-supported trimaran	60
Figure 5.6: Front foil position, relative to LCG vs. trim angle	62
Figure 5.7: Front foil position, relative to LCG vs. required horsepower	62
Figure 5.8: Front foil size vs. operating trim angle	63
Figure 5.9: Front foil size vs. estimated required horsepower	64
Figure 5.10: Speed vs. required horsepower	65
Figure 5.11: Final foil specifications	66
Figure 5.12: Final hull-foil configuration	67
Figure 6.1: Data collection equipment and model layout	68
Figure 6.2: Hull model	70
Figure 6.3: ITTC Prescribed test measurement system	72
Figure 6.4: Model test photo for determining wetted surface area	73
Figure 7.1: Resistance coefficient comparison for various hull configurations	74
Figure 7.2: Resistance coefficient comparison between test results and theory prediction for the centre hull	75

Figure 7.3: Resistance coefficient comparison between test results and theory prediction for the trimaran configuration	76
Figure 7.4: Resistance coefficient comparison between test results and theory prediction for the trimaran with foils configuration	77
Figure 7.5: Comparison between trimaran with and without foils	78
Figure 7.6: A comparison of the hydrofoil supported trimaran with various seagoing craft	79
Figure B-1: Section cut-outs from polyurethane foam	114
Figure B-2: Faired hull, ready for glass coating	114
Figure B-3: Model plug for centre hull and outrigger under vacuum	115
Figure C-1: Froude depth number vs. change in residuary resistance at various length to depth ratios	117



List of Tables

	p.
Table 2.1: A comparison of results for an example problem	20
Table 2.2: Hydrostatic properties of the hull	26



1 Introduction

1.1 Background

Multi-hull vessels have been around as long as any other boat shape; fishing canoes have been making use of “outriggers” for stability for centuries, as a matter of fact it is thought that the Polynesians started doing ocean voyages on catamaran-like boats and monohulls with outriggers as early as 2000 BC (Wikipedia, 2006). Probably the most obvious reason for having more than one hull is to provide lateral-stability on a long-slender boat; the other option would be to go short-fat, but it is well known that this has some very detrimental effects on hydrodynamic performance.

The main advantage of having the trimaran arrangement is the fact that one can have a very long-slender centre hull with all its hydrodynamic advantages and still have lateral stability with the aid of the outriggers.

With recent developments, it has become clear that the trimaran configuration offers, other than stability, many hydrodynamic, manoeuvrability, comfort and layout advantages above mono-hull and even twin-hull vessels. These advantages are obviously included in a design at the cost of others, i.e. one cannot expect a trimaran to be faster, handle better, and have more space while being more fuel efficient than a monohull or catamaran of similar size.

The building of trimarans has recently escalated, since 2001 a number of passenger ferries were built; the 55 m *Dolphin Ulsan*, the 127 m *Benchijigua Express* were both built in 2001.

Another trimaran, which has made a large impact on the high speed boating industry, is the *BladeRunner*, designed by ICE Marine (ICE Marine, 2006). It has set various offshore speed records including the fastest boat around Britain. This boat with its unique air cushion channels formed by the slender outriggers is capable of reaching speeds of up to 80 kn.



Figure 1: ICE Marine BladeRunner (ICE Marine, 2006).

The search to further improve the performance of boats has led to the development of hydrofoils. Hydrofoils are successfully used in various arrangements on both monohulls and catamarans but very little research has been done in the area of hydrofoil-assisted trimarans. Moolman (2005) researched the efficiency of such boats but this research was mainly aimed at larger ferry-like boats. It is the aim of this project to research the possible advantages of hydrofoils on smaller faster craft similar to the BladeRunner.

The theory behind a hydrofoil-assisted trimaran is to have the initial lateral stability provided by the outriggers and then as the boat accelerates up to its design speed and lifts out the water with the aid of the hydrofoils, it starts acting more like a monohull than a trimaran with the hydrofoils providing the lateral stability.

1.2 Objectives

The ultimate objective of the project is to design a high-speed planing trimaran making use of hydrofoil assistance. This design will then be experimentally tested and compared to similar boats with and without hydrofoils.

Briefly the objectives can be summarised as follows:

- Develop an ideal hull and outrigger configuration for hydrofoil support.
- Undertake an experimental analysis through testing of a scaled model of the design, with and without hydrofoils.
- Carry out a theoretical analysis of experimental results in order to investigate hydrodynamics.

- Compare the test results with that of typical Hysucat and planing craft tests to establish advantages and disadvantages.
- Provide guidelines for the future design of similar craft.

1.3 Layout

Chapter 2 presents the basis of the theory used to design the planing hulls of the trimaran. An introduction to the applications of planing hulls as well as the prediction of lift and resistance of such hulls is explained in detail. The theory is then applied in a mathematical model, which is then used as an aid in designing the trimaran centre hull.

The addition of outriggers to a monohull to form a trimaran has several practical and hydrodynamic implications. These implications are described and analysed in chapter 3. The theory is then applied to the design of the fully planing trimaran.

The prediction of the lift and drag produced by hydrofoils is summarized and applied in a mathematical model in chapter 4. In chapter 5 the hydrofoil model is combined with the planing trimaran model developed in chapter 3 to aid in the design of the best hull and foil configuration for the planing trimaran with hydrofoil support.

Chapters 6 and 7 are concerned with the model test and the results of those tests. Chapter 7 also compares the test results firstly to the theoretical predictions used in the design process and then to other seagoing craft to be able to draw conclusions as to how the boat performs.

Chapter 8 gives a conclusion and suggestions for future developments of the boat.

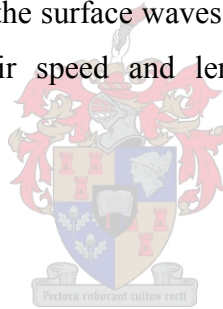
2 Planing Hulls

It was decided that it was essential to design an effective planing trimaran as a prerequisite to the design of a planing trimaran with hydrofoil support. This was decided to ensure an accurate analysis and fair comparison between the trimaran with and without foils. In order to design an efficient planing trimaran, the individual hulls need be as efficient as possible without compromising stability and safety.

2.1 Planing Hull Theory

There are three basic hull types: displacement, high speed displacement or semiplaning and planing hulls. The hull type is closely associated with the relative speed of the boat which is directly associated with the speed of the surface waves created by the hull. These surface waves have a fixed relation between their speed and length illustrated in the Froude number (Savitsky, 1985):

$$Fr = \frac{V}{\sqrt{gL}} = 0.4 \quad (2.1)$$



Since the waves created by a hull travel at the same speed as the hull itself, the critical speed to length ratio $\left(\frac{V}{\sqrt{L}}\right)$ where a hull creates a wave the same length as its waterline length is 1.34.

This is illustrated in figure 2.1.

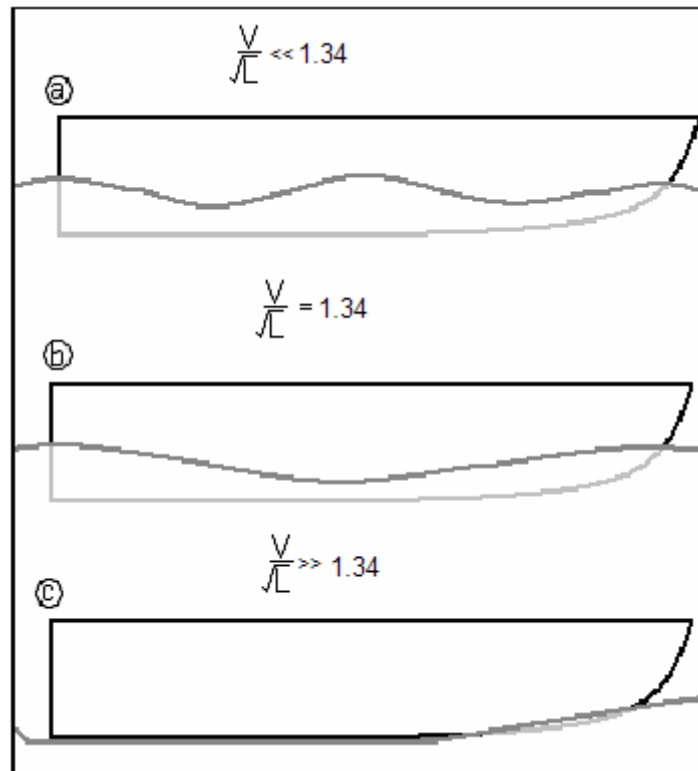


Figure 2.1: Wave-making at various speed/length ratios

Figure 2.1-a, illustrates a typical slow displacement ship. The wetted length is longer than two or more wave lengths. The hydrodynamic forces acting on the hull are negligible meaning the hull is almost entirely supported by buoyant forces. This means that there is hardly any change in trim angle or draft. According to Savitsky (1985), up to a Froude number of 0.27 the drag forces are predominantly frictional. As the Froude number increases from 0.27 the wave-making drag increases; once the Froude number reaches 0.4 (figure 2.1-b) the wave-making resistance is a virtual barrier to further speed increase for the purely displacement hull. From here some alterations can be made to a hull such as giving it a flat transom-like stern to prevent negative pressures caused by a rounded stern and promote clean flow separation as is shown in figure 2.1-c. This type of hull, known as semiplaning hull, can effectively operate between Froude numbers of 0.39 to about 0.9. For Froude numbers above 0.6, the wave-making resistance again becomes unimportant as the main drag forces are due to frictional resistance (Yeh, 1965). Because the frictional resistance is the predominant drag force it becomes necessary to minimise the wetted area. To do this, the hull is flattened out to produce a high lift to drag ratio resulting in a planing hull.

The 3 operating regimes of the three hull forms are illustrated in figure 2.2.

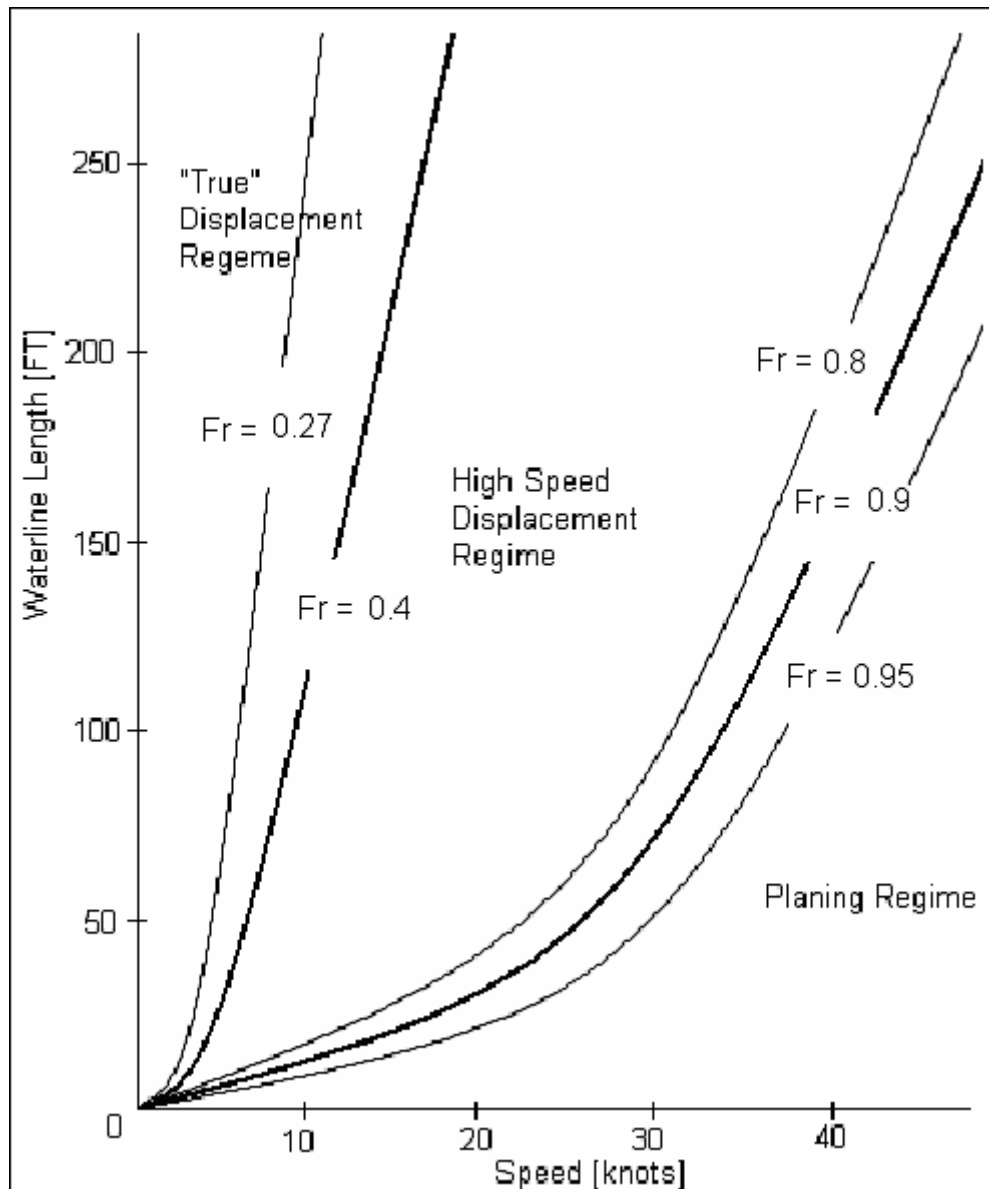


Figure 2.2: Operating regimes of different hull-forms (Savitsky, 1985)

During operation, the volume of water a planing hull displaces, is less than the displacement of the boat. This differs from displacement hulls, where the volume of water displaced, is always equal to the displacement of the boat. This is achieved by a combination of factors, most of which are related to the shape of the hull. As shown in figure 2.3, a flat-bottomed planing hull acts much like a foil, where the angle of attack is equal to the trim angle of the boat.

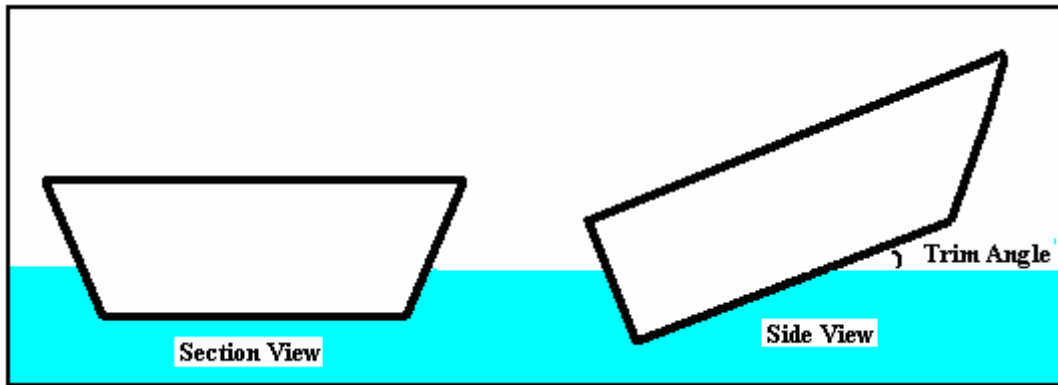
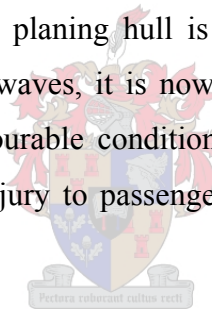


Figure 2.3: Flat-bottomed planing hull

When the boat is stationary or moving slowly, it is in effect a displacement hull. However, as more power is applied and speed increases the hull lifts out the water, because of the hydrodynamic forces acting on the hull, resulting in a smaller wetted area, which means less resistance. The result is a very effective hull at high speed.

The disadvantage of a flat-bottomed planing hull is that because the hull is now no longer displacing water and going through waves, it is now going over waves causing slamming or pounding. This can in the most favourable conditions lead to passenger discomfort while in rough-sea conditions, it can cause injury to passengers and damage to the boat structure and equipment (Powerboat, 2007).



To counteract this slamming, planing hulls generally have a “V” shape (vee-bottomed-hull), sacrificing lifting efficiency but providing a much needed dampening effect on vertical acceleration as the hull moves through waves. This shape is illustrated in figure 2.4.

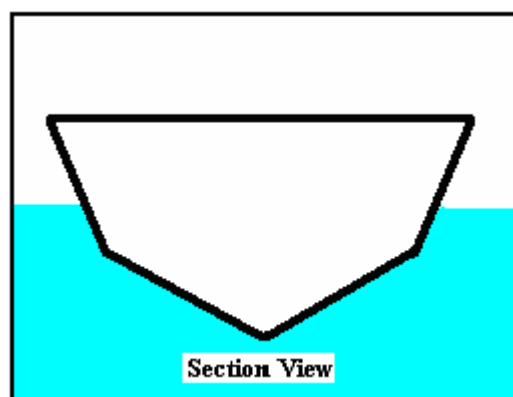


Figure 2.4: Vee-bottomed planing hull

There are various variations of the vee-bottomed-hull, some are vee shaped forward and flatten out toward the stern or others become more rounded toward the stern. These variations are all to try to accomplish a certain quality of passenger comfort while still producing sufficient lift for an efficient hull at various operating speeds.

The most common terms describing these hulls are as follows:

- Warped plane: a hull having a fine entry fanning out to flat or near flat at the transom.
- Constant section or monohedron: a hull having constant section planing surfaces aft with planing surfaces up to an angle of 15° .
- Deep vee: a hull having an angle of deadrise of over 20° at the transom, with or without constant sections but with longitudinal strakes (Levi, 1971)

Although the flat-bottomed hulls (warped plane and constant section or monohedron) are more efficient at lower speeds, the deep-vee hulls become more efficient and more comfortable at higher speed ranges (Froude numbers over 1.5). At lower speeds the flat-bottomed hull is more efficient and planes more easily because of its greater effective planing area. Because its centre of pressure is further aft, the flat bottomed hulls' trim angle is reduced more than that of the deep-vee hull as speed increases. The result is an increase in wetted length, which due to viscous drag causes the flat-bottomed hull to have a greater resistance than the deep-vee hull. Also the deep-vee hull has a reduction of wetted beam because of the deadrise angle, which the flat-bottomed hull lacks. This is illustrated in figure 2.5.

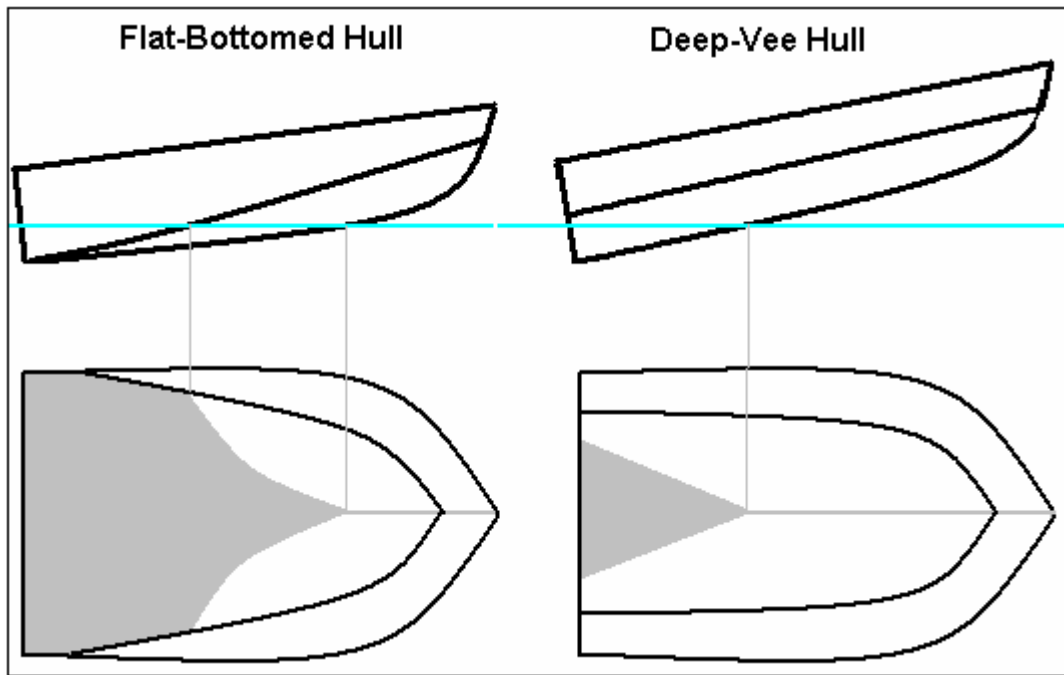


Figure 2.5: Wetted area of flat-bottomed vs deep-vee hull

In addition to the reduction of wetted length and beam, the deep-vee hull has the additional advantage of spray rails all along its length adding more lift and further decreasing wetted area.

With regards to performance and passenger comfort in rough water, as earlier stated, the deep-vee hull is far superior to the flat-bottomed hull. At high speeds any planing hull is bound to leave the water on coming into contact with a wave. The last part of the hull to leave and re-enter the water is usually the transom. If the transom is flat, the impact loads will be much greater than for a deep-vee hull; the larger the deadrise angle, the greater the dampening of the impact load.

Also in moderate conditions, where the boat never fully leaves the water, the deep-vee hull offers a much more comfortable ride. The reason for this is the more even pressure distribution allowing less abrupt correcting accelerations. These correcting accelerations are a result of the centre of pressure shifting because of a change in trim angle, causing an unbalance in the sum of the moments acting on the hull. The greater the correcting moment, the greater the acceleration. Because the pressure distribution is more concentrated for a flat-bottomed hull, the force lever is longer causing a larger correcting moment. This is illustrated in figure 2.6 for the case of pitching, but it also applies for yawing.

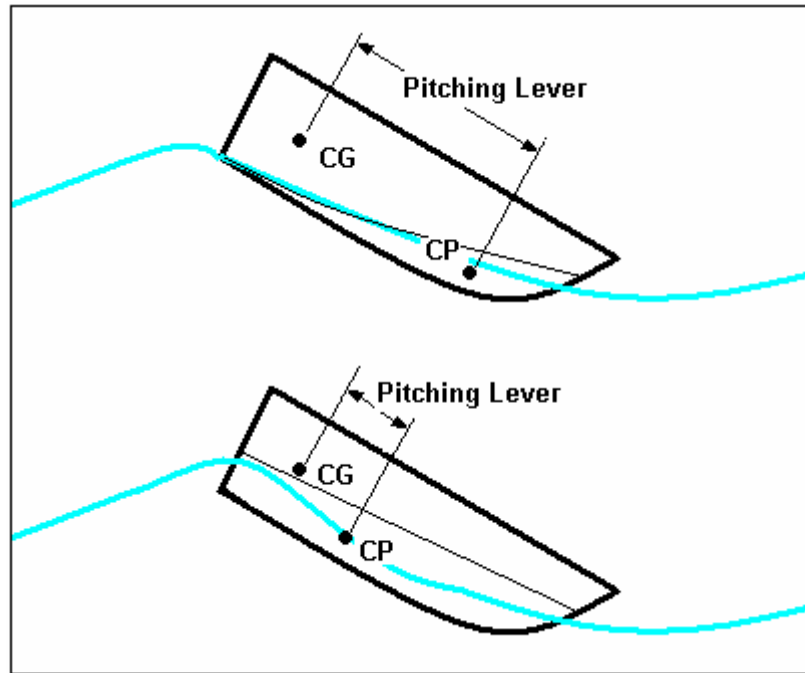


Figure 2.6: Pitching lever for flat-bottomed vs deep-vee hull

Deep-vee hulls are also more directionally stable than flat-bottomed hulls. Finally, in turning the deep-vee hull tends to turn much smoother because of the phenomenon of inward bank, stabilising the boat in the turn. Flat-bottomed hulls on the other hand tend to bank outward which can lead to instability because the outboard chine digs in. At high speed this can even lead to capsizing (Levi, 1971).

Another variation in hull shapes is the section shapes. The three basic shapes are convex, straight and concave sections. These are illustrated in figure 2.7. There are numerous variations and combinations of these basic sections, but the most practical; structurally and hydrodynamically is the convex section. This section offers very high rigidity of form thus requiring less material for additional stiffening of panels compared to the straight and concave sections. This of course leads to a reduction of weight. Another advantage of the convex section is the impact dampening effect, similar to the deadrise angle of the deep-vee hull, if the boat hit the water on its side on re-entry (Levi, 1971). The downside of convex sections is the low pressure caused by the transverse flow of water around the rounded hull, effectively sucking the hull into the water. This can be prevented if transverse flow around the hull is separated by spray-rails.

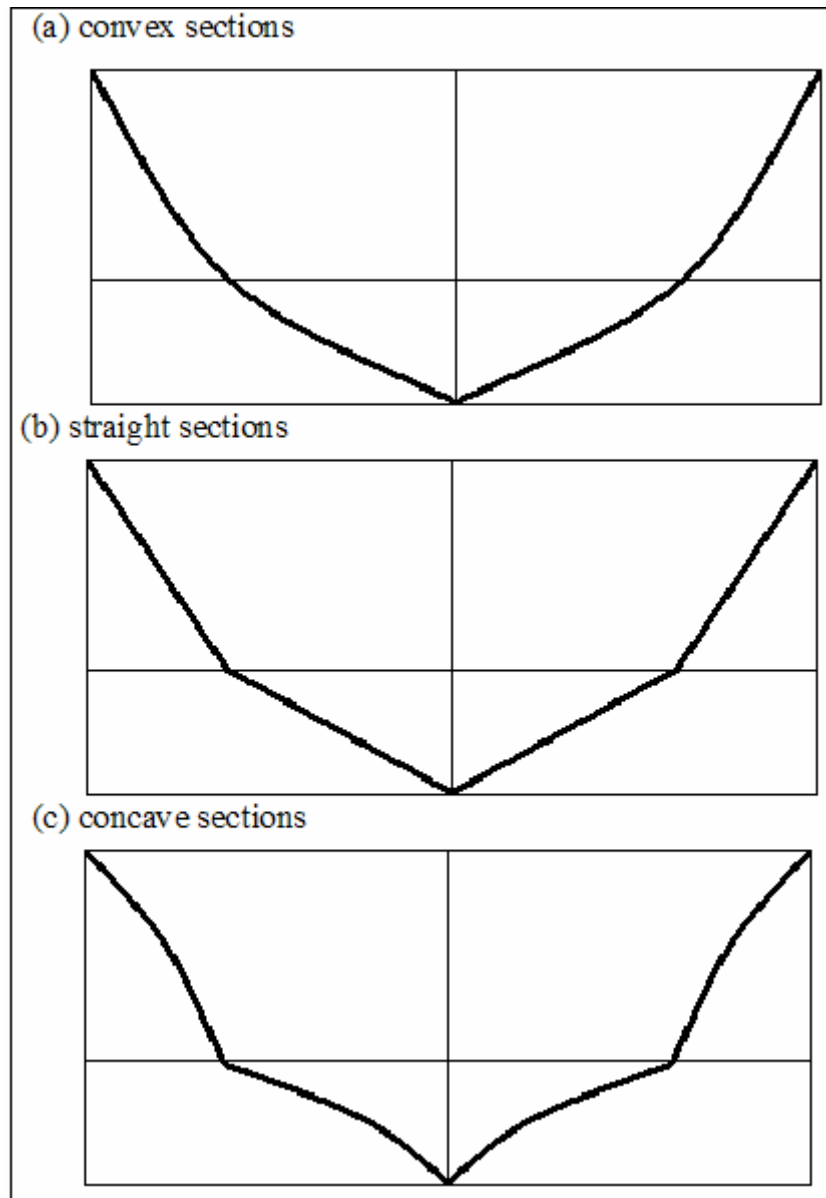


Figure 2.7: Transverse sections of planing hulls

There are various appendages, which further improve hull efficiency, the most common of which are the addition of spray-rails. The shape, size, number and position of spray rails affect its efficiency. Although some research has been done, most designers have their own theories regarding all the above variables. Müller-Graf (1991) developed a system for designing an optimum spray-rail system for round bilge hulls. This system is, however, only applicable to Froude numbers in excess of 0.85 (Damala and Grigoropoulos, 1999).

The basic function of spray-rails as far as hull efficiency is concerned is to create lift by deflecting downward a mass of water passing under them. Additional advantages are that large chine spray-rails prevent spray around the chine, thereby keeping the rest of the boat, including passengers, dry. For the same reason the spray-rails also reduce the wetted area, further improving efficiency. Furthermore the spray-rails improve directional and roll stability as any roll means an increase in spray rail surface in contact with the water on the lower side, increasing lift, and less on the higher side, decreasing lift, causing rapid correction of any roll.

The shapes of the spray-rails vary but the basic principal is a triangular cross-section with the bottom side deflecting the water. This is illustrated in the typical spray rail arrangement in figure 2.8

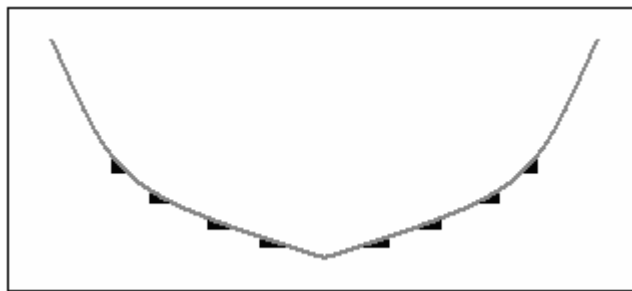


Figure 2.8: General spray-rail arrangement

The reflection angle of the bottom side of the spray-rail, relative to the water surface, may vary. In slower boats, where more lift is required from the rails, this angle should be smaller than for faster craft where more lift is produced by the hull. The number or total area of rails may vary similarly to the deflection angle; slower boats will require a greater area of spray rails to offer more lift.

2.2 Planing Hull Mathematical Model

Savitsky (1964) developed a series of equations to predict how a planing hull, given certain geometric parameters, will perform. Using the equations, one can calculate the wetted area, lift, drag, centre of pressure and stability limits of hard chine prismatic surfaces. The prismatic planing surface is assumed to have constant deadrise, constant beam and constant running trim

for the entire wetted planing area. The main hull/water interaction dimensions are shown in figure 2.9.

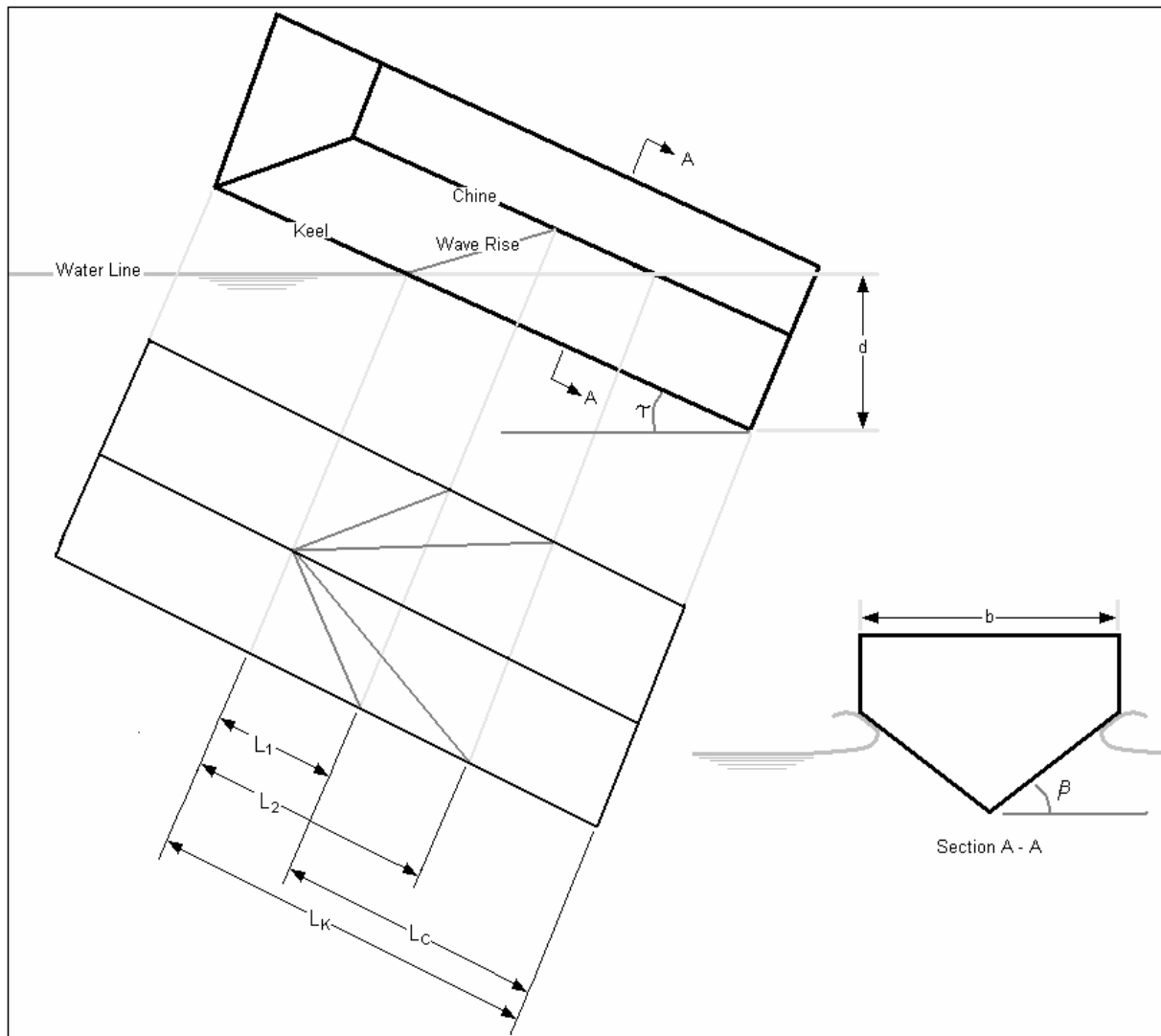


Figure 2.9: Waterline intersection for constant deadrise surface

Savitsky's method is explained below. The theory uses the beam as the prime nondimensionalizing dimension for the planing coefficients, rather than the wetted length, usually used by naval architects. This is because the wetted length for planing craft varies drastically with trim, speed and loading while the wetted beam remains almost constant.

The planing lift coefficient is firstly developed for a flat plate (see figure 2.10 and figure 2.11).

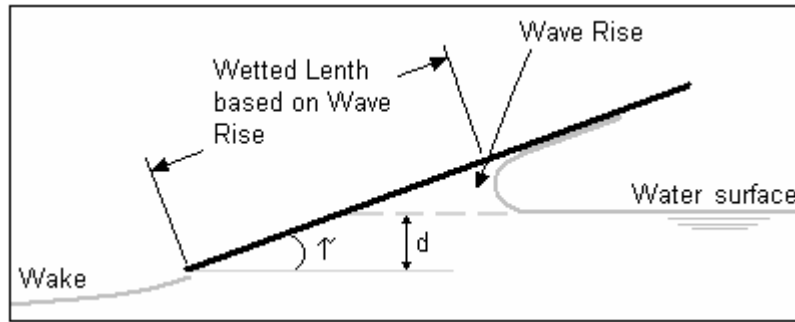


Figure 2.10: Wave rise on flat planing surface

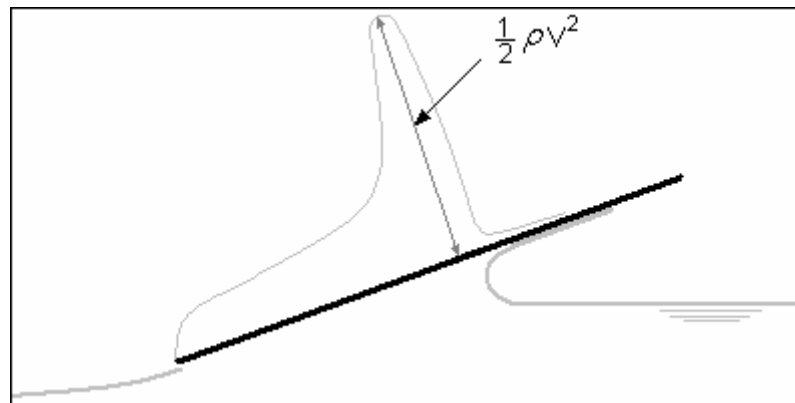


Figure 2.11: Typical pressure distribution on flat planing surface

The lift on a planing surface is due to two effects, firstly the buoyant or static forces related to the displacement of the hull and secondly the hydrodynamic forces acting on the hull as a result of the planing surface moving through the water. The formulation of a planing lift equation is based on a combination of these effects.

The static lift is of the form:

$$C_{Ls} = c\sqrt{\lambda} \tau^{1.1} \quad (2.2)$$

where c is a constant to be determined.

The dynamic lift component is of the form:

$$C_{Ld} = \frac{D\lambda^n}{C_v^2} \tau^{1.1} \quad (2.3)$$

where D and n are constants to be determined.

Adding equation 2.2 and 2.3 results in the empirical equation for the lift coefficient of a planing surface:

$$C_{L0} = \tau^{1.1} \left(c\sqrt{\lambda} + \frac{D\lambda^n}{C_v^2} \right) \quad (2.4)$$

The constants c, D and n are found by evaluating equation 2.4 for the large collection of test data resulting in:

$$C_{L0} = \tau^{1.1} \left(0.012\sqrt{\lambda} + \frac{0.0055\lambda^{5/2}}{C_v^2} \right) \quad (2.5)$$

This equation is applicable for $0.6 < C_v < 13$; $2^\circ < \tau < 15^\circ$ and $\lambda < 4$.

For a planing surface with the same trim angle and mean wetted length to beam ratio, the planing lift is reduced as the deadrise is increased. This reduction in lift is due mainly to a reduction in stagnation pressure at the leading edge of the wetted area.

Korvin-Kroukovsky et al. (1949), found that that the lift of a deadrise planing surface can be represented by the following equation:

$$C_{L\beta} = C_{L0} - 0.0065\beta \times C_{L0}^{0.6} \quad (2.6)$$

The centre of pressure is calculated by separately considering the buoyant and dynamic components of lift. The centre of pressure of the dynamic component is taken to be 75 % of the mean wetted length forward of the transom and the buoyant component 33 %. Using the values of buoyant and dynamic lift as calculated in equation 2.6, and adding the moments around the transom gives the following expression for the centre of pressure forward of the transom:

$$C_p = 0.75 - \frac{1}{5.21 \times \frac{C_v^2}{\lambda^2} + 2.39} \quad (2.7)$$

The resistance components are shown in figure 2.12:

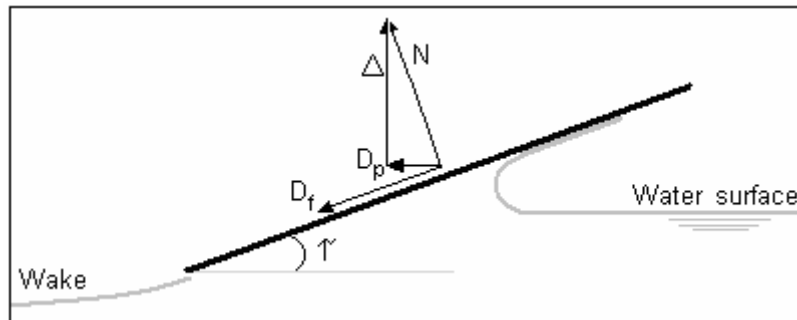


Figure 2.12: Resistance components of a planing surface

From figure 2.12 it can be seen that for a displacement Δ , trim angle τ , and a normal force N , the total resistance is:

$$D = D_p + \frac{D_f}{\cos \tau} = \Delta \tan \tau + \frac{D_f}{\cos \tau} \quad (2.8)$$

The friction drag component is shown to be calculated by the following equation (Korvin-Kroukovsky et al., 1949):

$$D_f = \frac{C_f \rho V_m^2 (\lambda b^2)}{2 \cos \beta} \quad (2.9)$$

The mean bottom velocity is less than the forward planing velocity because the bottom planing pressure is larger than the free-stream pressure. It can be shown that the mean bottom velocity for a flat plate can be calculated as follows (Savitsky and Ross, 1954):

$$V_m = V \left(1 - \frac{0.012 \tau^{1.1}}{\sqrt{\lambda} \cos \tau} \right)^{0.5} \quad (2.10)$$

To calculate the mean bottom velocity for any deadrise angle, the following alterations were made by Savitsky (1964):

$$V_m = V \left(1 - \frac{0.012 \tau^{1.1} (-1.5\beta + 95)}{\sqrt{\lambda} \cos \tau} \right)^{0.5} \tag{2.11}$$

The perpendicular height above the keel of the line of action of the friction drag component on a deadrise planing surface is assumed to be:

$$VCG - a = \frac{b}{4} \tan \beta \tag{2.12}$$

The above set of equations can be used to build a mathematical model for any planing hull given the following variables:

- Beam
- Deadrise angle
- Displacement
- LCG position
- VCG position
- Thrust angle and line



Using the information given and finding the lift and drag (illustrated in figure 2.13) as predicted by Savitsky (1964), a set of force and momentum balance equations can be set up as follows:

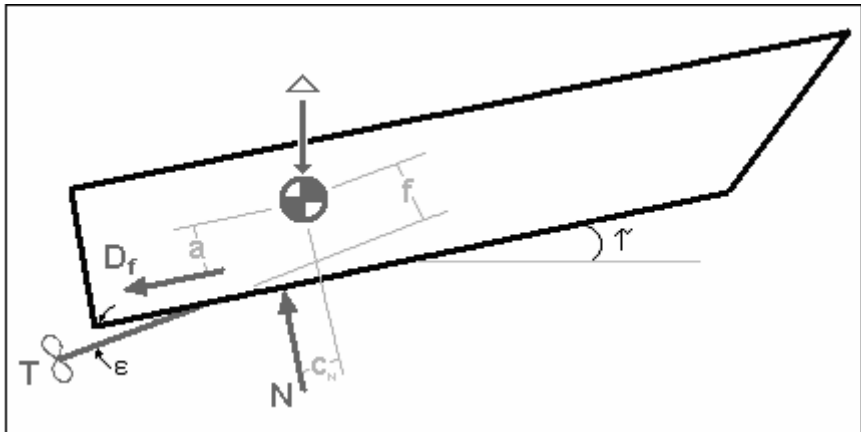


Figure 2.13: Force and moment equilibrium diagram

Summing vertical forces:

$$\Delta = N\cos(\tau) + T\sin(\tau + \varepsilon) - D_f\sin(\tau) \quad (2.13)$$

Summing horizontal forces:

$$T\cos(\tau + \varepsilon) = D_f\cos(\tau) + N\sin(\tau) \quad (2.14)$$

For equilibrium of pitching moments:

$$Nc_N + D_f a - Tf = 0 \quad (2.15)$$

The simultaneous solution of this set of equations will provide the following information:

- Equilibrium trim angle
- Required thrust
- Wetted keel length
- Wetted chine length
- Draft at stern



The Savitsky method as described above is applicable for speed ranges where the speed

coefficient $\left(C_v = \frac{V}{\sqrt{gb}} \right)$ is above 1 and for trim angles above 1° .

The necessary calculations were done using Matlab (version 7) and the three equations were solved iteratively. The text for the solution is included in appendix A. The following is a copy of an input file and figure 2.14 and figure 2.15 are solution plots showing the equilibrium trim angle and required horsepower for the centre hull with varying speed.

- Weight of boat [kg]: 5000
- Av. Beam [m]: 2
- Av. Deadrise [deg]: 24

- LCG from aft [m]: 4
- VCG from keel line [m]: 0.3
- Thrust inclination to keel line [deg]: 0

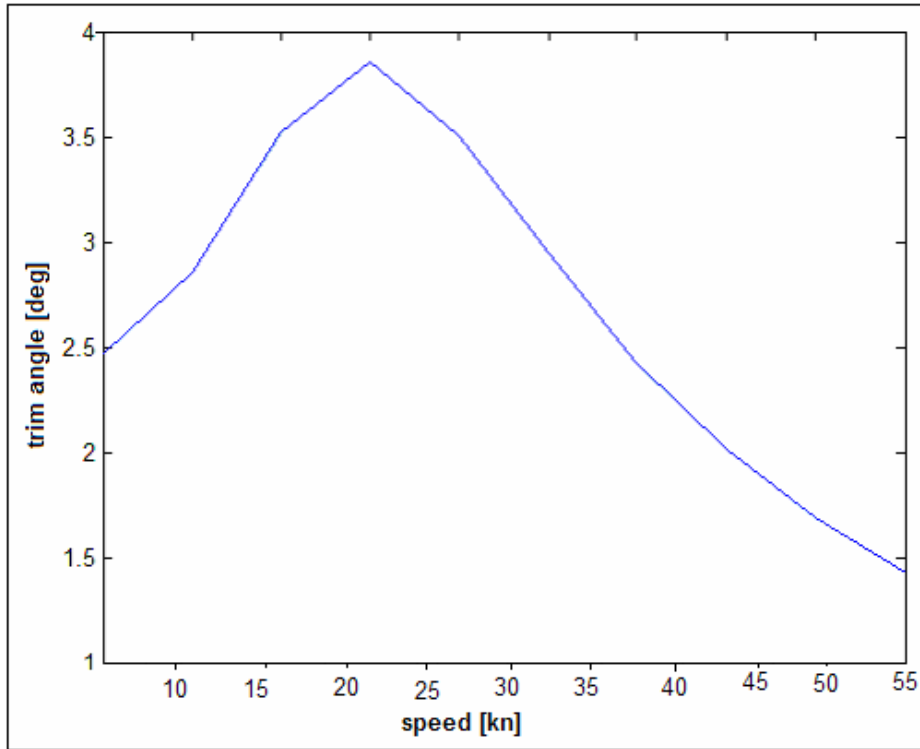


Figure 2.14: Solution of trim-angle

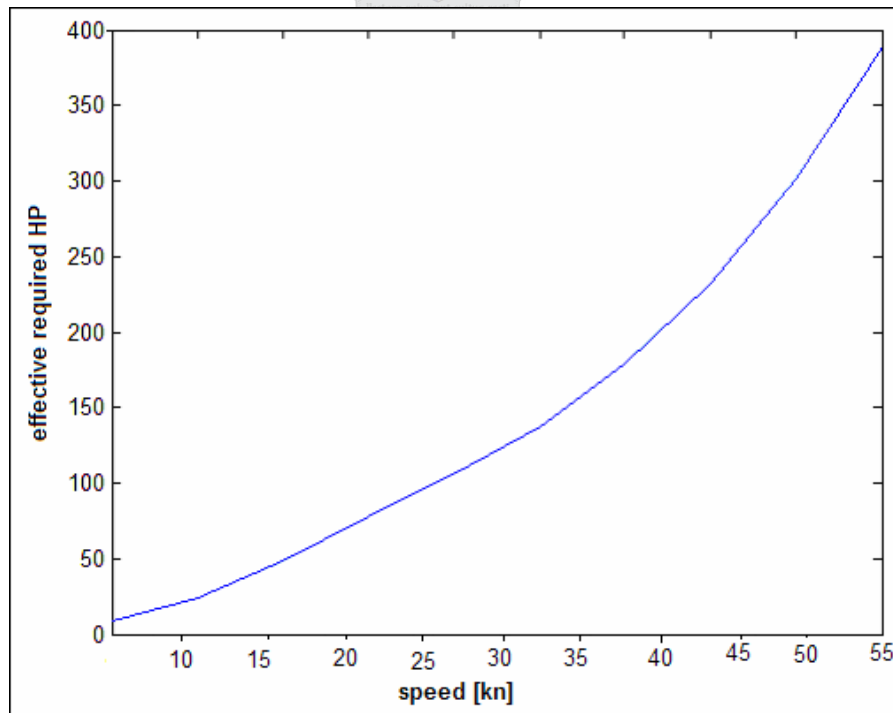
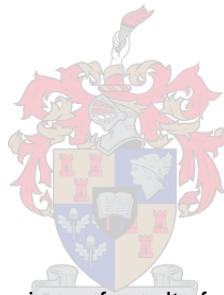


Figure 2.15: Solution of required effective horsepower

2.3 Program Verification

The accuracy of the program was verified by comparing it to an example provided by Savitsky (1964) calculated by interpolation between solutions for various trim angles. The solution is for the following hull:

- Displacement = 27.22 t
- LCG = 8.84 m
- VCG = 0.61 m
- Beam = 4.27 m
- Deadrise = 10°
- Speed = 40 kn
- Thrust inclination = 4°



The results are shown in table 2.1:

Table 2.1: A comparison of results for an example problem

	Savitsky Interpolation	Matlab Program
Equilibrium trim [deg]	2.3	2
Required effective HP	1115	975
Wetted keel length [m]	17.04	17.98
Wetted chine length [m]	11	10.97
Draft to keel @ transom [m]	0.68	0.61

The small variation in results are due to rounding errors in the Savitsky example and the fact that the solutions were found by hand calculation and interpolation, therefore not resulting in the exact answer.

2.4 Hull Design Process

For the centre hull the following design variables were considered

- Beam
- Deadrise angle
- Section shape
- Spray–rail configuration

It will be noticed that the total length is not a design variable. This is because the design is based on the Savitsky (1964) planing model, in which the wetted length is not specified but is calculated as a function of the beam, thrust, displacement and various other variables.

Firstly, the beam of the hull has to be decided on taking the following into consideration:

- Optimal hydrodynamic performance (lift to drag ratio)
- Equipment dimensions and
- Required deck area



The hydrodynamic performance can be assessed by looking at the lift to drag ratio for varying beam. This is illustrated in figure 2.16 and figure 2.17, as calculated by the Savitsky (1964) model .

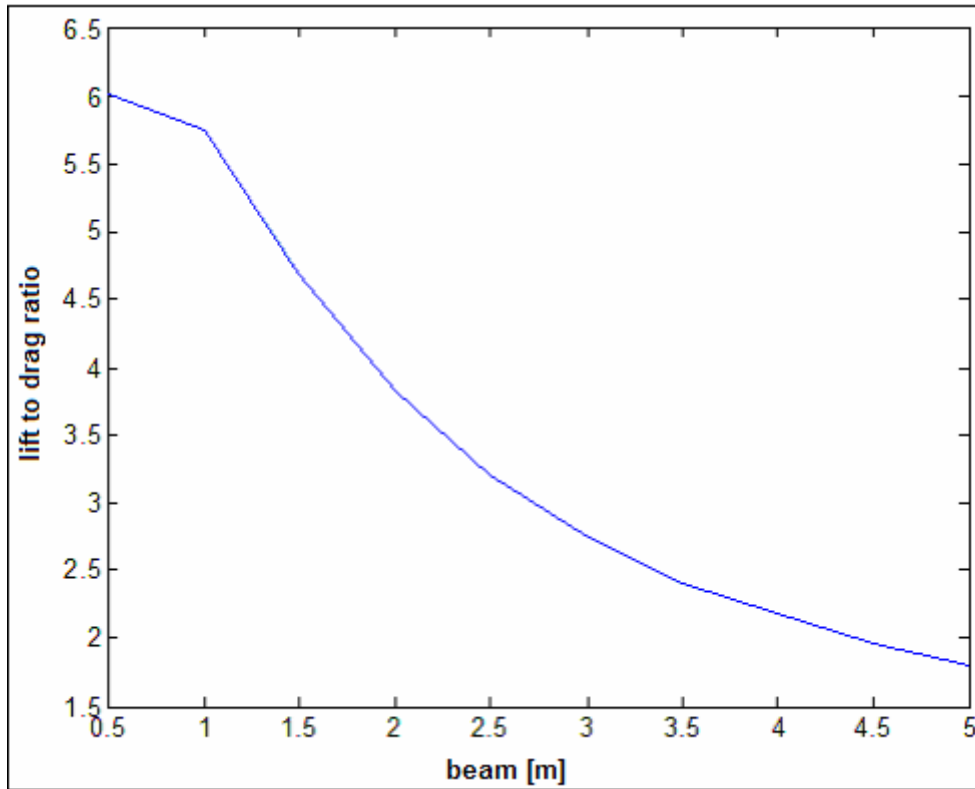


Figure 2.16: Beam vs. lift to drag ratio

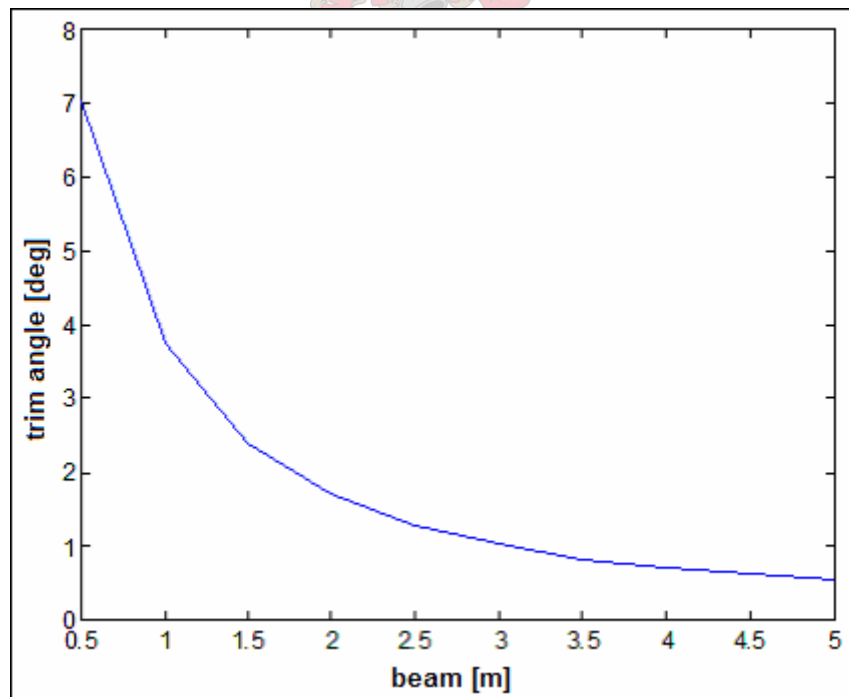


Figure 2.17: Beam vs. trim angle

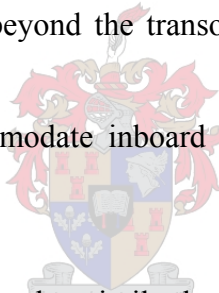
From these figures it is clear that the smaller the beam, the more efficient the hull. This notion is also an advantage when adding hydrofoils, which operate more efficiently the deeper they are

submerged. As the beam is reduced, the draft increases, therefore making the addition of hydrofoils more efficient. A limiting factor however, is that the equilibrium trim angle should not exceed a certain value to prevent porpoising instability. For a boat with a displacement of 5 tonnes and a design speed of 65 kn this limit is about 2.5° , which means the beam cannot be smaller than about 1.5 m.

Because this is the centre-hull for a trimaran, the required deck area does not limit the beam because the deck extends beyond the beam of the hull. The only other limit of the beam therefore is the equipment dimensions, the most limiting of which are the engines.

It was decided to use outboard engines for various reasons:

- The simplicity with which the engines can be installed and removed
- The compactness of the engine
- Because the engine is outboard, it does not take up valuable space on board
- Because the engine extends beyond the transom, it potentially shifts the LCG further back.
- The required beam to accommodate inboard engines is larger than that required for outboard engines



Because the boat is to be compared to other similar boats such as the ICE Marine BladeRunner, it was decided to design the hull to use similar engines. The engines prescribed therefore, was the Optimax range (225 and 250 HP) and the 300 HP Promax from Mercury. Twin engines will be used and in order for these engines to be installed, as prescribed by the manufacturer, the required minimum beam is 2 meters.

It was decided to make the deadrise angle 24° at the transom, varying to the stern to about 45° . This decision was based on the literature on deep-vee hulls as well as the numerous testimonials about offshore racing boats with 24° deadrise, being the best performing offshore boats. The main concern about hulls with such large deadrise is that they roll a lot. This is however not a concern as the trimaran configuration prevents rolling.

As shown in the solution plot in figure 2.18, the lift to drag ratio is compromised on at 24° , in order to accommodate seaworthiness.

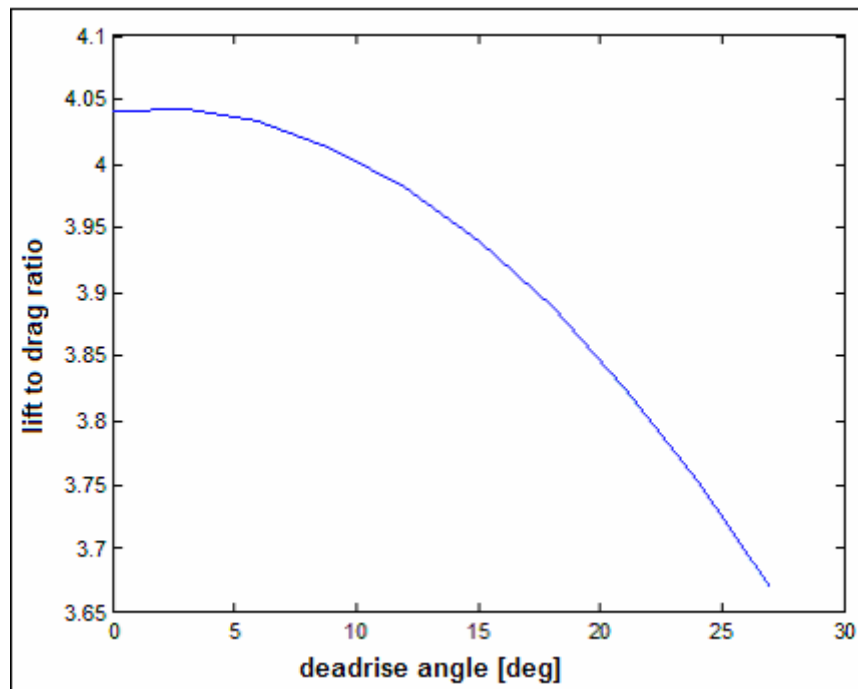
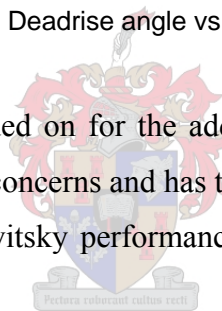


Figure 2.18: Deadrise angle vs. lift to drag ratio

The convex section shape was decided on for the added structural rigidity without additional weight as weight is one of the major concerns and has to be minimised.

The final hull specifications and Savitsky performance calculations input and output data are shown below:



- Mass of boat [kg]: 5000
- LCG from aft [m]: 4
- VCG from keel line [m]: 0.3
- Speed [kn]: 65
- Av. Beam [m]: 2
- Thrust Inclination to keel line [deg]: 0
- Av. Deadrise [deg]: 24

- The equilibrium planing trim angle is: $\tau = 1.6$ deg
- Effective power requirement: EHP = 452 HP
- The wetted centre keel length is: 10.0 m [32.8 ft]
- The wetted centre chine length is: 1.6 m [5.4 ft]

- The draft to keel at transom is: 0.27 m [0.89 ft]

The overall length (LOA) of the boat will be 12 m. This decision was made based on the calculations above and the fact that if the hull is 12 m or below, the boat certification based on the Recreational Craft Directive _2003/44/EC (2006), is much less stringent.

The first decision made regarding the spray-rail arrangement was to make a large rail at the chine. This was decided to prevent transverse flow around the chine, forming a low pressure and sucking the hull down. In addition, the draft at the stern was calculated to be fractionally deeper than the chine line. By positioning the large spray-rail at the chine, any increase in draft due to shifting LCG or any wave induced change during operation, will be countered by the lift produced by the large spray-rail.

Another smaller spray-rail was positioned halfway between the keel and the chine. This rail was shortened to only become active once the boat is planing at high speed. The final arrangement is shown in figure 2.19.

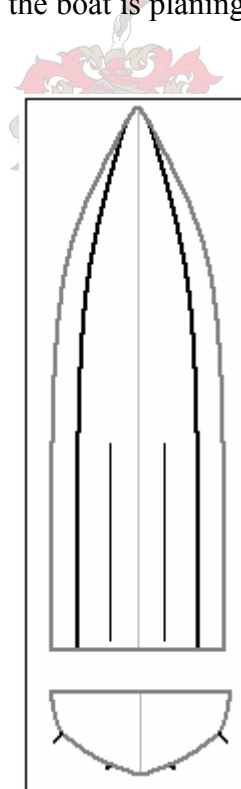


Figure 2.19: Final spray-rail arrangement

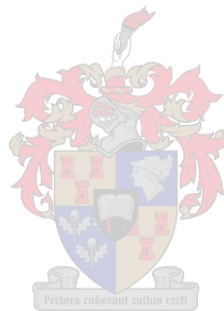
2.5 CAD Model

The hull was drawn and analysed using a student version of MaxSurf (student version 11.0), a computer aided design (CAD) program specifically developed for the design of boats and ships.

The hydrostatic analysis and the CAD model are presented in table 2.2 and figure 2.20 respectively.

Table 2.2: Hydrostatic properties of the hull

Displacement	5.000	tonne
Volume	4.878	m ³
Draft to Baseline	1.005	m
Immersed depth	0.52	m
L _{wl}	11.303	m
Beam _{wl}	1.679	m
Max cross sect area	0.583	m ²
Waterplane area	16.151	m ²



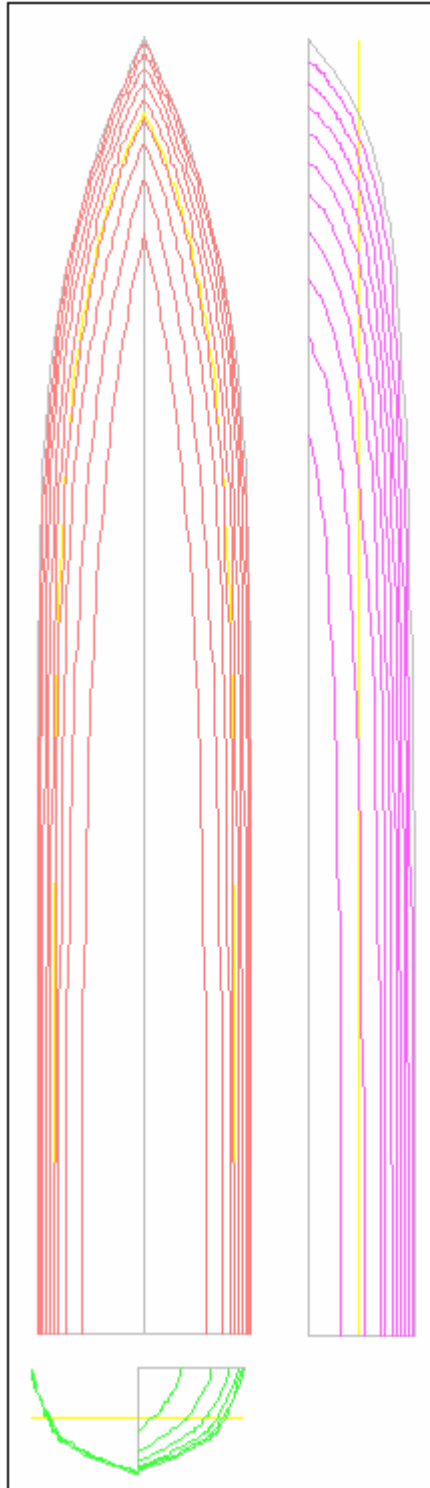


Figure 2.20: Hull lines from CAD model of centre hull

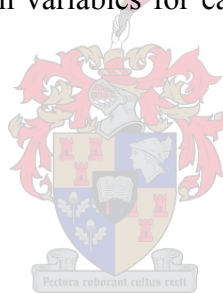
3 Trimaran Design

In order to reduce wave-making resistance, a hull should be as narrow as possible. However, once a hull's slenderness, or length to beam ratio, nears 4, it easily becomes laterally unstable. With the addition of outriggers the slenderness ratio can be much larger. Most trimarans have a slenderness ratio in the range of 12 to 19 for the centre hull and 18 to 35 for the outriggers (Seung-Hee et al. , 2004). Although the outriggers add to the wetted surface area, the total resistance can still be reduced further by positioning the outriggers so that wave interference further reduce the wave making resistance of the boat.

3.1 Trimaran Theory

In the design of a trimaran the design variables for each individual hull is similar to that of a monohull:

- Displacement
- Beam
- Deadrise
- Length
- Section shape
- Spray rail arrangement



Some consideration must however be given to how each of these variables will not only influence the performance of the hull they apply to, but also how it will influence the interaction between the hulls. The main interactions between the hulls are as follows:

- Wave formation by each hull can influence the performance of the adjacent hulls (wave interference)
- Wetting from spray, caused by an adjacent hull, can increase resistance of a hull (spray interference)

- When two surfaces plane in close proximity to one another, the sum of the lift produced by both the surfaces is more than the sum of the lift of the two when planing alone

Taking the above into consideration, the following design variables, which apply to the relation between the centre hull and outriggers, are included:

- The distance between the centre hull and the outriggers (clearance)
- The height difference between the centre hull and outrigger keel
- The displacement ratio of the outriggers to the centre hull
- The longitudinal position of the outriggers (stagger)

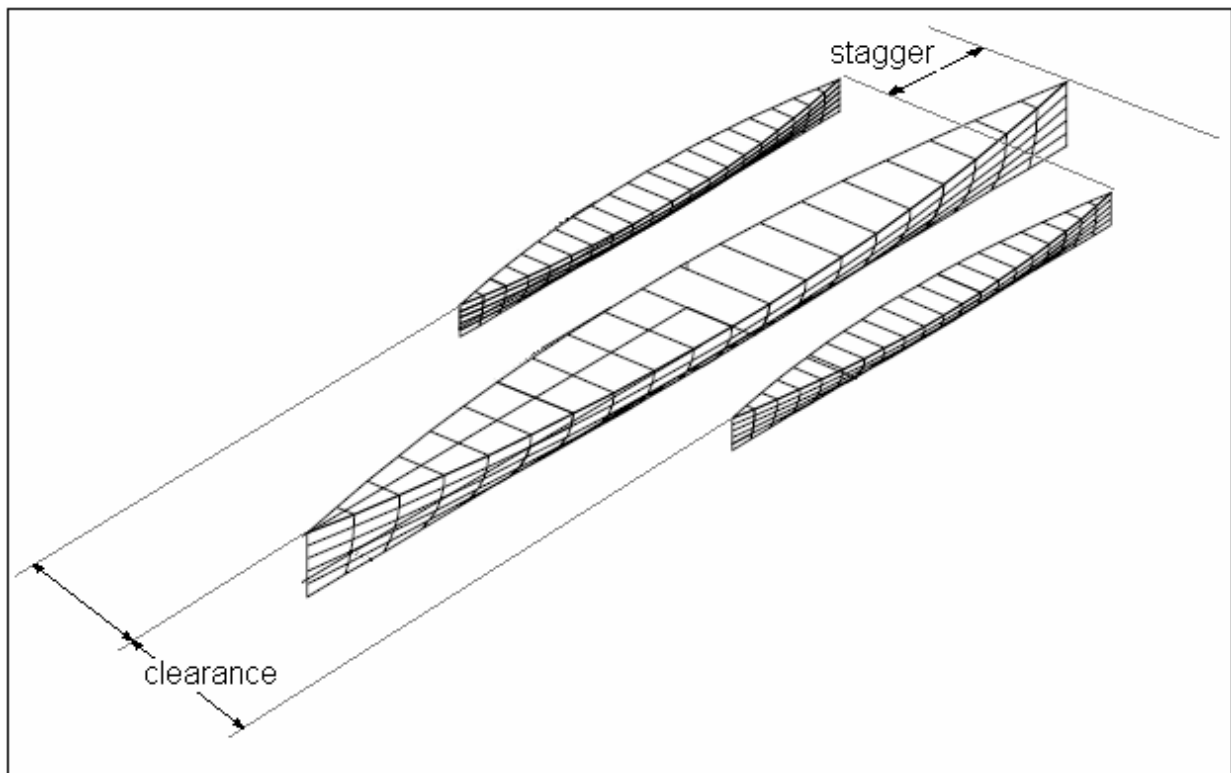


Figure 3.1: Outrigger terminology for a trimaran

3.1.1 Wave interference

Wave interference between hulls can both be an advantage (positive interference), reducing resistance or a disadvantage (negative interference), increasing resistance of each hull compared to its performance as a single hull. The resistance components related to wave interference are firstly the constructive or destructive interference in wave formation between the hulls and

secondly the wetted area of the hulls as affected by the wave formation of the other hulls. This viscous interference is concerned with the change of flow about one hull due to the presence of the other two hulls (Degiuli et al., 2005). The destructive interference effect of positioning a hull at the correct clearance and stagger is illustrated in figure 3.2:

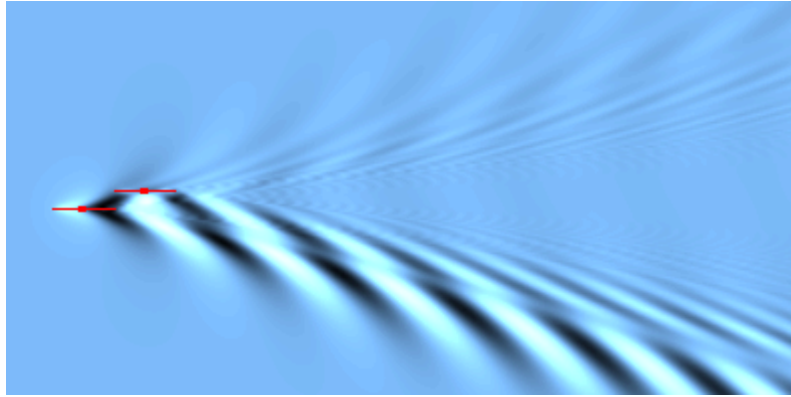


Figure 3.2: Destructive wave interference (Weinblum, 2006)

This figure shows a staggered arrangement of hulls, sometimes referred to as a Weinblum configuration (Weinblum, 2006). The position of the starboard hull is such that it cancels out the wake of the leading hull.

Because the wave formation of a hull varies with speed, it is not possible to position the outriggers so that there is always positive interference. The optimum positioning should therefore be at the design speed and it can be assumed, that at other speed ranges there will be negative interference.

Although a resistance model for trimarans was proposed by Dubrovsky (2004), using an interaction coefficient based on various tests, the preferred method for predicting resistance is still model testing. The resistance as shown by Dubrovsky is as follows:

$$R_T = 0.5\rho V^2 S_{w_{mh}} (C_F + \Delta C + C_R I_i) + R_0 \quad (3.1)$$

Here V is in m/s. I_i can be read off a series of graphs determined for various outrigger configurations.

The frictional coefficient for the main hull can be determined according to the ITTC-57 model-ship correlation line as follows:

$$C_F = \frac{0.075}{(\log_{10} Rn - 2)^2} \quad (3.2)$$

where Rn is the Reynolds number of the main-hull.

It was found (Begovic et al., 2005) that for a trimaran with hard chine centre hull and round-bilge type outriggers, the best position of the outriggers to reduce resistance in the Froude number range 0.25 – 0.60, is at 0 % stagger (i.e. the stern of the outriggers are in the same lateral position as that of the centre hull). It was also found that the resistance was reduced with smaller clearances. Similar results (Brizzolara et al., 2005) show that for the hard chine centre hull, the best resistance reducing configuration is to have stagger of 0 % and clearance as small as possible.

These findings mostly apply to lower speed ranges, i.e. Froude numbers below 0.5. For increasing Froude numbers the wave interference becomes less. This is because the angle of the bow wave becomes smaller relative to the hull. This is illustrated in the fact that for Froude numbers above 0.5, the interaction coefficient in the Dubrovsky (2004) model is taken as $I_i = 1$.

3.1.2 Spray interference

Spray interference is simply caused when spray formed by one hull wets another hull. This increases wetted surface area and interferes with the flow of water past the hull being sprayed, thereby possibly reducing its efficiency. It was found (Cardo et al., 2003) that on ordinary semi-displacement centre hull trimarans, hard chine outriggers caused large amounts of spray. This is because the smaller outriggers have a larger volumetric Froude number and therefore begin to plane before the centre hull does. However, because they are held submerged by the centre hull, they cause an unusually large amount of spray.

Dubrovsky and Matveev (2005) found that the relative speed of the outriggers should be limited. Once the Froude number of the outrigger, based on length, reaches 1.1-1.3, there is a very intense growth of spray resistance.

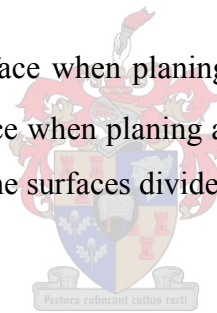
In order to prevent this situation, the keel line of the outriggers should be positioned at a height above the centre hull, which would allow it to plane without producing abnormal amounts of spray. Another solution would be to manipulate the planing characteristics of the hulls (beam, deadrise angle and displacement) so that the hulls start planing at the same speed.

3.1.3 Hull proximity lift effect

There is an increase in the velocity of flow between the centre hull and the outriggers (Migeotte, 1997). This is probably the cause for the fact that when two surfaces are planing in close proximity of each other, there is an increase in each surfaces' lifting ability. This was investigated by Savitsky and Dingee (1954), who plotted the increase in lift as a function of the distance between the surfaces. The plot can be well represented by the following equation:

$$\frac{\Delta_1}{\Delta} = -0.0002C^5 + 0.0053C^4 - 0.0471C^3 + 0.207C^2 + 1.45 \quad (0 < C < 4) \quad (3.3)$$

where Δ_1 is the lift for a single surface when planing adjacent to another at a given trim and speed. Δ is the lift for a single surface when planing alone at the same trim and speed. C is the ratio of the lateral distance between the surfaces divided by the beam of each surface.



3.2 Trimaran Mathematical Model

Using the Savitsky (1964) model described in chapter 2, the lift and drag coefficients for each hull can be calculated individually. These calculations are based on the displacement of each hull. This of course changes with speed as the trim angle changes and the boat lifts out the water as it starts planing. It was therefore necessary to calculate the submerged volume of each hull at a certain speed after calculating the equilibrium trim and draft based on an initial estimate of the displacement of each hull. This process was repeated iteratively until a predetermined accuracy was satisfied.

The equilibrium equations solved to find the equilibrium trim angle (illustrated in figure 3.3) are as follows:

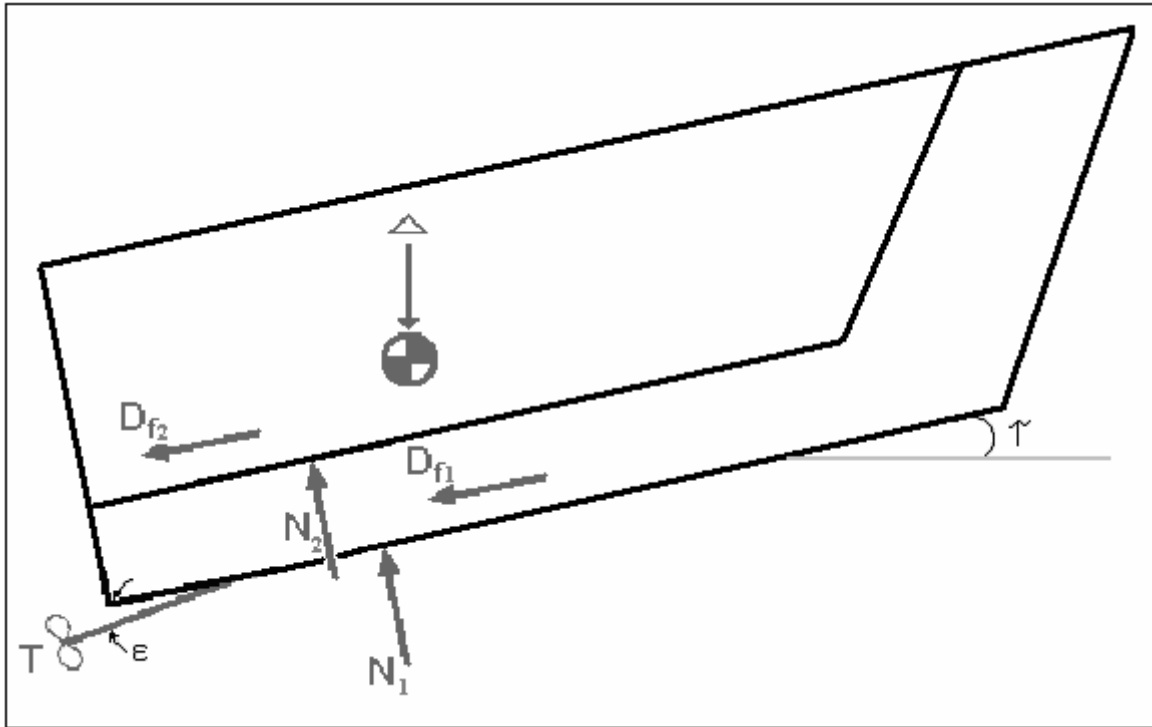
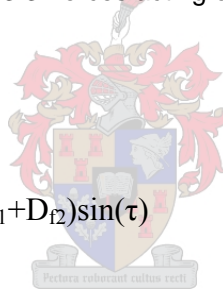


Figure 3.3 Forces acting on trimaran

Summing vertical forces:

$$\Delta = (N_1 + N_2)\cos(\tau) + T\sin(\tau + \epsilon) - (D_{f1} + D_{f2})\sin(\tau) \quad (2.13)$$



Summing horizontal forces:

$$T\cos(\tau + \epsilon) = (D_{f1} + D_{f2})\cos(\tau) + (N_1 + N_2)\sin(\tau) \quad (2.14)$$

For equilibrium of pitching moments:

$$N_1c_1 + 2N_2c_2 + D_{f1}a_1 + 2D_{f2}a_2 - Tf = 0 \quad (2.15)$$

N and D_f are found similarly as for the single hull situation (chapter 2) except the increase in lift produced because the hulls are planing close together.

The simultaneous solution of this set of equations will provide the following information:

- Equilibrium trim angle
- Required thrust
- Wetted keel length for centre hull and outrigger
- Wetted chine length for centre hull and outrigger
- Draft at stern for centre hull and outrigger

It will be noted that the effects of wave interference and spray interference are not taken into account. This is simply because this hull will be operating in Froude ranges above 0.5 where the wave interference can be neglected. Also, the inclusion of wave interference, should one wish to do calculations at lower speeds, is beyond the scope of this project. Spray interference has not been researched enough to produce a reliable model to predict the added resistance. A copy of the solution code is provided in appendix A.

3.3 Trimaran Design Process



For each individual hull, the following variables had to be considered:

- Displacement
- Beam
- Deadrise
- Length
- Section shape
- Spray rail arrangement

while the following relations had to be fixed:

- The distance between the centre hull and the outriggers (clearance)
- The height difference between the centre hull and outrigger keel
- The displacement ratio of the outriggers to the centre hull

- The longitudinal position of the outriggers (stagger)

Many of these variables are directly linked; for instance the displacement of each individual hull, the displacement ratios and the beam of each hull. The initial start point was to fix as many variables as possible. The centre hull was already decided on based on various other factors. The centre hull specifications are as follows:

- Beam: 2 m
- LOA: 12 m
- Deadrise at stern: 24°
- Displacement of boat: 5 tonnes

In tests it has been found that outriggers with a planing hull are inefficient because they produce large amounts of spray (Cardo et al. , 2003). This was however the case when having a semi displacement centre hull which doesn't plane. In this case the project aim is to have a fully planing trimaran. This would mean that the centre hull will lift out the water together with the outriggers preventing the large spray situation found by Cardo et al. , (2003). It would however still be necessary to determine the ideal draft of each hull when planing at the design speed. Because all three hulls are planing hulls, there will be a significant amount of spray produced, as is the case for all planing hulls. This spray will however not cause any interference, as at the design speed, all the spray will pass by the adjacent hull and come out the back of the tunnel between the centre hull and outriggers.

Another variable that would differ greatly from the proposed arrangements in literature is the relative displacement of the outriggers. The proposed and accepted displacement of the outriggers is in the range of 3 to 5 % (Seung-Hee et al., 2004) of the total displacement. In this case, however, because the outriggers will also be hard chine planing hulls and the planing lift to drag ratio is more favourable for more slender hulls, it will be advantageous for them to have a much larger displacement volume.

It was decided to make the outriggers half the length of the centre hull. This would provide sufficient deck space for recreational use, allow a large length to beam ratio and also provide the length required for the larger volume of the outriggers. The beam of the outriggers was fixed at

0.3 m with a deadrise of 24° , the same as that of the centre hull. The beam was fixed as small as possible for a favourable length to beam ratio, while still being large enough to provide the structural rigidity required.

The planing draft of the outriggers, when planing alone at the design speed and at the same trim angle as the centre hull, was calculated to be 0.2 m where that of the centre hull was found to be 0.24 m. This means that the keel height difference, to prevent excessive spray, would have to be at least 0.04 m. Figure 3.4 shows the solution of the centre hull/outrigger height difference vs. the trim angle, using the proposed mathematical model. The trim angle was not to exceed 2.5° to insure porpoising stability. The height difference was therefore fixed at 0.059 m.

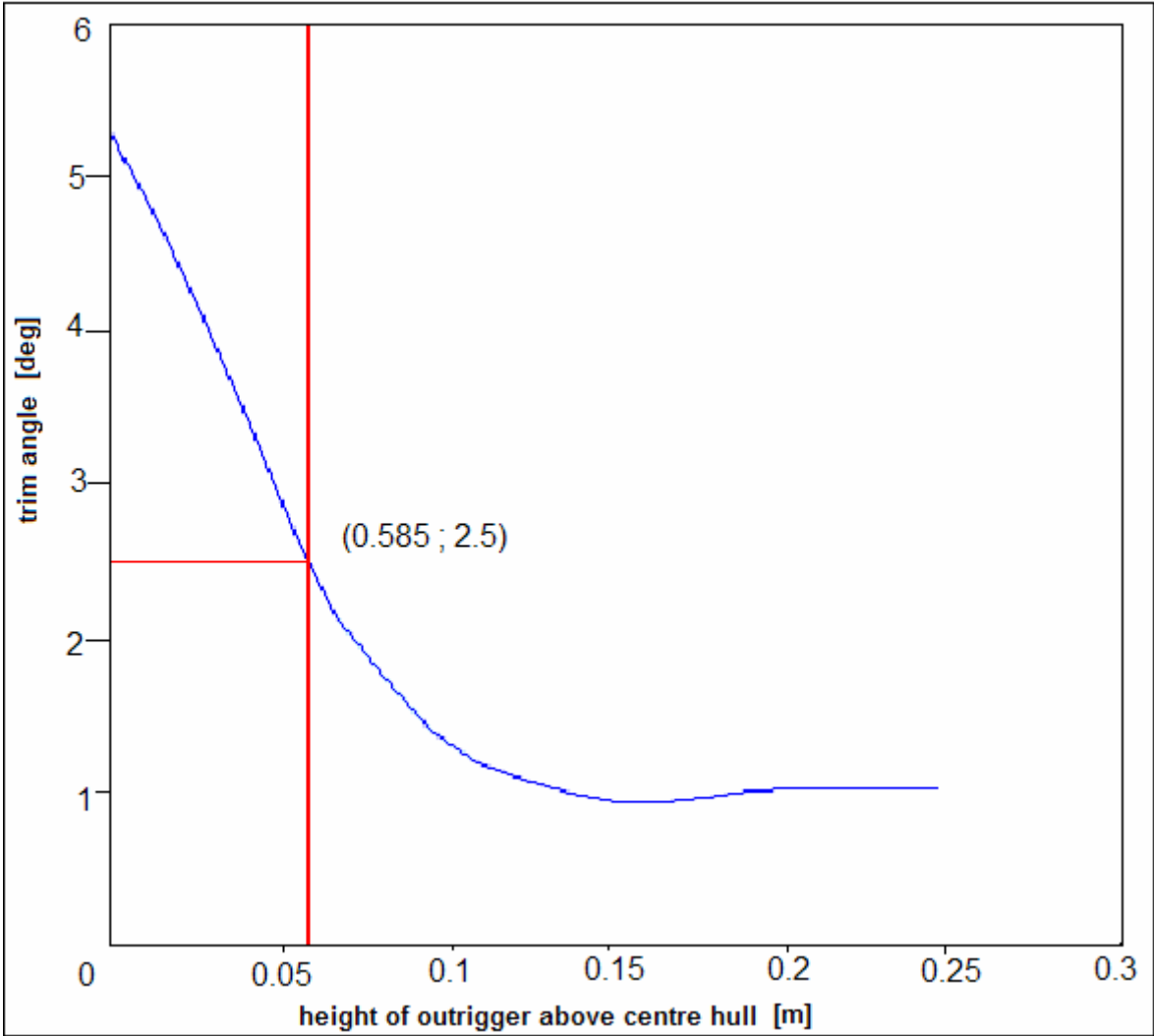


Figure 3.4: Keel height difference vs. trim angle

It was decided to position the outriggers so that the stern of the centre hull and outriggers are level (0 % stagger). This was based on tests by Begovic et al. (2005) and Brizzolara et al. (2005). It was decided that the clearance should to be minimised. This was done to reduce the resistance as shown in tests done by Doctors and Scrace (2003), indicating that for larger outriggers the clearance should be minimized. The clearance was fixed at 2 m to still provide enough deck space for a leisure craft.

A large spray rail was positioned at the chine of the outriggers to prevent transverse flow.

The final principal dimensions of the trimaran are listed below:

- LOA-centre hull: 12 m
- LOA- outriggers: 6 m
- Beam centre hull: 2 m
- Beam outriggers: 0.3 m
- Deadrise centre hull: 24°
- Deadrise outriggers: 24°
- Clearance: 2 m
- Stagger: 0 %
- Keel height of outriggers: 0.059 m



The equilibrium planing condition output file, as calculated is shown below:

- The equilibrium planing trim angle is: $\tau = 2.45$ deg
- Effective power requirement: EHP = 396 HP
- The wetted centre keel length is: 3.8 m [12.4 ft]
- The centre-hull-chine is out the water
- The draft to keel at transom is: 0.16 m [0.53 ft]
- The wetted outrigger keel length is: 2.4 m [7.9 ft]
- The draft to keel at outrigger transom is: 0.1 m [0.34 ft]

4 Hydrofoils

Hydrofoil supported vessels are characterized by the highest lift to drag ratio among all types of water-borne craft within the optimal regime for them. Hydrofoil-assisted ships and boats use foils to partially or fully support a ship's weight. To reduce hydrodynamic resistance, a significant fraction of the ship hull is lifted out of the water. Hydrofoils can also be very effective in mitigating motions in rough seas (Matveev and Duncan, 2005)

4.1 Hydrofoil Theory

Hydrofoils, similarly to airfoils, produce lift when moving through a fluid (water) because of the formation of a pressure gradient between the fluid above and below the foil. This is illustrated in figure 4.1.

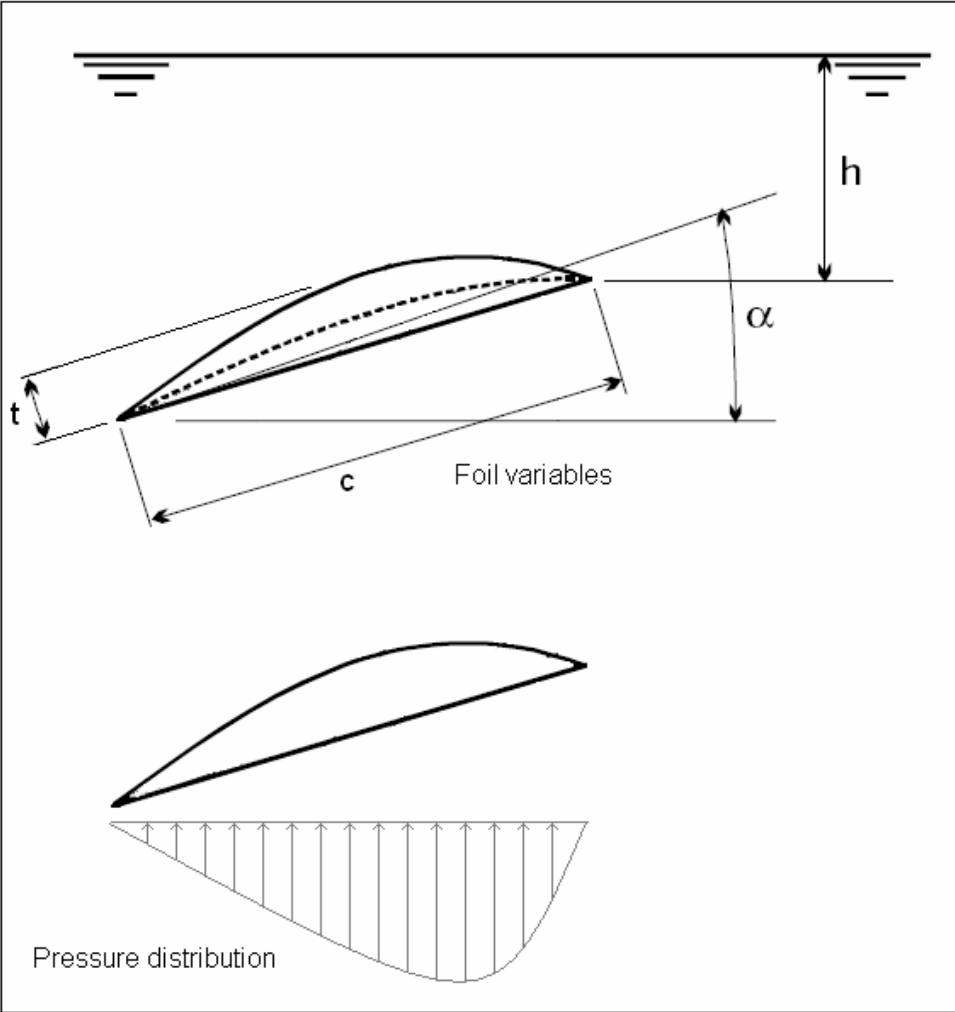


Figure 4.1: Hydrofoil variables and typical pressure distribution

Hydrofoil profiles are varied according to the conditions they are to operate in. The basic variables are the chord: c ; the thickness: t ; the span: s , which is the length of the foil; the camber: f ; the dihedral angle: Γ , which is the angle measured from the horizontal to the foil; and the sweep angle: Λ , which is the angle with which the foil is swept back or swept forward measured from a line perpendicular to the direction of motion. The operating depth of the foil has a large affect on its efficiency and is denoted as h .

4.1.1 Hydrofoil configurations

Hydrofoils can be used in various configurations. The distribution of the hydrofoil area relative to the craft’s centre of gravity defines the “configuration” of the foil system (Du Cane, 1972). The most common of these configurations are shown in figure 4.2.

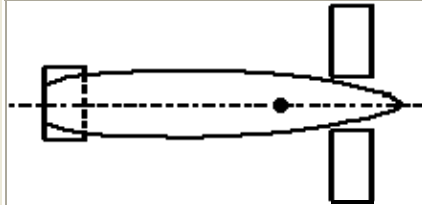
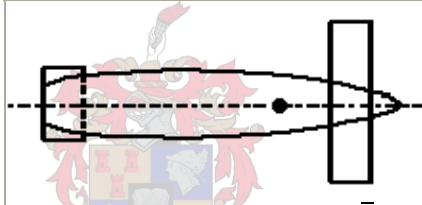
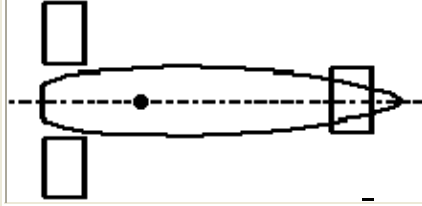
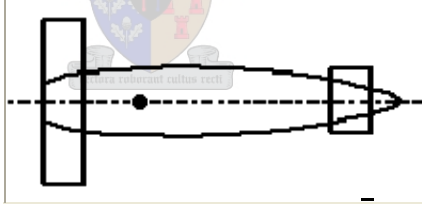
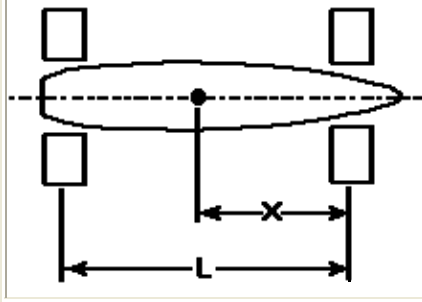
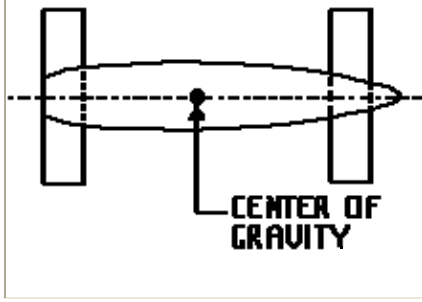
<i>SPLIT</i>	<i>NON-SPLIT</i>	<i>ARRANGEMENT</i>
		CONVENTIONAL
		CANARD
		TANDEM

Figure 4.2: Most common hydrofoil configurations

A variation of the conventional or aeroplane configuration which has been very successful is the patented Hysucat (hydrofoil supported catamaran). It was developed by Hoppe (1989) in the late 1970’s at the, Mechanical Engineering department of the University of Stellenbosch. It comprises a fixed hydrofoil system, consisting of a main-foil near the centre of gravity

(LCG) and a pair of stern foils. The stern foils are also referred to as trim foils as they control the trim of the boat. This is achieved by the fact that the foils operate near the surface of the water where large changes in lift capability is associated with vary slight changes of operating depth. This automatic trim control system is used because shifts in the position of the LCG can largely affect the performance by altering the trim; this system prevents large trim changes.

The basic Hysucat layout is shown in figure 4.3.

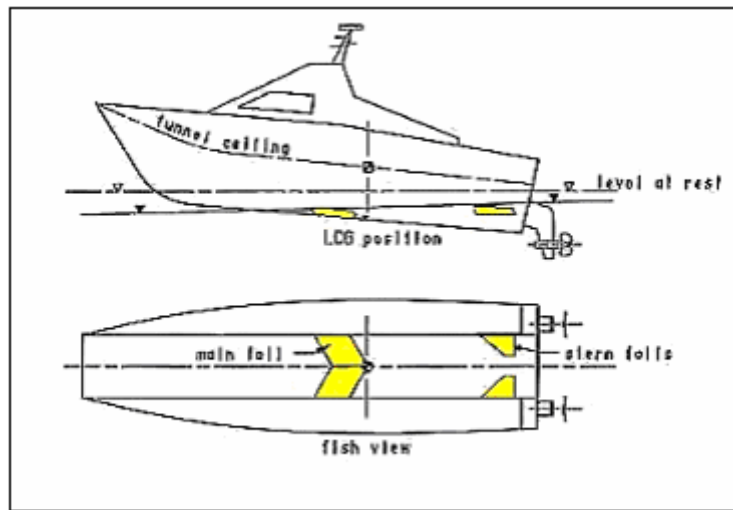


Figure 4.3: Hysucat configuration (Unistel Technologies (Pty) Ltd.)

There are two other main categories in which hydrofoil systems may be classified; these are surface piercing and fully submerged as shown in figure 4.4.

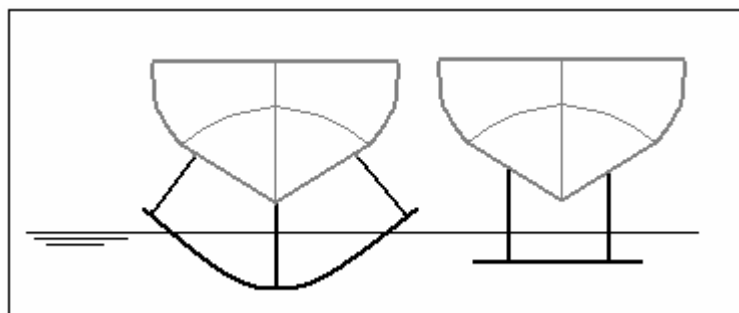


Figure 4.4: Surface piercing vs. fully submerged hydrofoils

Surface piercing foils provide automatic altitude and trim stability since the foil area decreases as the hull lifts up reducing the lifting capability of the foil, the opposite is true if the hull dips or goes through a wave. Fully submerged foils can be controlled with the aid of an automatic-control-system by changing the foil geometry (flaps) or angle of attack, or they

can be designed to operate near the surface where control is automatic due to the free-surface-effect.

4.1.2 Hydrofoil-craft size limit

The size of hydrofoil-supported craft is limited by the so called “square-cube” law. The lift developed by the foils is proportional to their planform area which is a square of a linear dimension, while the weight to be supported is proportional to a volume which is the cube of a linear dimension. This means that as the size of the craft to be supported increases, the necessary size of the foil increases much faster. Aircraft solve this problem by increasing speed and wing loading as size is increased, but practical hydrofoil speeds are limited by cavitation (Meyer, 2006). For the same reason hydrofoils are also not practical at low speeds. This is illustrated in figure 4.5 (Du Cane, 1972).

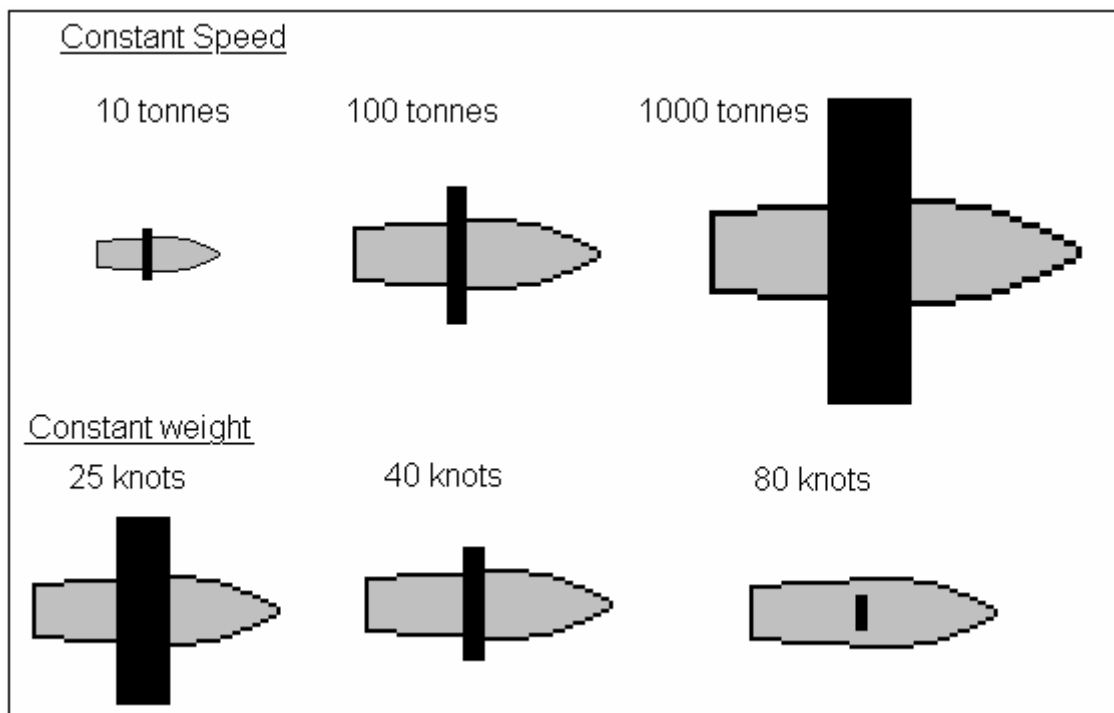


Figure 4.5: Required sizes of hydrofoils for various boat sizes and various speeds

4.1.3 Resistance and powering

The main function of hydrofoils is to lift the hull out of the water thereby reducing the wave-making resistance and the wetted surface area, reducing the friction drag. Because the foils only become useful near their design speed, the boat hull will spend a considerable amount of time operating as an ordinary hull without the lift support of the foils but with their added drag. For this reason, hydrofoil supported hulls need to be designed as efficiently as possible,

particularly at speeds lower than the design speed of the foils. Figure 4.6 shows a typical comparison between a hydrofoil supported craft and a planing craft.

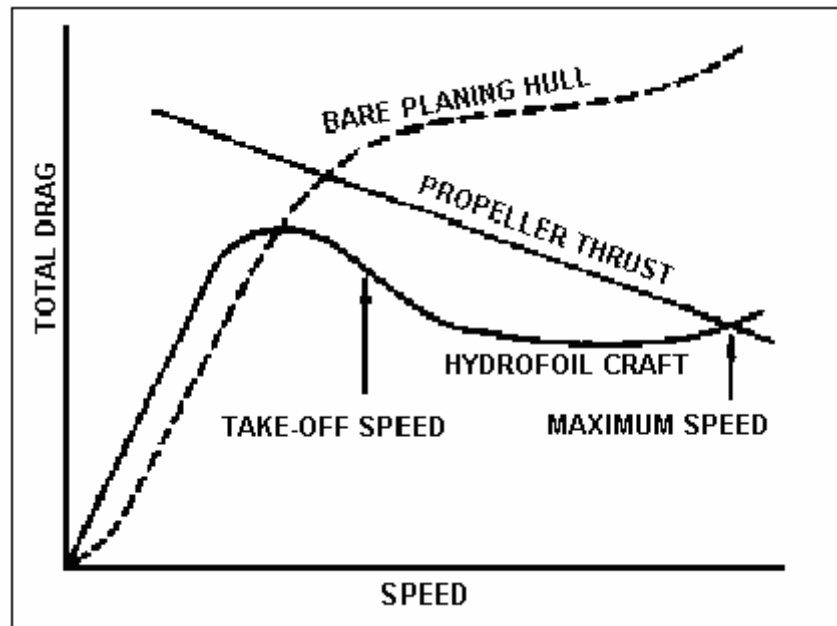


Figure 4.6: Comparison of hydrofoil supported craft vs. planing craft
(Meyer, 2006)

Here the added resistance of the foils can be seen below the takeoff speed for the hydrofoil craft. Noticeable is the hump on the hydrofoil craft curve. The hump in the resistance is the transition speed between hull-borne and foil-borne operation. Once the craft becomes foil-borne, it is clearly a lot more efficient than the bare planing hull because of the total reduction in resistance. Takeoff in rough water is more difficult and requires a power margin over smooth water operating power estimations. U.S. Navy, hydrofoil supported craft tests have shown that a 20 to 25 % margin is sufficient to permit rough water takeoff (Meyer, 2006).

4.1.4 Sea-keeping and manoeuvring

Hydrofoil supported craft are able to operate more efficiently than any conventional ship type in almost any sea environment. A submerged foil ship with an automatic-control-system can operate in high sea states at speeds only slightly lower than that in calm water. The hydrofoils provide continuous dynamic control of the ship right through takeoff, during operation to landing. The automatic-control-system reduces rolling and pitching and also controls the height of the hull above the water surface, providing a comfortable work platform for passengers. Figure 4.7 shows operating data points for three submerged-foil hydrofoil ships in

actual sea conditions clearly showing only a modest reduction in speed as wave heights increase.

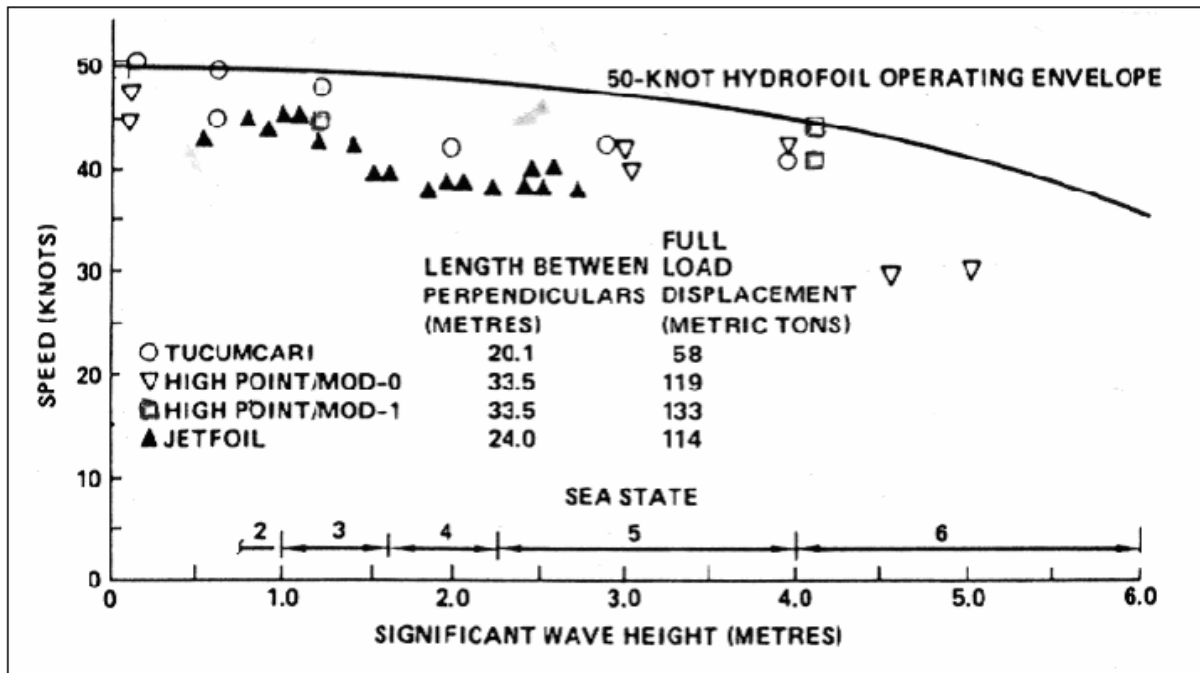


Figure 4.7: Typical hydrofoil supported craft operation in various sea-states (Meyer, 2006)

In addition to higher speeds, hydrofoil craft are more manoeuvrable in any sea-state than conventional boats. When foil-borne, turns are accomplished in a banked fashion, similarly to that of deep-vee planing hulls. Because the turn is banked-in, the centrifugal reaction force is provided by the efficient lift force of the hydrofoils. This banked turn provides passenger comfort because acceleration reaction forces due to turning are experienced as small vertical forces rather than a lateral forces. For example, a 0.4g turn is felt as only 0.08g vertical acceleration increase while the lateral acceleration is zero. For this reason, hydrofoil craft have design turn-rates of two to four times that of conventional ships in both calm and rough water (Meyer, 2006).

4.2 Hydrofoil Performance Prediction

The major obstacle to increasing speed for hydrofoil assisted boats is the occurrence of cavitation. Cavitation not only leads to higher resistance and lower lift, but can cause major corrosive damage to foil systems. Cavitation can be limited but above 60 kn. it becomes necessary to design foil sections capable of performing in the presence of cavitation.

There are various basic foil sections which are applicable to different speed ranges. For speeds above 60 kn it is suggested (Lewis, 1988) that super-cavitating foil sections should be used.

4.2.1 Super-cavitating foils

There are two basic super-cavitating foil sections. The first, used for speeds of up to 80 kn, is displayed in figure 4.8-a. This is referred to as a fully wetted base-ventilated super-cavitating foil. The cavitating blunt trailing edge of the foil is ventilated by natural ventilation along the cavitating surface piercing foil.

In figure 4.8-b is the section of a fully ventilated super-cavitating foil. This section is most successful at speeds above 80 kn. The sharp leading edge causes the formation of a fully developed cavity over the entire upper surface of the foil. Because the cavity only collapses well aft of the trailing edge of the foil, corrosive damage is absent.

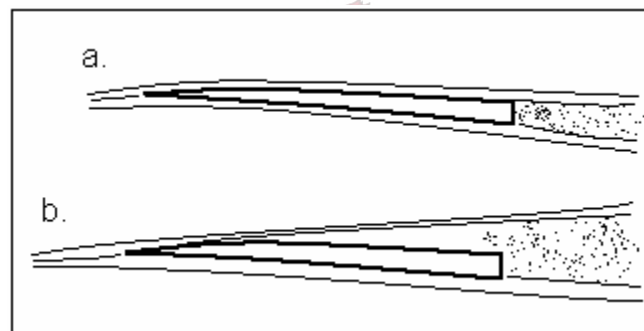


Figure 4.8 Super-cavitating sections

4.2.2 Sub-cavitating foils

At speeds below 60 kn foils can be designed with sections to limit cavitation. There are various standardized foil sections designed to maximize the lift to drag ratio while delaying the onset of cavitation, the most well known of which are from the NASA design literature such as the 16 or 63 series (Lewis, 1988) and the Göttingen K-series profiles. These foils are designed to produce a flat pressure distribution at the design speed and angle of attack. This flat pressure distribution prevents cavitation because of the absence of pressure peaks.

Although foil sections can be designed to minimize cavitation, there are various factors which cause cavitation on most foils. These include the flow interaction at foil struts and pod intersections, surface roughness and discontinuities, and the craft motions in a seaway combined with the orbital wave velocities (Lewis, 1988).

Hydrofoil lift

For foils operating in the subcavitating regime, lift and drag forces can be calculated according to aeronautical practice with corrections for the presence of the free surface. The lift force can be calculated using the standard equation for a three-dimensional lifting surface:

$$C_L = C_{L\alpha}(\alpha - \alpha_0) \quad (4.1)$$

Egrov and Sokolov (1965) proposed the following variation to correct the zero lift angle-of-attack affected by the free surface:

$$C_L = C_{L\alpha}(\alpha + \alpha_0 - \Delta\alpha_0) \quad (4.2)$$

where

$$\Delta\alpha_0 = \frac{t/c}{2} \left(\frac{1}{k_\phi} - 1 \right) \quad (4.3)$$

and

$$k_\phi = 1 - (0.5 + t/c) \exp[-2(h/c)^{0.6}] \quad (4.4)$$



The zero lift angle-of-attack in this equation is calculated as follows:

$$\alpha_0 = 110 \frac{f}{c} @ 0.1 \tau_c^{0.6} @ \log R_n^c \quad (4.5)$$

Alternately α_0 corresponds to $d\alpha/dC_L$ (Hoerner, 1965) for circular foil sections and can be calculated as follows:

$$\alpha_0 = -2 \frac{f}{c} = - \left(\frac{360}{\pi} \right) \left(\frac{f}{c} \right) = -115 \left(\frac{f}{c} \right) \text{ [deg]} \quad (4.6)$$

where f is the camber of the foil.

The three-dimensional lift curve slope depends on various factors that including sweep angle, dihedral angle and aspect ratio. These factors are also associated with airfoils and aircraft wings but the hydrofoil lift curve slope also incorporates submergence. Although there are various equations for calculating the lift curve slope available, most of these have similar results. Equation 4.7 was proposed by Migeotte (1997). It is a combination of the equations from various sources. Du Cane (1972) provides alternate equations similar to equation 4.7 and Tweedie (1996) shows that although the equations presented by Du Cane do not include some of the interference factors present in 4.7, the accuracy of prediction is similar.

$$C_{L\alpha} = \frac{2\pi \cdot P \cdot AR \cdot \cos \Lambda \cos^2 \Gamma}{AR + 2P(1 + \sigma)(1 + \xi) \cos \Lambda \cos^2 \Gamma \left[1 + \left[1 + \left(\frac{AR}{2P \cos \Lambda \cos^2 \Gamma} \right)^2 \right]^{0.5} \right]} - AR(1 + \sigma)(1 + \xi) \quad (4.7)$$

Where P is estimated for high speeds by (Lewis, 1988):

$$P = \frac{16 \left(\frac{h}{c} \right)^2 + 1}{16 \left(\frac{h}{c} \right)^2 + 2} \quad (4.8)$$

σ Corrects for the influence that the free surface has on the trailing vortex system associated with the three-dimensional flows around a hydrofoil of finite span. This factor can be calculated with bi-plane theory since the interference of the free surface is similar the bi-plane interference effect:

$$\sigma = 1.73 + 0.694 \frac{h}{s} - 2.127 \sqrt{\frac{h}{s}} - 0.514 \exp\left(\frac{h}{s}\right) \quad (4.9)$$

Du Cane (1972) presents the following approximation for the plan form correction factor which corrects the elliptical foil lift distribution for rectangular foils:

$$\xi = 1 + \frac{2}{AR^2} \quad (4.10)$$

Hydrofoil drag

The drag coefficient is made up of various different drag components shown in equation 4.18 as proposed by Lewis (1988) with an added term for separation drag as proposed by Migeotte (1997).

$$C_D = C_{DP} + \delta C_{DP} + C_{Di} + C_{Dw} + C_{DS} + C_{Dsep} \quad (4.11)$$

C_{DP} is calculated differently for various Reynolds numbers as proposed by Kirkman and Kloetzli (1980):

for laminar flow: $Rn < 5 \cdot 10^4$

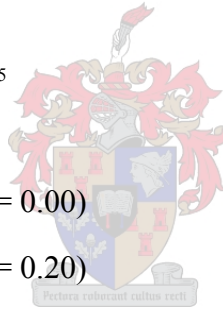
$$C_{DP} = 1.46Rn^{-0.507} \quad (\text{for } t/c = 0.00) \quad (4.12)$$

$$C_{DP} = 0.466Rn^{-0.259} \quad (\text{for } t/c = 0.20) \quad (4.13)$$

for first transition: $5 \cdot 10^4 < Rn < 5 \cdot 10^5$

$$C_{DP} = 0.172Rn^{-0.310} \quad (\text{for } t/c = 0.00) \quad (4.14)$$

$$C_{DP} = 181Rn^{-0.810} \quad (\text{for } t/c = 0.20) \quad (4.15)$$



for second transition: $5 \cdot 10^5 < Rn < 1 \cdot 10^7$

$$C_{DP} = 2.93 \cdot 10^{-3} \left[1 + 2 \left(\frac{t}{c} \right) + 60 \left(\frac{t}{c} \right)^4 \right] \quad (4.16)$$

and for turbulent flow: $Rn > 1 \cdot 10^7$

$$C_{DP} = 0.03Rn^{-0.1428} \left[1 + 2 \left(\frac{t}{c} \right) + 60 \left(\frac{t}{c} \right)^4 \right] \quad (4.17)$$

Migeotte (2001) suggested that the hydrofoil pressure drag will decrease as the foil approaches the free surface. The following formula, determined by

Egorov and Sokolov (1965) and presented by Migeotte (2001), accounts for the influence of the free surface:

$$C_{DP} = C_F \left[1 + \left[(m_p + 0.5) \frac{\varphi}{k_\varphi} - 0.5 \right] C_L \right] \quad (4.18)$$

C_F can be determined according to the ITTC 1957 formulation as follows:

$$C_F = \frac{0.075}{(\log_{10} Rn - 2)^2} \quad (4.19)$$

m_p can be determined with linear interpolation as follows:

$$m_p = \frac{2C_L}{3} + 0.3833 \quad (4.20)$$

φ Can be determined as follows:

$$\varphi = 1 - \exp \left[-2 \left(\frac{h}{c} \right)^{0.6} \right] \quad (4.21)$$



The lift curve slope correction factor k_φ is determined as follows:

$$k_\varphi = 1 - \left(0.5 + \frac{t}{c} \right) \exp \left[-2 \left(\frac{h}{c} \right)^{0.6} \right] \quad (4.22)$$

δC_{DP} is a profile drag increment due to angle of attack and can be approximated by (Lewis, 1988):

$$\delta C_{DP} = 0.005 C_L^2 \quad (4.23)$$

Wave drag (C_{Dw}) is caused by the formation of waves as the foil approaches the free surface. These waves are caused by the pressure fields around the foil, deforming the water surface. Riegels (1961) presented the following equation to calculate wave drag:

$$C_{Dw} = \frac{0.5C_L^2}{F_h^2 \exp\left(\frac{2}{F_h^2}\right)} \quad \text{where} \quad F_h = \frac{V}{\sqrt{gh}} \quad (4.24)$$

The induced drag is caused by the downward velocity induced over the foil by the foil-tip vortices (Houghton and Carpenter, 1993). The induced drag can be calculated in accordance with standard aeronautical practice including the bi-plane interference effect:

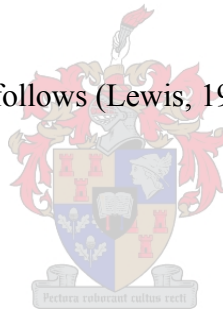
$$C_{Di} = \frac{C_L^2}{\pi \cdot AR \cdot P \cdot \cos \Lambda \cos^2 \Gamma} (1 + \sigma)(1 + \xi) \quad (4.25)$$

Surface piercing strut drag is made up of various different drag components:

$$C_{DS} = C_{Dspr} + C_{Dint} + C_{DSP} + C_{DSw} \quad (4.26)$$

The spray drag can be determined as follows (Lewis, 1988):

$$C_{Dspr} = C_F \left[7.68 - 6.4 \left(\frac{t \cos \beta}{c} \right) \right] \quad (4.27)$$



where β is the angle of the strut measured normal to the free surface.

The interference drag occurring at the joints between the foil and struts or the foil and hull. The boundary layers of the two joint surfaces joins together resulting in them being retarded (Hoerner, 1965). This leads to an increase in profile pressure drag arising due to the adverse pressure gradient at the rear of the foil. The angle of the joint is important in that angles smaller than 90° lead to larger interference drag. This is illustrated in figure 4.9, which shows how the drag of a wing fuselage configuration changes with respect to corner angle. A similar tendency can be expected for hydrofoil-hull configurations (Hoerner, 1965).

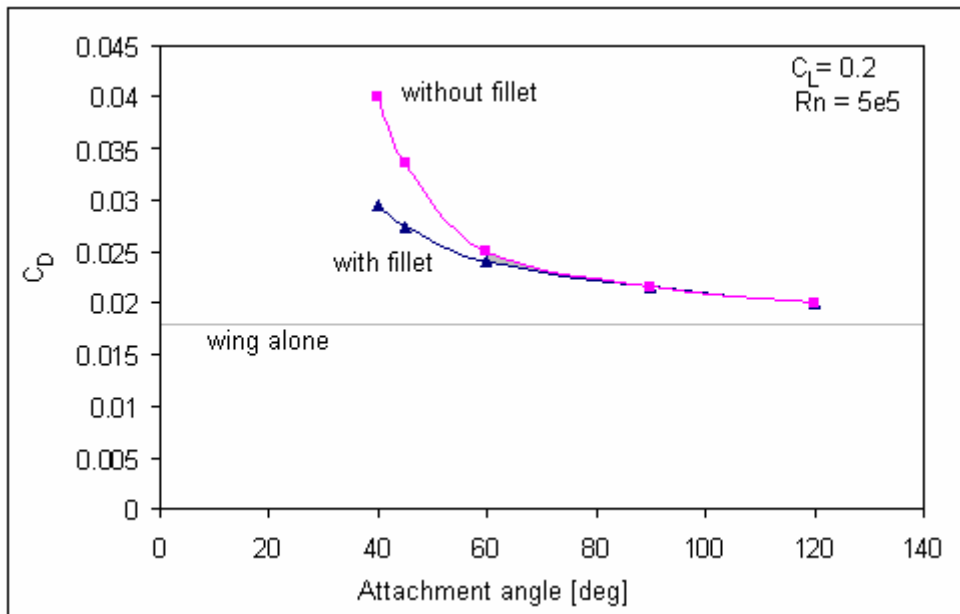


Figure 4.9: Drag of wing fuselage configuration as a function of the angle along the wing roots (Hoerner, 1965)

Also indicated in figure 4.9 is the effect of incorporating a fillet between the two surfaces. Hoerner (1965) proposed the following equation for the calculation of the interference drag at 90°:

$$C_{D_{int}} = 0.75 \left(\frac{t}{c} \right) - \frac{0.0003}{\left(\frac{t}{c} \right)^2} \quad (4.28)$$

For $t/c < 0.08$ the interference drag is negative. Since hydrofoils rarely have t/c values exceeding 0.08, this can be considered beneficial.

The wave-making drag can be ignored for Froude numbers larger than 0.7 since the wave-making decreases rapidly at these high speeds (Migeotte, 2001).

The separation drag ($C_{D_{sep}}$) due to thin airfoil stall has to be included because thin airfoil theory assumes potential flow. The following equation (Migeotte, 1997) for separation drag can be derived from empirical equations provided by Hoerner (1965):

$$C_{Dsep} = \frac{\sin^2 \alpha}{0.222 \sin \alpha + 0.283} - \frac{\left(\frac{\sin \alpha \cos \alpha}{0.222 \sin \alpha + 0.283} \right)^2}{\pi AR} \quad (4.29)$$

4.3 Hydrofoil Calculations

The theory discussed above was implemented in a Microsoft Excel (2000) spreadsheet to test its validity and applicability to the design problem at hand. In figure 4.10 and 4.11 the theory prediction is compared to experimental data from tests by Scheepers (1988).

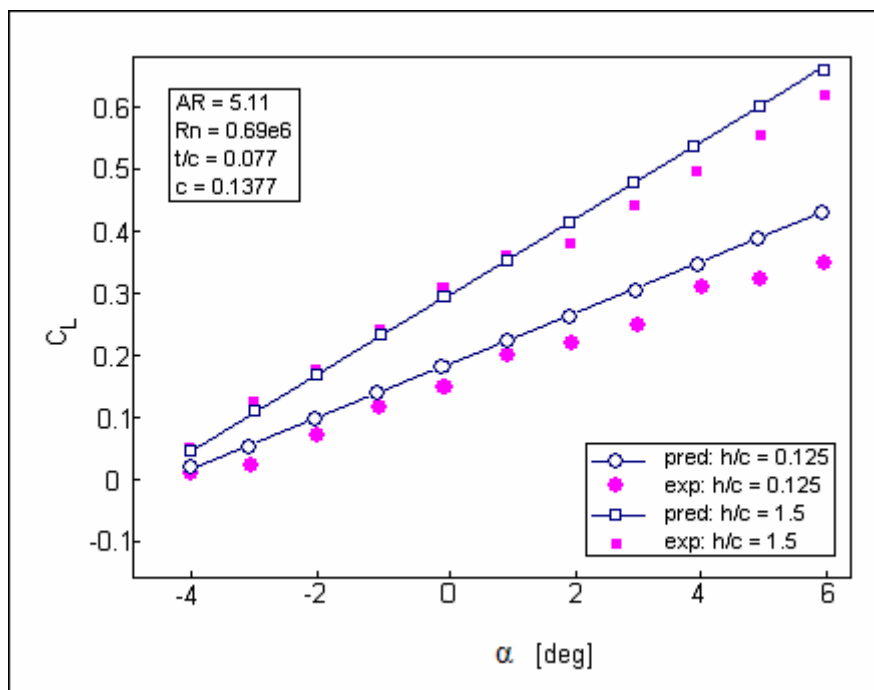


Figure 4.10: Prediction of hydrofoil lift compared with experimental results for various submergence ratios

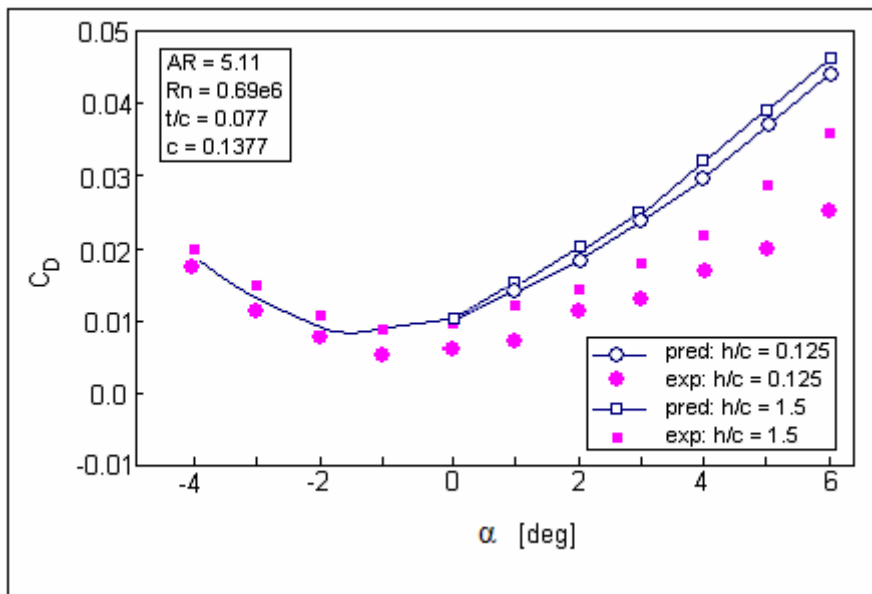


Figure 4.11: Prediction of hydrofoil drag compared with experimental results for various submergence ratios

As can be seen in figure 4.10, the lift is predicted sufficiently accurate particularly in the regions of interest where foils are most often used between an angle of attack of -1° to 2° . The drag is slightly over predicted for most angles of attack.

In the above prediction C_L was calculated with equation 4.1 where α_0 was calculated with equation 4.6. The drag includes all the drag components in equation 4.11 except for spray drag. Equation 4.29 is used to calculate separation drag only for negative angles of attack as there is no separation drag for small positive angles.

5 Planing Trimaran with Hydrofoil Support

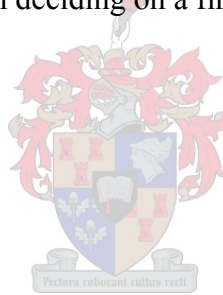
The design process is initiated by finding the best operating foil system and then the hulls are accommodated around that system.

5.1 Hydrofoil Design

A hydrofoil system has to be designed to support the planing hulls of the trimaran. The best hydrofoil design may not be the optimum foil arrangement design, as there are various limitations which have to be considered. These include: production of the foil, trimaran configuration, supports of the foil, structural limitations and cavitation.

The variables taken into account when deciding on a final foil system are the following:

- Foil configuration
- Depth of submergence
- Profile
- Chord
- Thickness
- Span
- Angle of attack
- Dihedral angle
- Sweep angle



5.5.1 Foil configuration

One of the most successfully used foil configurations, is the Hysucat design. The combination of lift with the front main foil and trim control with the smaller stern foils makes it the ideal configuration for a boat of this size. An additional advantage of the system is the large amount of test and prototype performance data that can be used to accurately predict performance as well as compare the current design to previous examples.

Another important decision regarding foil configuration is the operating depth of the foils. Foils become more efficient as their operating depth increases. For this reason it is desirable to have the foils operating as deep as possible, extending below the bottom of the hull keel where the free surface effects do not influence their operation. This, however, limits some of the practical applications of the boat. Once the foils extend below the keel, they are exposed, making it impossible to beach the boat or load it on a trailer. It also exposes the foils to bottom strike in shallow water and floating debris strike from which it would be protected would they have been above the keel line.

It was decided therefore to have the front foils level with the keel line, positioned only slightly in front of the LCG to provide pitch stability. The stern foils will be placed at a depth, calculated to be near the surface where the free surface effect will allow them to provide the trim stability for which they are intended. The final foil configuration is illustrated in figure 5.1.

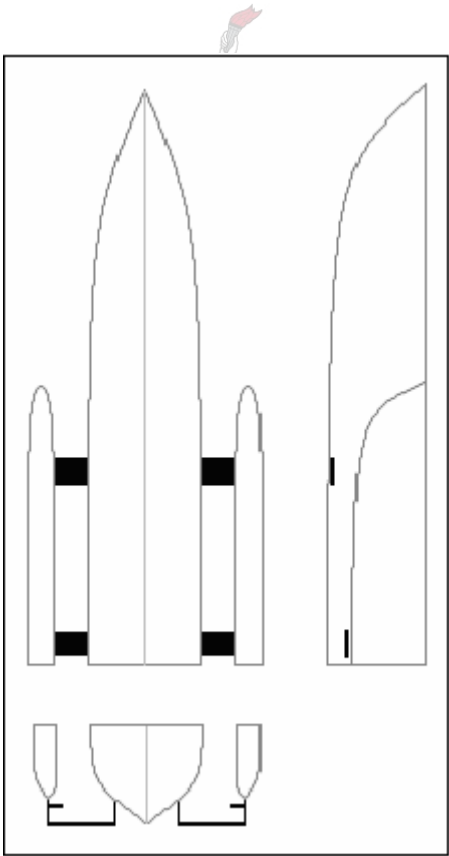


Figure 5.1: Hydrofoil configuration

5.1.2 Foil profile

The foil profile was chosen based on two important factors; delaying cavitation and ease of production. Profiles whose maximum thickness lies forward are unfavourable because of the high minimum pressure that causes premature onset of cavitation. Circular-arc-segment profiles have a very uniform pressure distribution and are therefore favourable for cavitation delaying purposes. They are also easily produced compared to other profiles because of their simple geometry.

The most commonly used circular arc segment profiles are the Göttingen K-series profiles, particularly the 5K to 16K profiles which have rounded leading edges and are more resistant to cavitation (Riegels, 1961). The basic circular-arc-segment profile is shown in figure 5.2.

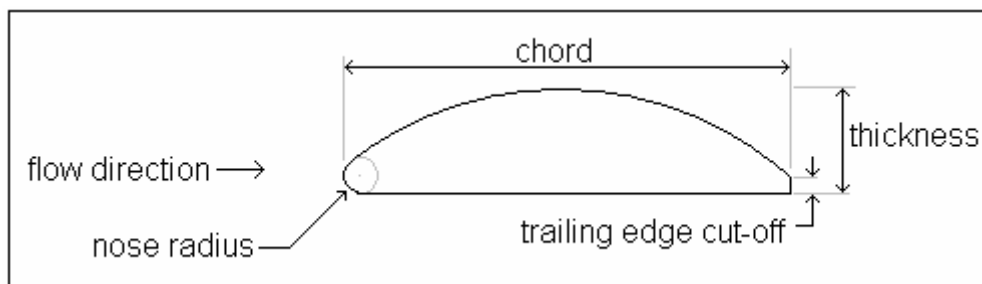


Figure 5.2: Circular arc segment foil profile

It is shown by Riegels (1961) that for the Göttingen 14K to 16K, cavitation will occur if the cavitation number is smaller than $\sigma < 3 \frac{t}{c}$. It is seen that foils with smaller thickness to chord ratios are more resistant to cavitation, this however is in conflict with the required strength of the foil which is higher for thicker profiles. For a foil travelling at 60 kn at a depth of 0.5 metres, the cavitation number is 0.21. This corresponds to a thickness to chord ratio of 0.07.

When considering the hydrofoil performance equations of chapter 4, it is clear that foils with high aspect ratios (span to chord ratios) will have a higher lift to drag ratio. It is therefore desirable to have a foil with as large a span as possible with a small a chord as possible. This is only limited by the required strength of the foil as longer narrower foils are not as strong as short wide foils, particularly if the thickness to chord ratio is constant as the thickness is the main factor determining the foil strength. It was therefore necessary to make an initial

estimation of the load each foil would have to carry, in order to do the necessary strength calculations.

The Hysucat hydrofoil configuration works well if the front foils carry 70 % and the stern foils 10 % of the total boat weight (Migeotte, 2005). This weight distribution will require each of the front foils to carry:

$$\frac{5000kg \times 70\%}{2} = 1750kg$$

and the stern foils:

$$\frac{5000kg \times 10\%}{2} = 250kg$$

The required strength was determined using simple beam theory as shown in figure 5.3 with both ends of the foil clamped in.

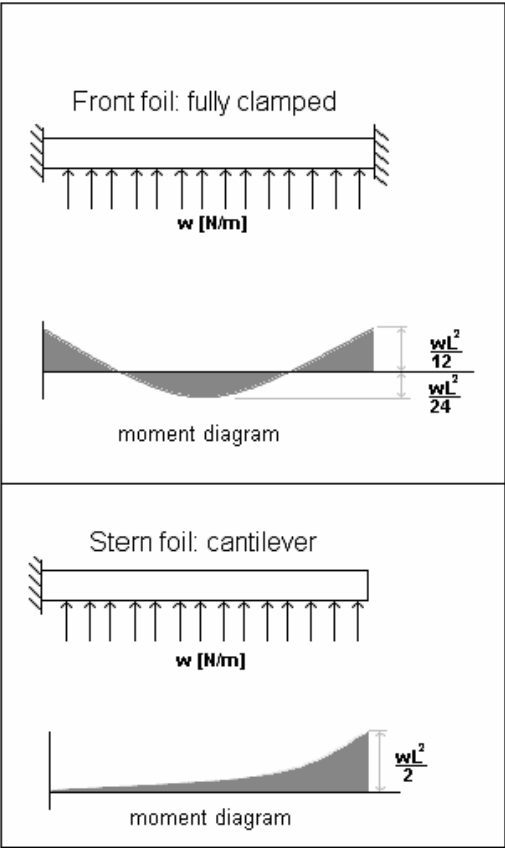


Figure 5.3: Simple beam theory for clamped in beam

Using this theory, structurally the most important points on the front foils can be identified as the ends where the moment is the greatest. The stress in the foil can be found at any point with the simple relation:

$$\sigma = \frac{My}{I} \quad (5.1)$$

where σ is the stress, M the bending moment, y the distance of the point in question to the centre of the cross sectional area, and I is the second moment of area.

To calculate the second moment of area (I) for the foil, it is divided into n squares as shown in figure 5.4.

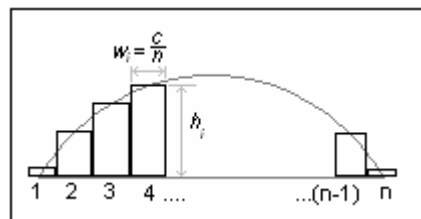


Figure 5.4: Integration across foil profile

The centre of area is then calculated for the foil as follows:

$$Y' = \frac{\sum_i^n (y'_i A_i)}{\sum_i^n A_i} \quad \text{where } i = 1 \text{ to } n \quad (5.2)$$

where y'_i is the centre of area for each division which is simply its height (h_i) divided by 2,

and A_i is the area of each division ($A_i = w_i h_i = \frac{ch_i}{n}$).

The second moment of area is then:

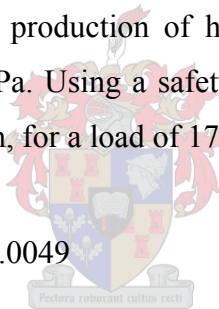
$$I_z = \sum_i^n \left(\frac{wh^3}{12} + A(Y' - y')^2 \right) \quad (5.3)$$

Given the thickness and chord the second moment of area can therefore be found for any circular arc profile. With a constant thickness to chord ratio, the second area moment and therefore also the stress in a foil can be found as a function of the chord. Given the maximum allowable stress for the material from which the foil is fabricated, the maximum span can be found as a function of the chord, thus maximising the aspect ratio. A copy of the Matlab solution is included in appendix A.

The stress in the horizontal plane, due to drag, was neglected because it is negligibly small. This is because firstly the lift to drag ratio is in the order of 15 and the second moment of area in the chordal direction is much larger than for the thickness.

The material commonly used in the production of hydrofoils is SAF 2205 stainless steel which has a yield strength of 620 MPa. Using a safety factor of two, the following relation was found between the chord and span, for a load of 1750 kg:

$$S = 121.69c^3 + 0.0597c^2 - 0.0309c + 0.0049$$



Once the thickness and span can be written as functions of the chord, which maximises the lift to drag ratio while still limiting cavitation, it becomes simple to calculate the necessary profile to produce the required lift. These relations were then used in the mathematical model discussed later.

5.1.3 Dihedral and sweep angle

Although there are various advantages; related to manoeuvring, sea-keeping and stability in including both a dihedral and sweep angle; to simplify the production of the foil system, particularly that of the model, it was decided not to have any dihedral or sweep angle.

5.1.4 Angle of attack

The most favourable angles of attack for the limitation of cavitation and maximising the lift to drag ratio are between -1° and 3° . The fixed foils will therefore be mounted with an angle of

attack of 0° which will then change with the trim angle of the boat. The maximum allowed trim angle of the boat is 2.5° which is still in the favourable range of angles of attack.

5.2 Hull Configuration

Once the hydrofoils are added, the main factor determining the hull configuration is the position and size of the foils. This is largely because the design is such that when operating at the design speed, the outriggers will be air-borne and all lateral stability will be provided by the foils. The hull configuration must be such that the hull, when in contact with the water, must not interfere with the operation of the foils.

It was accordingly decided to still have 0 % stagger as this does not in any way interfere with the foil operation and provides a practical base where the foils can be joined to the outriggers.

The clearance of the outriggers is only dependent on the necessary span of the foils. The front foil strut will be attached to the centre hull in line with the chine where hull-foil interference will not occur and structurally the joint will be easier. From this line, the clearance of the outriggers will be the same as the span of the foils to the centre of the outriggers where the outrigger-foil strut will be mounted.

The outrigger keel height will be calculated along with the clearance, so that the outriggers will come into contact with the water and provide additional stability only if the boat rolls more than 8° when the boat is operating at design speed.

5.3 Mathematical Model

Shown in figure 5.5 are the forces acting on the planing trimaran with hydrofoil support. Adding the lift and drag forces into the system, an altered version of the program used in chapter 3 to solve the equilibrium trim angle for a planing trimaran is used. The equilibrium equations are then solved to find the equilibrium trim angle.

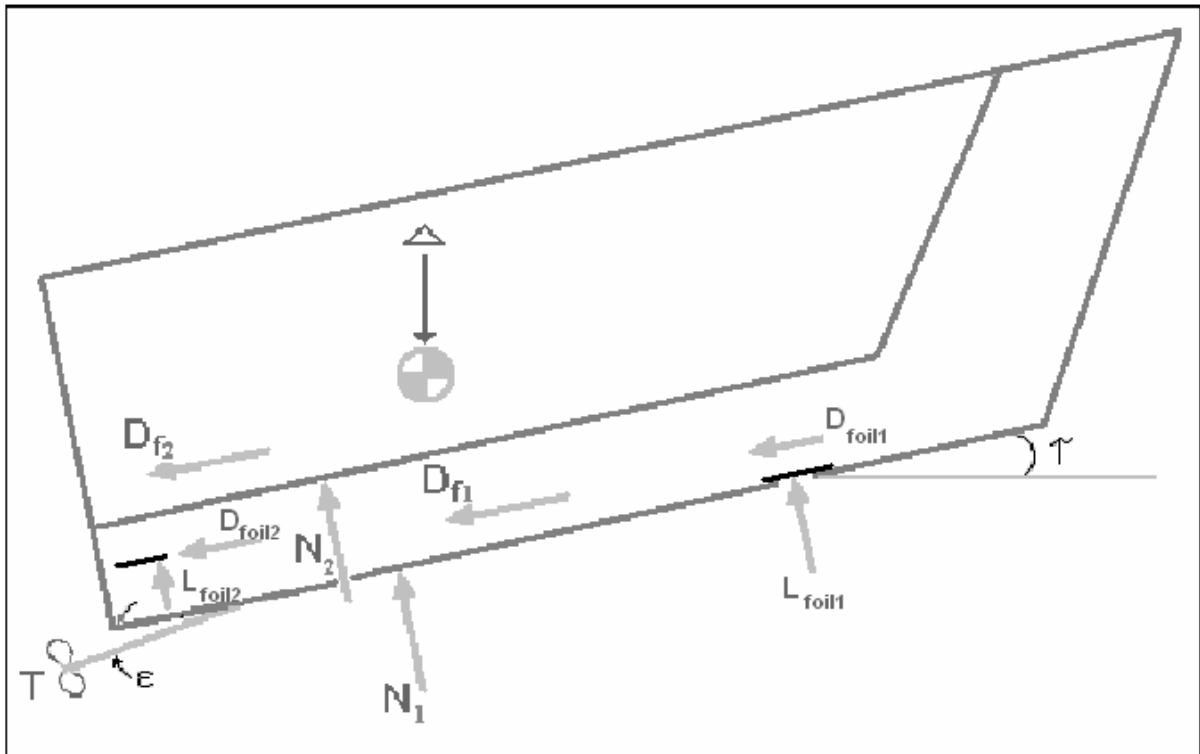


Figure 5.5: Forces acting on hydrofoil-supported trimaran

Summing vertical forces:

$$\Delta = (N_1 + N_2)\cos(\tau) + T\sin(\tau + \epsilon) - (D_{f1} + D_{f2})\sin(\tau) + (L_{foil1} + L_{foil2})\cos(\tau) - (D_{foil1} + D_{foil2})\sin(\tau) \quad (5.4)$$

Summing horizontal forces:

$$T\cos(\tau + \epsilon) = (D_{f1} + D_{f2})\cos(\tau) + (N_1 + N_2)\sin(\tau) + (D_{foil1} + D_{foil2})\cos(\tau) + (L_{foil1} + L_{foil2})\sin(\tau) \quad (5.5)$$

For equilibrium of pitching moments:

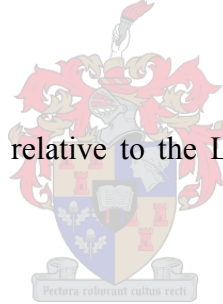
$$N_1c_1 + 2N_2c_2 + D_{f1}a_1 + 2D_{f2}a_2 - T_f - L_{foil1}(f_{l1} - LCG) + D_{foil1}(VCG - fh_1) + L_{foil2}(LCG - f_{l2}) + D_{foil2}(VCG - fh_2) = 0 \quad (5.6)$$

A copy of the solution code is provided in appendix A.

5.4 Optimisation analysis

The program was used to calculate the equilibrium drag, trim angle and wetted lengths for a range of foil positions and sizes. The aim was to find the best operating foil configuration to minimise the required horsepower while operating at the design speed of 60 kn. This was done for LCG positions of 31 %, 34 %, 37 % and 40 %. This represents a realistic range of practical operation conditions.

Firstly, the position of the front foil relative to the LCG was investigated. The results are shown in figure 5.6 and 5.7.



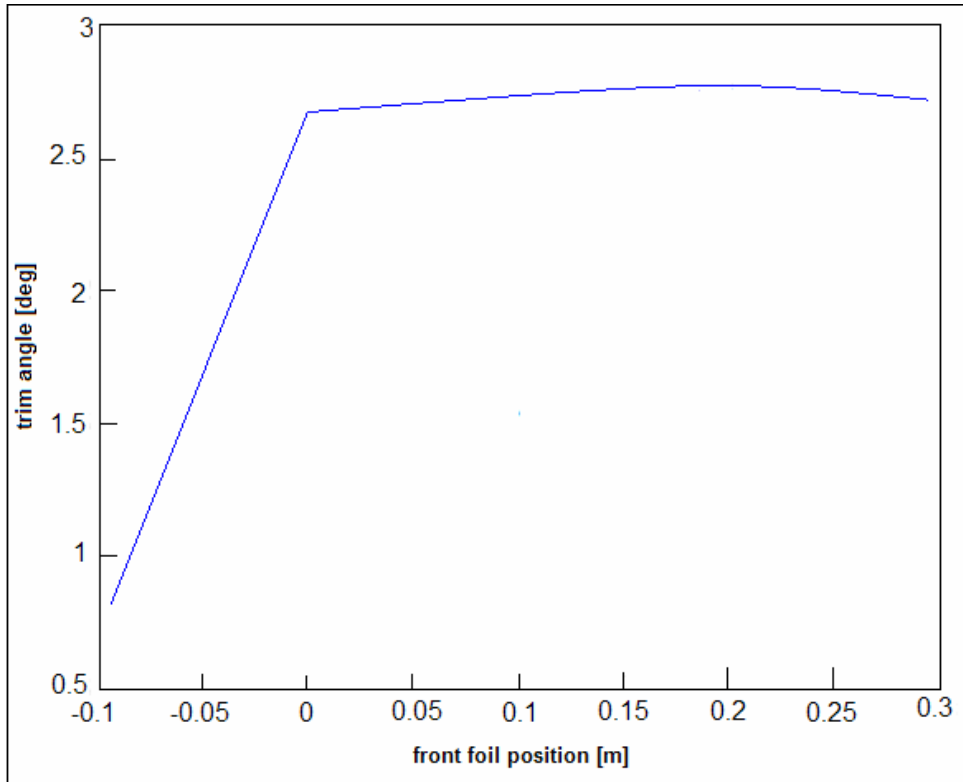


Figure 5.6: Front foil position, relative to LCG vs. trim angle

Here it can be clearly seen how the boat becomes unstable, trimming down, when the front foil is positioned behind the LCG. This is also noticeable in figure 5.7.

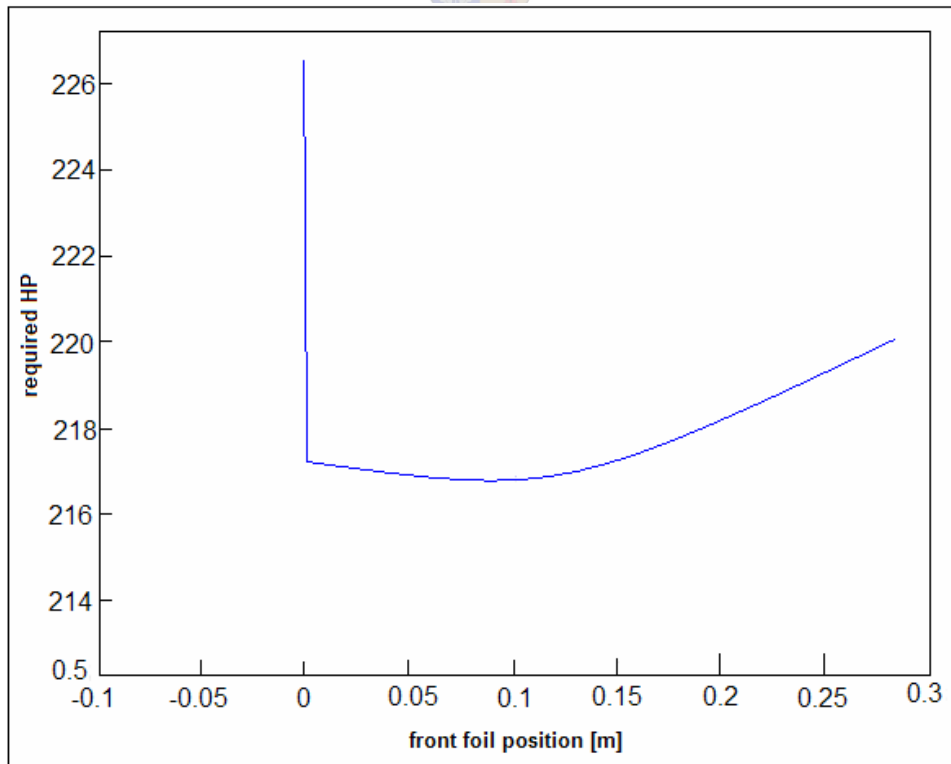


Figure 5.7: Front foil position, relative to LCG vs. required effective horsepower

Here it is clear that the foil must be positioned as close as possible to the LCG, without placing it too close, risking the boat becoming unstable with a forward shift in LCG. It was accordingly decided to position the front foil 0.1 m in front of the LCG.

Next the size of the front foil was varied for all the various LCG positions to find the optimum foil size. Firstly the front foil size, represented by the chord, was plotted versus the operating trim angle to determine the foil size at the maximum allowable trim of 2.5°. This is shown in figure 5.8.

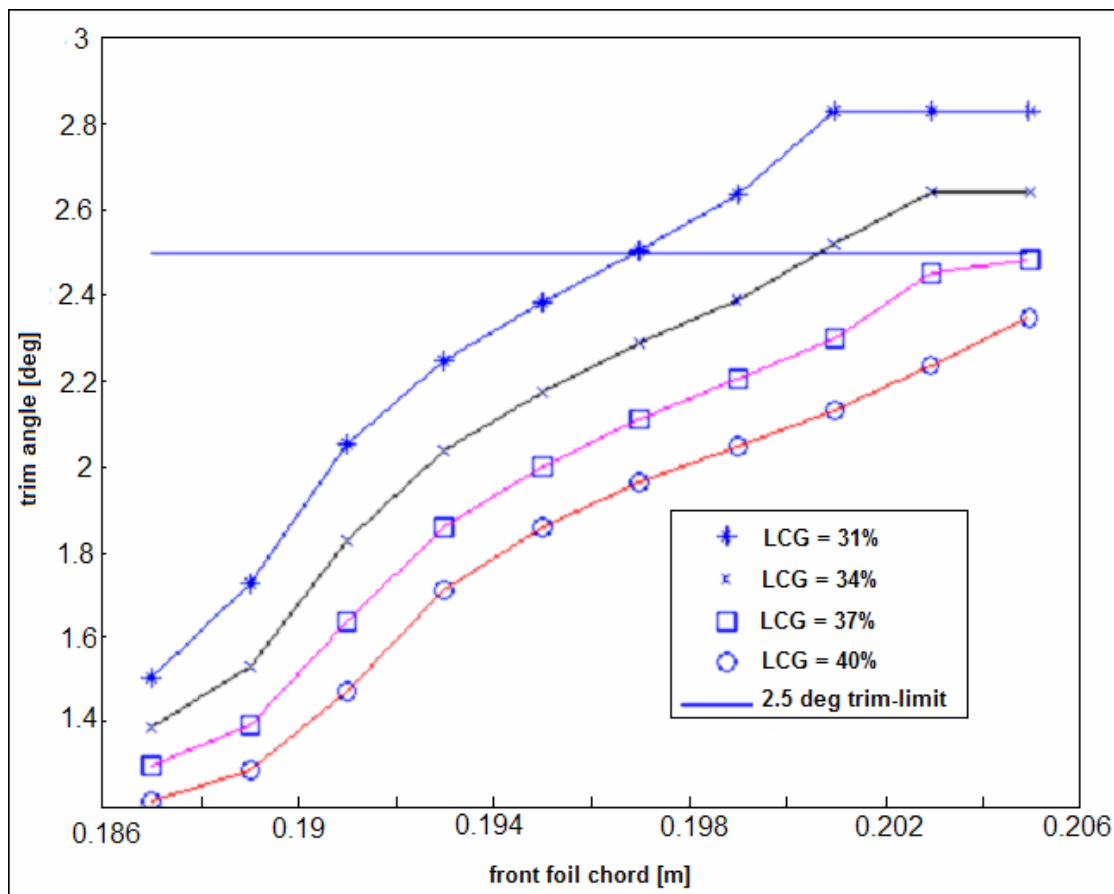


Figure 5.8: Front foil size vs. operating trim angle

From this figure it is clear that to limit the operating trim angle to 2.5°, the front foil chord length will have to be limited to 0.197 m. Although the foil can be larger for LCG positions larger than 31 %, this would endanger the boat of porpoising instability if the LCG were shifted back.

The corresponding foil size versus required horsepower plot is shown in figure 5.9.

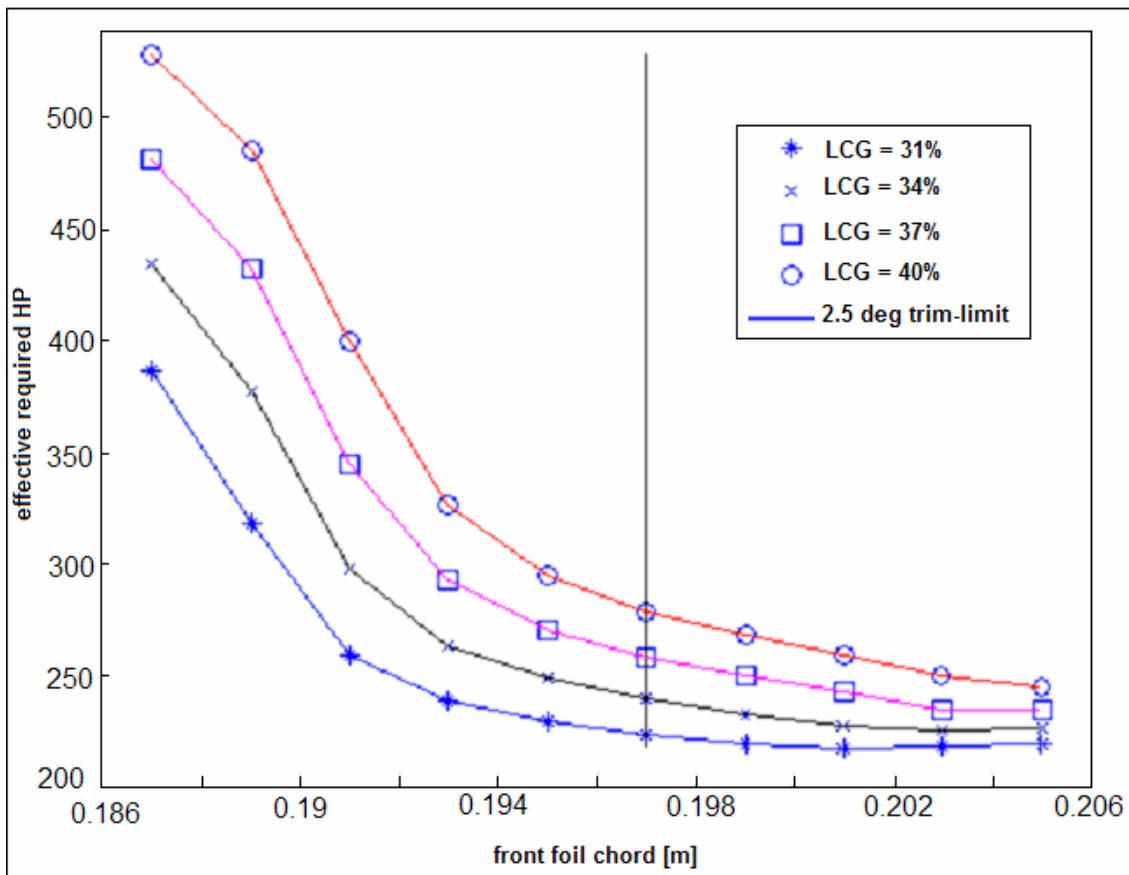


Figure 5.9: Front foil size vs. required effective horsepower

It can be seen from this figure that the required horsepower estimations corresponding to the 2.5° trim angle limit is 223, 239, 258 and 279 for the 31 %, 34 %, 37 % and 40 % LCG positions respectively.

All the above calculations were made while the stern foils are positioned at a depth of 0.1 m at design speed where the free surface effect allows trim stabilisation. They are sized to carry 10 % of the total boat displacement.

Next, an analysis was done to see how the boat is expected to perform through the speed range with the above foil configuration. The results are shown in figure 5.10.

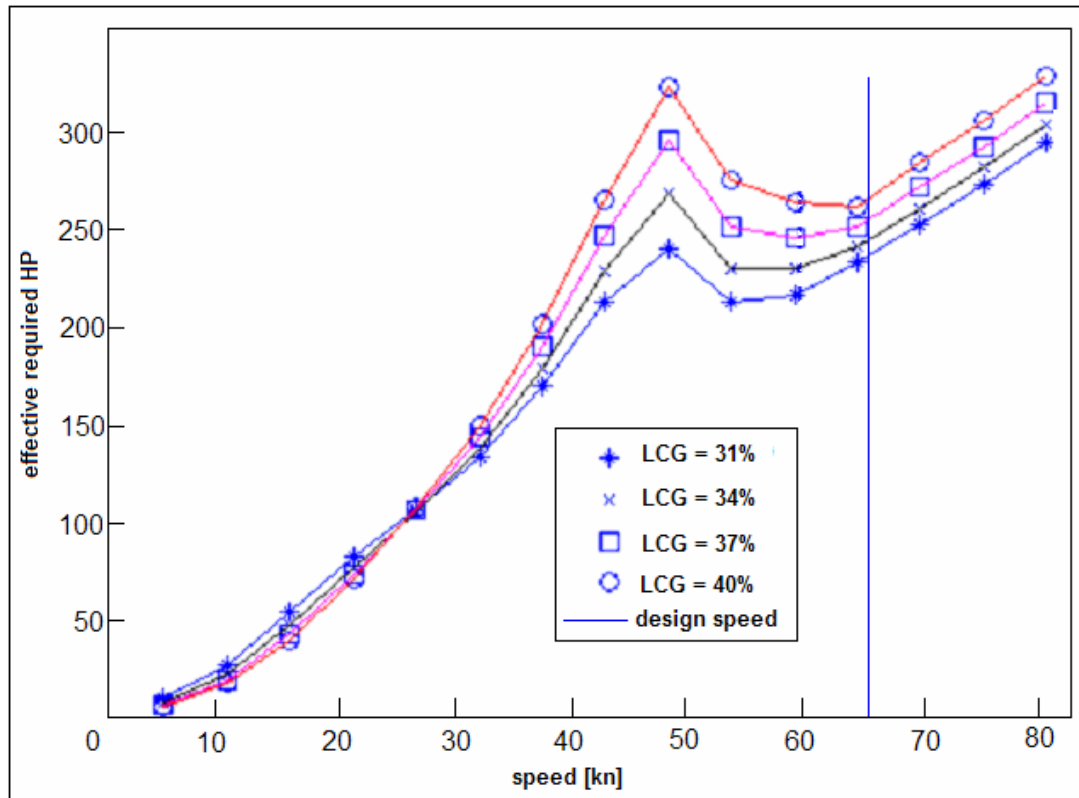


Figure 5.10: Speed vs. required effective horsepower

Here the typical hump can be seen in the resistance, only slightly prior to the takeoff speed. The analysis also indicates how the decisions taken to limit the resistance at the design speed have successfully allowed the hydrofoil configuration to operate at its optimum at that speed.

5.5 Final hull-foil configuration

The final foil profile is shown in figure 5.11:

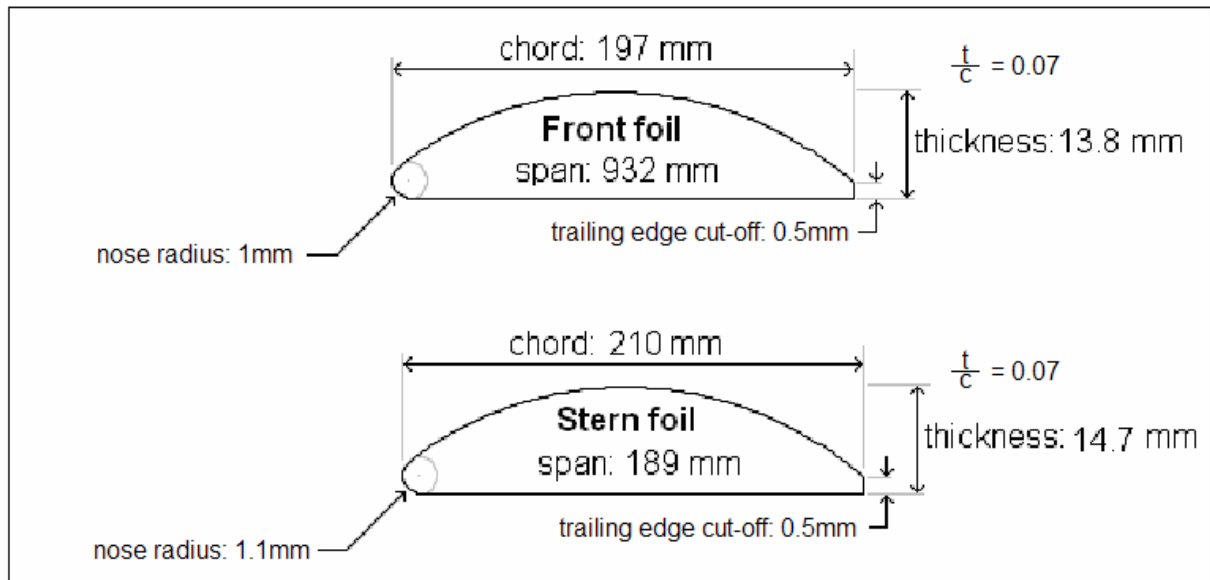


Figure 5.11: Final foil specifications

As earlier mentioned, the outrigger clearance will be based on the hydrofoil span. The distance between the foil strut and the centre hull keel is 667 mm, which brings the clearance to 1599 mm. The outrigger height will be such that if the boat rolls 8° , they will come into contact with the water; the corresponding height above the waterline is 225 mm. The calculated draft at the centre hull keel at design speed is 250 mm which, makes the keel height of the outriggers above the centre keel, 475 mm.

The stern foils will be operating at a depth of 100 mm. With the outrigger height above the water at 225 mm, the stern foil will be positioned 325 mm below the outrigger keel line with the foil trailing edge in line with the stern of the boat.

The final hull-foil configuration is illustrated in figure 5.12.

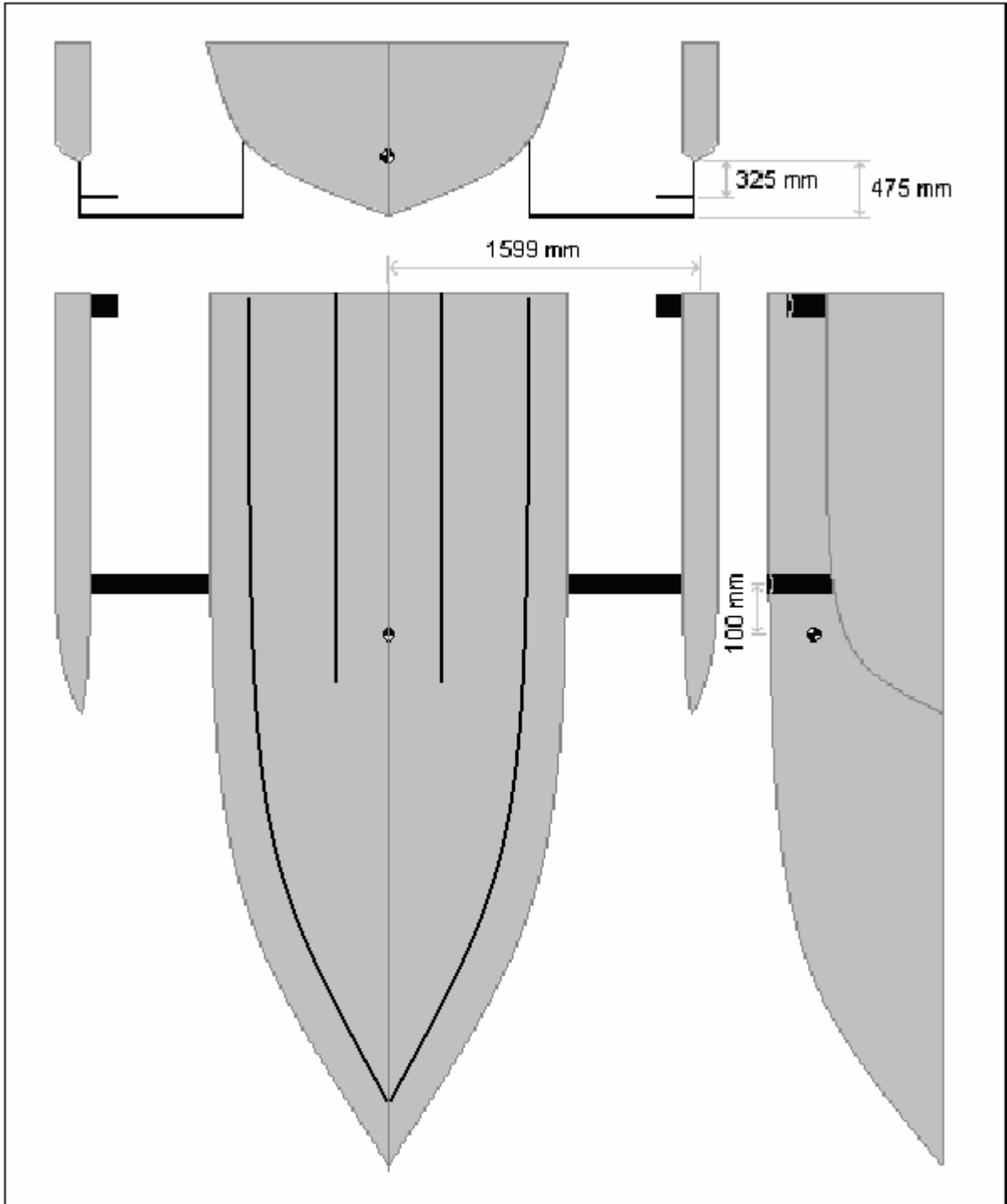


Figure 5.12: Final hull-foil configuration

6 Model Testing

In order to test and verify the theory thus far used to design the boat, it is necessary to test the hull to see how well the theory predicts the actual performance. In order to do the testing, a model of the boat was built which could then be tested in a towing tank.

6.1 Testing Facilities

The testing was done at the towing tank of the Mechanical Engineering department at the University of Stellenbosch. The towing tank has the following specifications:

- length: 92 m
- breadth: 4.5 m
- depth: 2.7 m
- maximum trolley speed: 8 m/s

The trolley is fitted with measuring equipment used to measure the speed, trim angle and resistance of the model. The equipment layout is shown in figure 6.1.

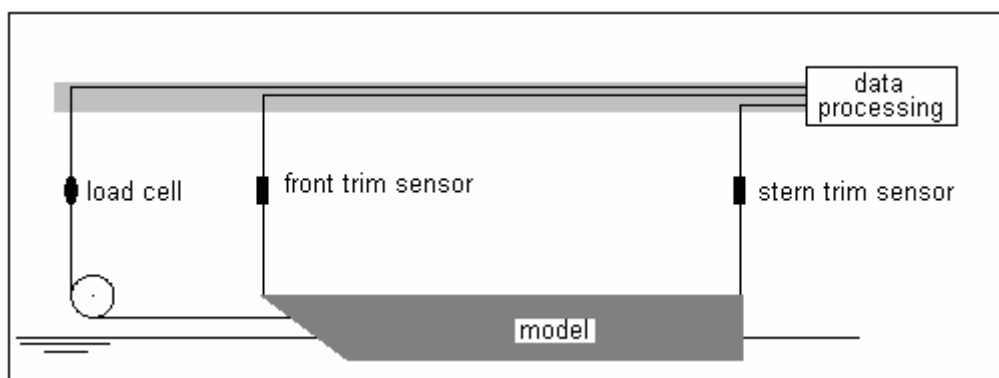


Figure 6.1: Data collection equipment and model layout

The hull resistance is measured with a load cell. The cord towing the model must be horizontal to ensure accurate results. The trim is measured by two linear displacement sensors, the cords of which must be attached to the model vertically.

6.2 Model Production

6.2.1 Model scaling

Before the model could be produced the correct scaling factor had to be determined, based mainly on the speed capability of the towing tank trolley. The model and the prototype has to be dynamically similar. To ensure dynamic similitude the Froude number for both the model and prototype must be equal. The model has to be made as large as possible to limit viscosity scaling effects and to limit measurement errors. The model will be tested for a range of speeds from 25 % below to 25 % above the design speed. The maximum prototype testing speed is therefore 75 kn. The model was therefore scaled to have the maximum trolley speed of 8 m/s be dynamically similar to the prototype at 75 kn. The appropriate scaling factor was 23,53. This resulted in a model with an overall length of 510 mm.

6.2.2 Final model

The model was made from a clear plastic to simplify the determination of the wetted surface area during testing. Instead of having to estimate the wetted surface area from oil-smudge marks, as is traditionally done, the clear hull made it possible to simply take a photograph and measure the wetted area from the photograph. The production process of the model is included in appendix B. The final model is shown in figure 6.2.

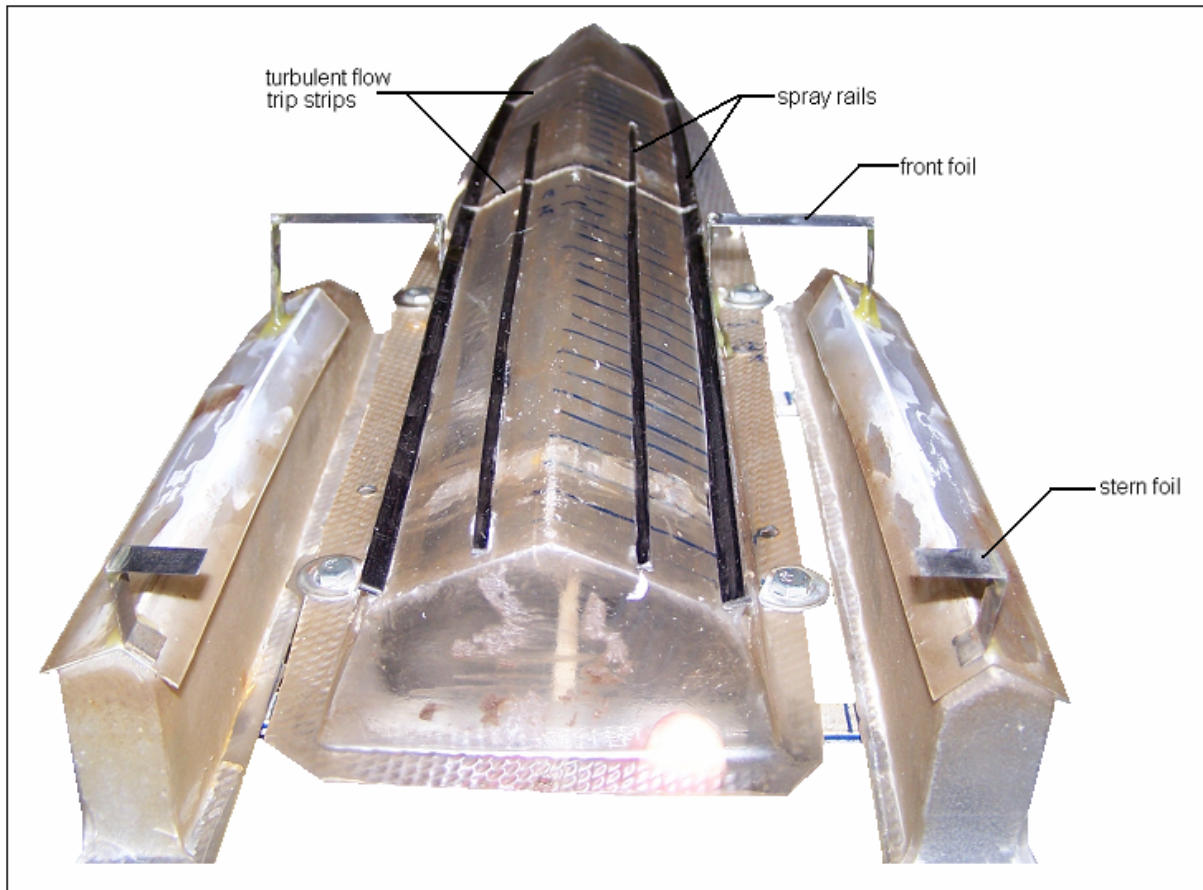


Figure 6.2: Hull model

The turbulent flow trip strips indicated in the figure are attached to the hull to trip turbulent flow. This has to be done because the model is smaller and travels slower than the prototype and therefore the Reynolds number is much lower. This causes the flow transition from laminar to turbulent to occur farther down the hull of the model than on the prototype. To ensure turbulent flow and therefore dynamic similarity as is required by Froude's law of scaling, the rough strips are added to trip the flow. The ITTC requires one such strip for displacement hulls. This however is unpractical for planing hulls because the wetted length changes drastically with speed. It was therefore decided to have two strips, one to trip the flow at low speed and another to trip the flow at high speed, positioned according to the mathematical model, when the wetted length is shorter.

6.3 Test Procedure

6.3.1 Test set-up

The model was tested for a speed range between 4.8 and 8 m/s, corresponding to full-scale speeds between 45 and 75 kn. Tests were done on the bare centre hull, the centre hull with spray rails, trimaran without foils and the trimaran with foils. The tests on the centre hull alone were done to be able to compare the hull performance with and without the spray rails. This could then also be compared to the trimaran performance to gain knowledge of the effect of adding the outriggers.

The tests on the centre hull alone were done for a LCG position of 37 %, while the tests on the trimaran with and without foils were done at LCG positions of 31 %, 34 %, 37 % and 40 %.

Testing of the hull without foils was done at 0.5 m/s intervals while when the foils were added, the speed intervals were shortened to about 0.3 m/s. This was done because the presence of wind blown particles in the water caused some of the tests to give inaccurate results as the particles were caught on the foils. The larger number of tests ensured that these inaccurate tests could be excluded without affecting the results.

The ITTC testing regulations require that the resistance sensor should measure the horizontal tow force to within 0.2 % of the maximum capacity of the sensor or 0.05 N, whichever is the larger. The speed of the model should be measured to within 0.1 % of the maximum speed or to within 3 mm/s, whichever is the larger. The trim should be measured to within 1.0 mm.

The basic test set up as prescribed by the ITTC is shown in figure 6.3 (Sname, 2006).

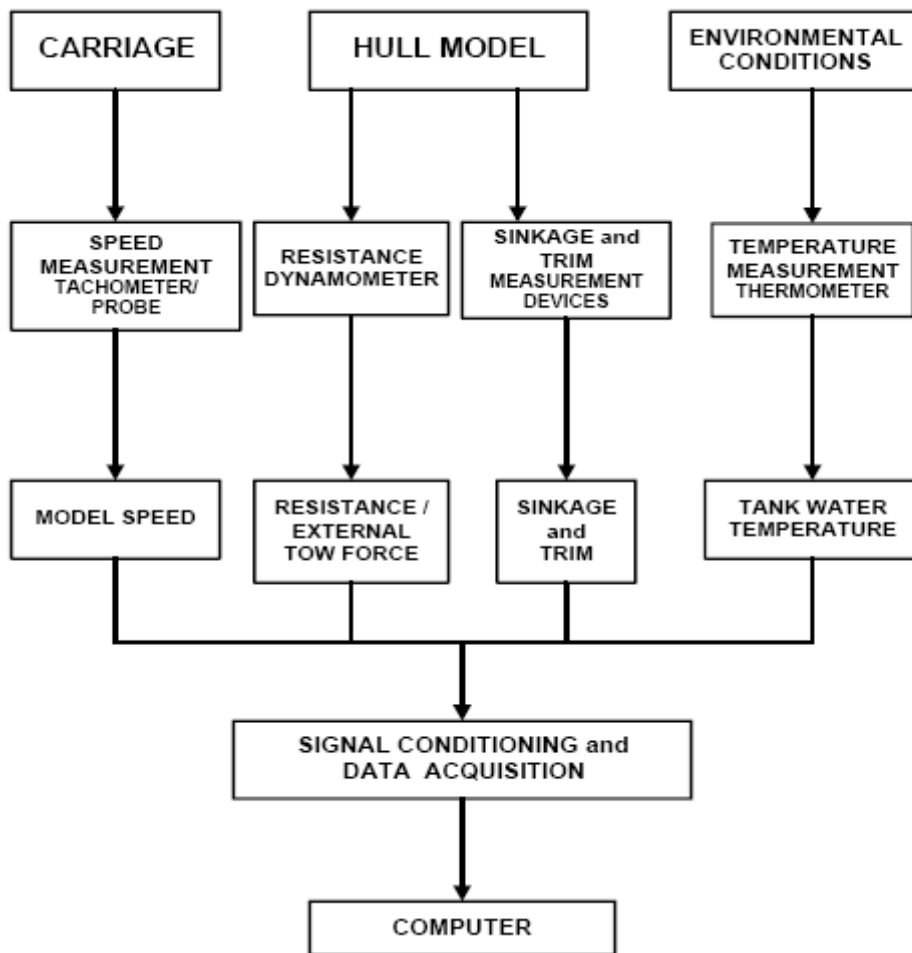


Figure 6.3: ITTC Prescribed test measurement system (Sname, 2006)

There are various limitations on tank testing such as shallow water affects and blockage (lateral flow restriction). These limitations and their applicability to this project is discussed briefly in appendix C. Taking into account these limitations, calibration, measuring and scaling errors, the total error in the results is between 5 and 10 percent for the towing tank in which the tests were performed (Migeotte, 2005).

6.3.2 Test procedure

Before each test the test conditions had to be determined. This includes the measuring of the water temperature to determine the water density and viscosity. The atmospheric temperature also affects the instrumentation and therefore the measurements. For this reason the measuring instrumentation was calibrated before each test. The resistance sensor (load cell)

was calibrated using a known mass while the trim sensors were calibrated using a known displacement.

The model was prepared by first cleaning it up, removing any impurity deposits from the water from the previous tests. The LCG was then shifted to the desired position. This was done by simply moving a weight along a slide on the model, when the model balances on a sharp edge at the required LCG position, the shifting weight is fixed.

The model is then placed in the water and the towing harness as well as the trim sensor lines are attached. The tow pulley is then vertically positioned so that the towing harness is perfectly horizontal. The towing harness is then taut or loosened and the trim sensors positioned to ensure that the trim sensor lines are normal to the water surface when the towing harness is tensioned to the zero resistance load. All equipment is then zeroed and the data measurement is started. The trolley is then accelerated to the required speed and kept at that speed for as long as possible before braking. The measured data is then analysed and an averaged value for the resistance and trim is stored for the data range where the speed was constant at the required value. A photo is taken of the model while it is travelling at constant speed to determine the wetted surface area at that speed. An example of such a photo is shown in figure 6.4.



Figure 6.4: Model test photo for determining wetted surface area

7 Test Results

Test results for the resistance, trim and wetted surface area at various speeds for each model configuration with different LCG positions were written into Microsoft Excel where the necessary analysis and scaling was performed. The correlated prototype results are presented.

7.1 Hull Configurations and Appendages

The resistance results for the various hull configurations are displayed in figure 7.1.

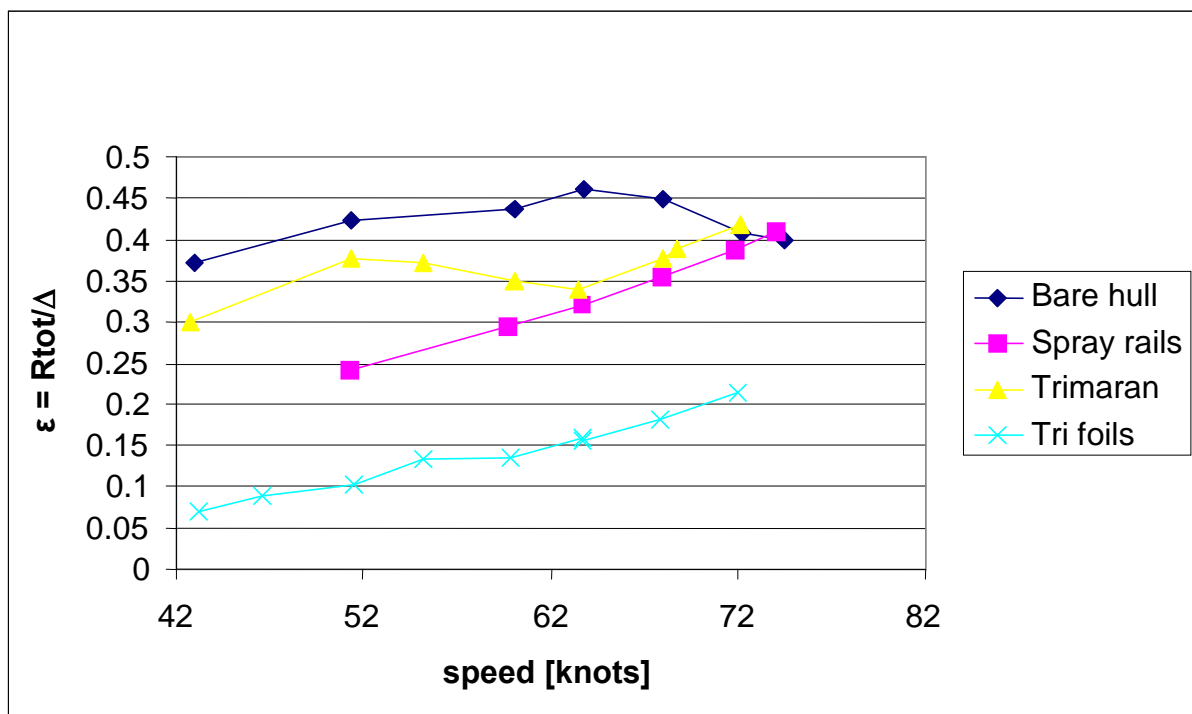


Figure 7.1: Resistance coefficient comparison for various hull configurations

The effect of adding the various appendages is clearly seen in figure 7.1. The simple bare hull is seen to have a relatively large resistance. This resistance coefficient is large even for a monohull even though the hull is very slender. This is because the convex section shape is sucked into the water and therefore has a much larger viscous and wave-making resistance.

It is seen that once the spray rails are added, the resistance coefficient is reduced dramatically. The fact that the transverse flow is now separated from the hull, no longer causing a low pressure sucking the hull down into the water, means a considerable total resistance reduction.

With the addition of the outriggers, the resistance increases a little. This is because of the added wetted surface area and wave making resistance of the outriggers.

Finally the hydrofoils are added and the result is a drastic reduction in resistance. The outriggers are not touching the water at all anymore and the wetted area of the centre hull is greatly reduced. It is clear that even operating near the surface as the foils are on this model, the foils are a lot more efficient than the planing hull.

7.2 Design Theory Verification

It is necessary to compare the theory which was used to design the hull to the test results to be able to judge whether or not the theory sufficiently predicts the hull performance. In figure 7.2 to 7.4 various comparisons are made.

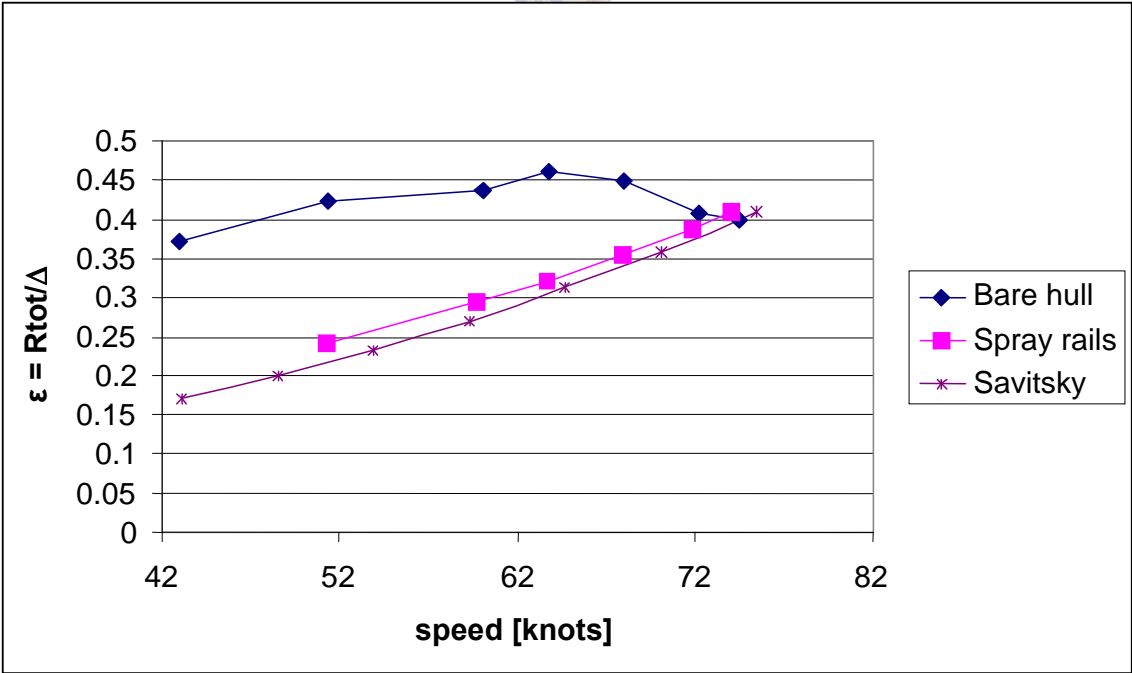


Figure 7.2: Resistance coefficient comparison between test results and theory prediction for the centre hull

It can be seen in figure 7.2 how the prediction by the Savitsky (1964) theory corresponds closely with the tests of the centre hull with spray rails. The theoretical prediction is for prismatic hulls with straight sections while this hull has convex sections. As described earlier, the convex sections have a larger resistance without the addition of spray rails. The centre hull with spray rails therefore performs more like the straight section prismatic hull prediction than the bare hull without spray rails.

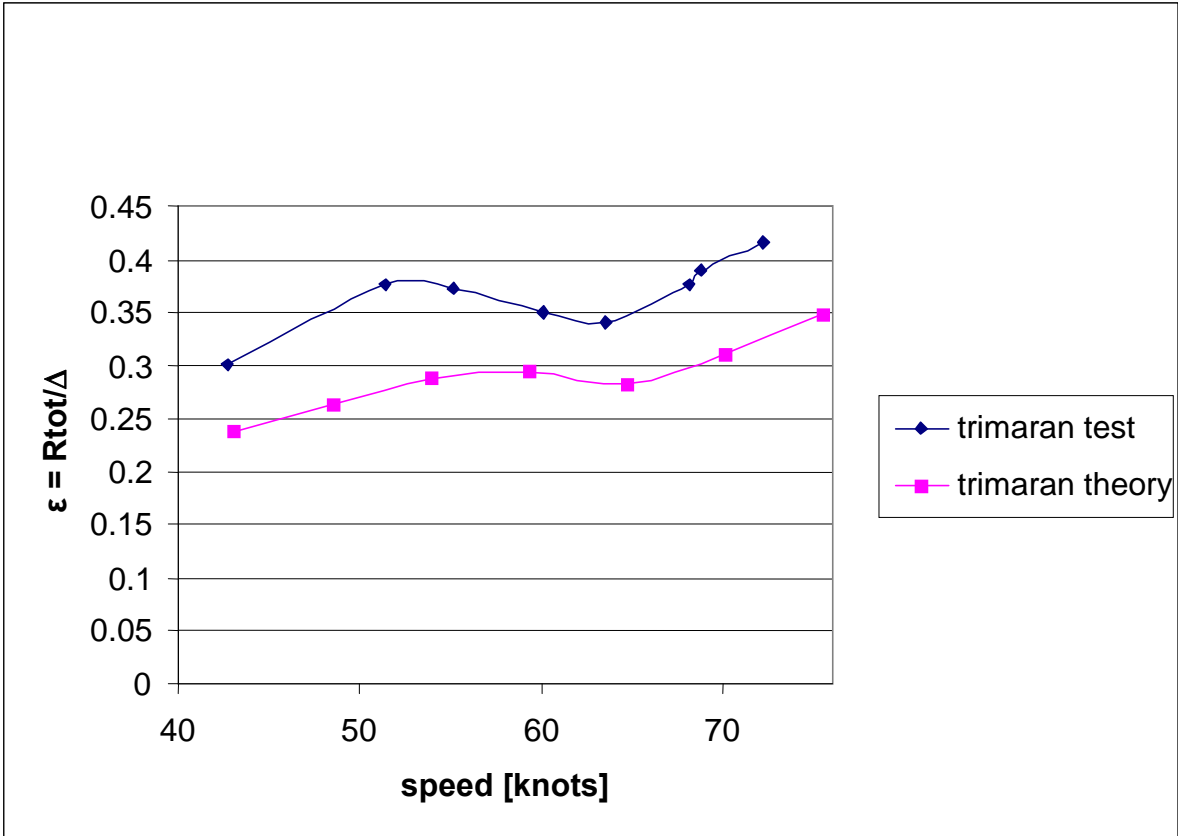


Figure 7.3: Resistance coefficient comparison between test results and theory prediction for the trimaran configuration

The theory for the trimaran configuration accurately predicts the trend shown by the tests although there is an under-prediction for the resistance. This is due to various resistance adding factors on the model. Firstly, the theory neglects air resistance, which, for fast craft of this nature, can be as much as 30 percent of its total resistance. In addition, the model contains small manufacturing errors and surface flaws not accounted for in the theory, further increasing the resistance.

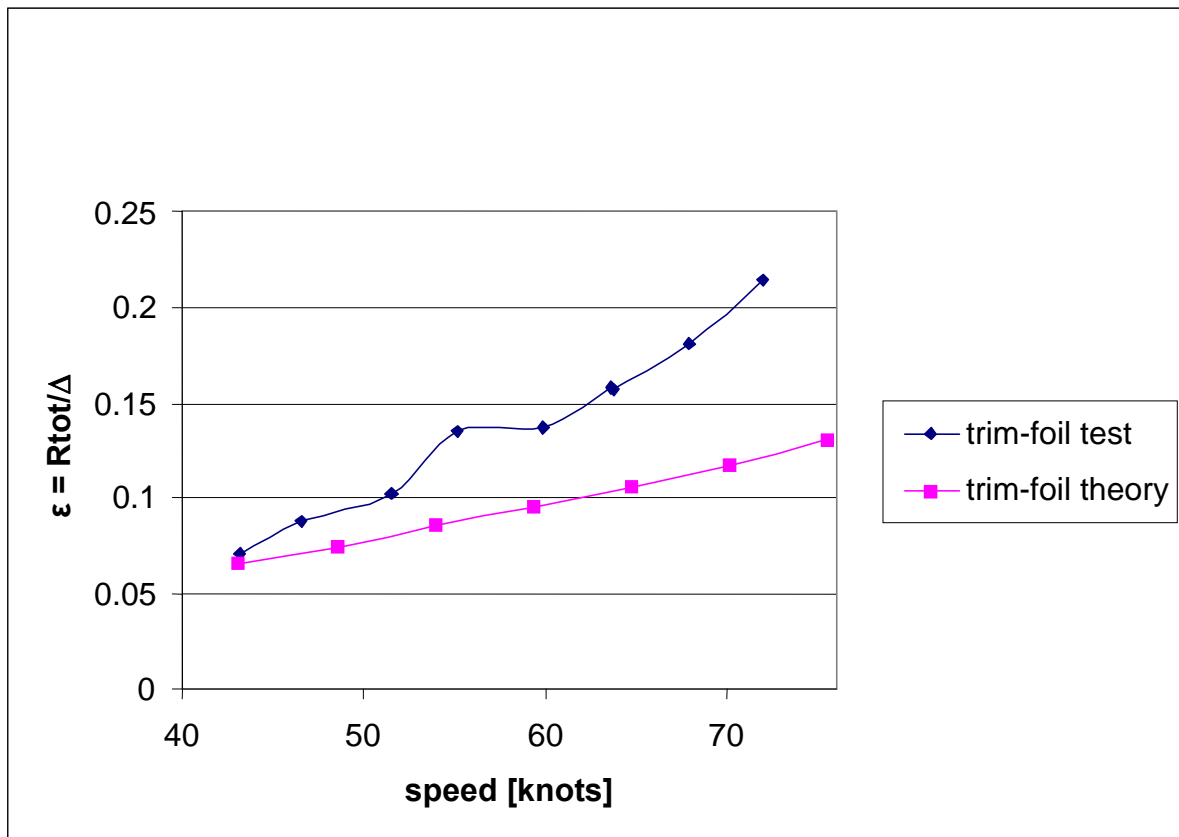


Figure 7.4: Resistance coefficient comparison between test results and theory prediction for the trimaran with foils configuration

A similar resistance under prediction is seen for the configuration with the added foils. This deviation can again be ascribed to air resistance and surface flaws on the model. In addition, the very small model hydrofoils add to the increased resistance; according to Migeotte (2001), the model will experience additional viscous pressure drag due to the thicker laminar boundary layer across the foil; the full scale foil has a thinner turbulent boundary layer because the foil is larger and travelling faster. The laminar flow separates more easily at places of the profile curvature with positive pressure gradient, which increases the drag and reduces the lift, particularly for larger angles of attack (Hoppe, 1989). This results in the test and theoretical data deviating further at higher speeds.

7.3 Trimaran With and Without Foils

The trimaran was designed to be able to perform without hydrofoils. The addition of foils however greatly reduced its resistance, particularly for the lower LCG positions. Figure 7.5

shows a comparison between the trimaran with and without hydrofoils for LCG locations of 31 % and 34 %.

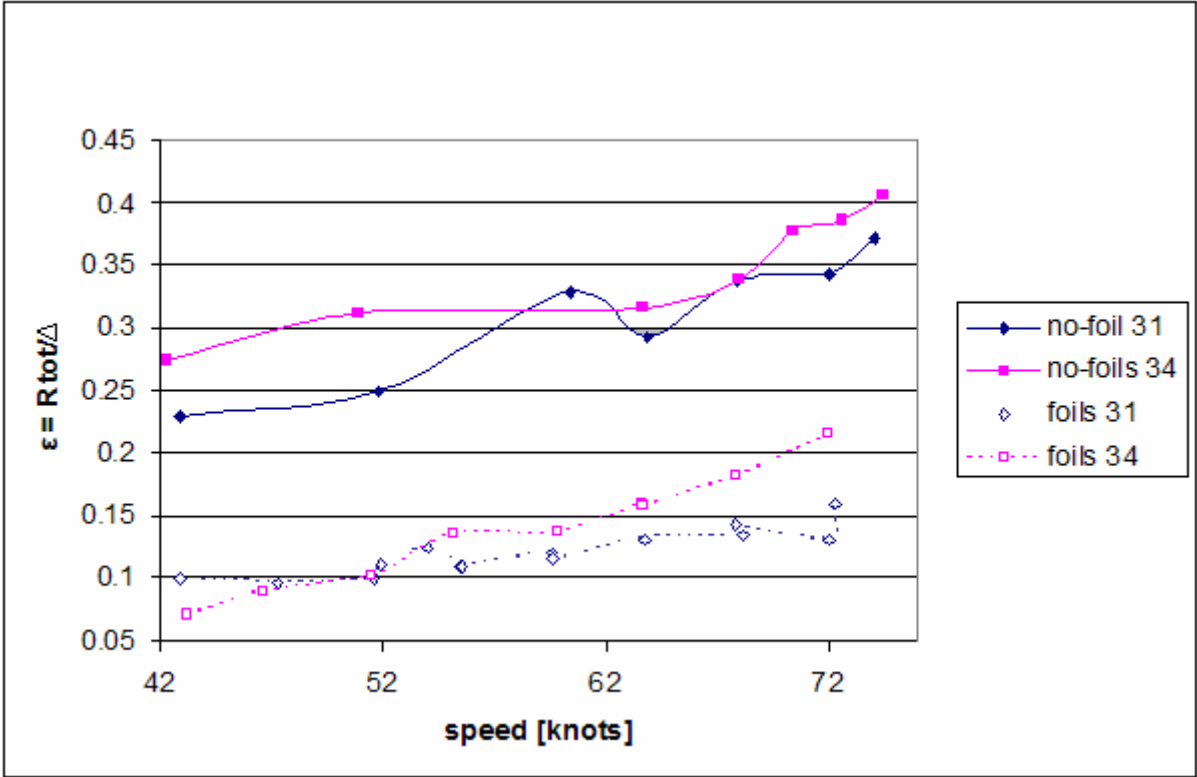


Figure 7.5: Comparison between trimaran with and without foils



7.4 Comparison to Other Craft

Finally, the boat is compared to other craft. Because this boat was designed for and tested at very high speed it is difficult to compare it to other craft as most of the boats operating at such high speeds are offshore racing boats. For these boats, any test performance data is a highly guarded secret. A comparison was therefore made on a more general scale. Figure 7.6 shows a comparison between various types of craft. Included are the resistance tests for a 10 metre, 7 tonne Hysucat. Because the plot compares craft of various sizes as well as hydrofoil craft, the resistance coefficient is plotted against the volumetric Froude number. The tendency curves for the various seagoing vessels were published by Von Schertel (1973).

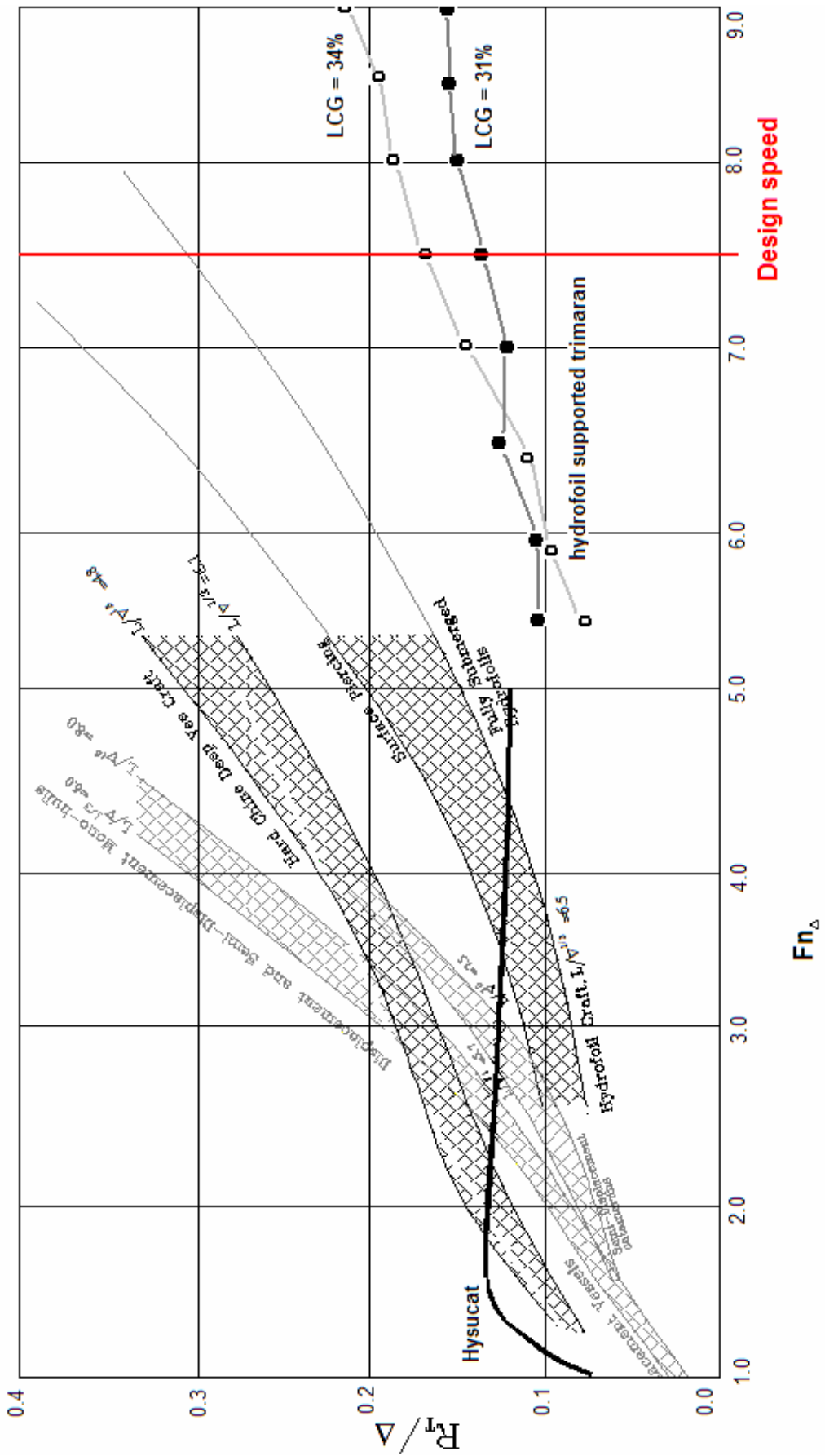
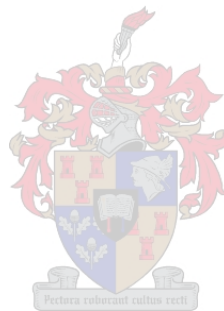


Figure 7.6: A comparison of the hydrofoil supported trimaran with various seagoing craft

The low resistance of the Hysucat can be ascribed to the efficient way in which the stern foils carry part of the boat weight (Hoppe, 1989); where other craft only perform well over a small speed range, the Hysucat foil configuration allows the vessel to trim optimally over a very large speed range, thus making it very efficient. This is clearly visible in the low resistance coefficient shown in figure 7.6 for both the Hysucat and the hydrofoil supported trimaran. In addition, for the trimaran, only the very efficient planing centre hull and not the outriggers are not touching the water at the applicable speeds, thus further improving its efficiency.



8 Conclusion

A fully planing trimaran was designed and a model was manufactured to allow towing tank testing. A hydrofoil support system was designed for the trimaran and the model was altered and the foil system added for further tank testing

The tests supported the theory used in the design process, in showing that for both the trimaran with and without hydrofoils, the best LCG position for reduced resistance is at 31 % of overall length.

The model test results were scaled up using a scaling method taking into account the different hull lengths of the trimaran. The scaling method is based on Froude's scaling law and it is included in appendix D.

Considerable resistance improvements at the design speed were achieved with the addition of the hydrofoils. Reductions of 25 %, 17 %, 60 % and 62 % were achieved for the 40 %, 37 %, 34 % and 31 % LCG positions respectively.

In comparison to other seagoing craft the planing hydrofoil supported trimaran has a substantially reduced resistance. Its resistance coefficient can be compared to that of a Hysucat, this comparison is however made at a Froude number of almost twice that of the Hysucat. The resistance of the trimaran will most probably not be better at lower speeds, as the lift produced by the hydrofoils will not be as substantial. In addition, at lower speeds the outriggers will come into contact with the water further increasing the resistance.

Recommendations for further development would be to further optimise the hydrofoil system. The addition of a sweep angle for the front foils to improve handling and a dihedral angle to further aid in lateral stability can be considered. Further, the stern foils can be tapered to further improve their lift to drag ratio, which would lead to a further reduction in resistance. Further testing, to investigate the performance of the boat through the speed range may also be required.

References

Begovic E, Bove A, Bruzzone D, Caldarella S, Cassella P, Ferrando M, Tincani E and Zotti I, 2005, *Co-operative Investigation of Different Trimaran Hull Forms and Configurations*, International Conference on Fast Sea Transportation, Russia.

Bertram V, 2000, *Practical Ship Hydrodynamics*, Butterworth Heinemann, Oxford.

Bricknell D and Carlisle C, 2004, *Power and Propulsion Systems for the New Naval Trimarans: RINA*, Design and Operation of Trimaran Ships, Conference Proceedings, London.

Brizzolara S, Capasso M, Ferrando M and Podenzana-Bonvino C, 2005, *Effect of Hull Form Variation on Hydrodynamic Performance of a Trimaran Ship for Fast Transportation*, Department of Naval Architecture and Marine Technologies – DINAV University of Genoa, Genoa, Italy.

Cardo A, Ferrando M and Podenzana-Bonvino C, 2003, *Influence of Hull Shape on the Resistance of a Fast Trimaran Vessel*, International Conference on Fast Sea Transportation, Italy.

Damala D P and Grigoropoulos G J, 1999, *Effect of Spray Rails and Wedges on the Performance of Semi-Displacement Hulls*, Department of Naval Architecture and Marine Engineering, National Technical University of Athens, Greece.

Degiuli N, Werner A and Zotti I, 2005, *An Experimental Investigation into the Resistance Components of Trimaran Configurations*, International Conference on Fast Sea Transportation, Russia.

Doctors L J and Scrace RT, 2003, *The Optimisation of Trimaran Sidehull Positioning for Minimum Resistance*, International Conference on Fast Sea Transportation, Italy.

Dubrovsy V, 2004, *Ships with Outriggers*, Backbone Publishing Company, Fair Lawn, USA.

Dubrovsy V A and Matveev K I, 2005, *Concept Design of Outrigger Ships*, International Conference on Fast Sea Transportation, Russia.

Du Cane P, *High Speed Small Craft*, 1972, David and Charles, Newton Abbot.

Egrov I T and Sokolov V T, 1965, *Hydrodynamics of Fast Craft*, In Russian (English translation: NTIS AD A032120; 1976).

Hoerner S, 1965, *Fluid Dynamic Drag*, 2nd Edition, Published by the author, New Jersey.

Hoppe K G, 1989, *The Hysucat Development*, Department of Mechanical Engineering, University of Stellenbosch.

Hoppe K G, 1995, *Ship Fluid Dynamics: Additional Notes and Data Collection*, University of Stellenbosch, Department of Mechanical Engineering.

Houghton E L and Carpenter P W, 1993, *Aerodynamics for Engineering Students*, 4th Edition, Arnold, London.

ICE Marine, 2006, <http://www.icemarine.com/models.html>, [8 March 2006].

Kirkman K L and Kloetzli J W, 1980, *Scaling Problem of Model Appendages*, ATTC, University of Michigan, Ann Arbor.

Korvin-Kroukovsky BV, Savitsky D and Lehman W F, 1949, *Wetted Area and Centre of Pressure of Planing Surfaces*, Stevens Institute of Technology, Davidson Laboratory Report No. 360.

Lewis E, 1988, *Principles of Naval Architecture*, vol. 2, Society of Naval Architects and Marine Engineers, Jersey City USA.

Levi R, 1971, *Dhows to Deltahs*, Nautical Publishing.

Matveev K and Duncan R, 2005, *Development of the Tool for Predicting Hydrofoil System Performance and Simulating Motion of Hydrofoil-Assisted Boats*, High Speed and High Performance Ship and Craft Symposium, ASNE, Everett.

Meyer J, 2006, *Hydrofoil Design Basics - A Brief Tutorial*, International Hydrofoil Society, <http://www.foils.org/basics.htm>, [15 March 2006].

Migeotte G, 1997, *Development for Hydrofoil Supported Catamarans with Semi-Displacement Hulls*, MScEng thesis, Mechanical Engineering Department, University of Stellenbosch, .

Migeotte G, 2001, *Design and Optimization of Hydrofoil-Assisted Catamarans*, Ph.D thesis, Mechanical Engineering Department, University of Stellenbosch, .

Migeotte G, 2005, *Personal Communication*, Stellenbosch.

Millward A, 1982, *Resistance of a Fast Round Bilge Hull in Shallow Water*, AIAA Journal, Vol. 20, No. 8.

Moolman R, *Comparitive Evaluation of Hydrofoil Assisted Trimaran*, MScEng thesis, Mechanical Engineering Department, University of Stellenbosch, , 2005

Müller-Graf B, 1991, *The Effect of Advanced Spray Rail System on Resistance and Development of Spray of Semi-Displacement Round Bilge Hulls*, 1st Intl.Conf. on Fast Sea Transport. FAST 91, Trondheim, Norway.

Powerboat, 2006, <http://powerboat.about.com/od/maintenance/l/aa012403b.htm>, [3 November 2007].

Recreational Craft Directive Compliance Guide, 2006, 1st Edition.

Riegels F W, 1961, *Airfoil Sections*, English version translated by Randall D G, Butterworths, London.

Savitsky D and Dingee D A, 1954, *Some Interference Effects Between Two Flat Surfaces Planing Parallel to Each Other at High Speed*, Stevens Institute of Technology, Hoboken.

Savitsky D and Neidinger J W, 1954, *Wetted Area and Center of Pressure of Planing Surfaces at Very Low Speed Coefficients*, Stevens Institute of Technology, Davidson Laboratory Report No. 493.

Savitsky D and Ross E, 1954, *Turbulence Stimulation in the Boundary Layer of Planing Surfaces*, Davidson Laboratory Report No. 44, Stevens Institute of Technology.

Savitsky D, 1964, *Hydrodynamic Design of Planing Hulls*, Stevens Institute of Technology.

Savitsky D, 1985, *Planing Craft*, Naval Engineers Journal, Chapter IV.

Scheepers S J, 1988, *Watervlak Profiel Toetse met Oppervlak Effekte [Surface Profile Tests with Surface Effect]*, University of Stellenbosch, Department of Mechanical engineering, Report in Afrikaans.

Seung-Hee L, Young-Gill L, Jae Wook L and NamChul K, 2004, *The Development of a Small Multi-Hull Pleasure Fishing Boat*, International Symposium on yacht design and production.

Sname, 2006, http://ittc.sname.org/2002_recomm_proc/7.5-02-05-01.pdf, [3 April 2006]

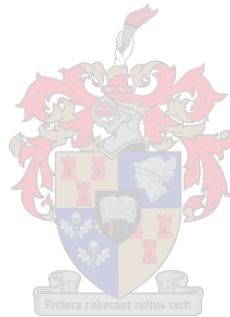
Tweedie M A, 1996, *Die Ondersoek van H_oe Spoed Watervlerke met Vryeoppervlak Invloed* [*Investigation of High speed Hydrofoils with Surface Effects*], MScEng thesis, University of Stellenbosch, Report in Afrikaans.

Von Schertel S, 1973, *The Design and Application of Hydrofoils and their Future Prospects*, IME, London.

Weinblum, 2006, <http://www.cyberiad.net/wakeweinblum.htm>, [3 April 2006].

Wikipedia, 2006, <http://en.wikipedia.org/wiki/Trimaran>, [16 March 2006].

Yeh H, 1965, *Series 64 Resistance Experiments on High speed Displacement Forms*, Marine Technology, Volume 2, No. 3.



Appendix A Matlab Code

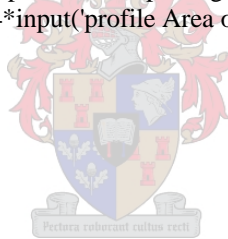
Bellow is the Matlab code used to solve the equilibrium planing condition, using the Savitsky method described in chapter 2.

```
close all
clear all
clc

disp('This Program calculates:');
disp(' the equilibrium trim condition of a planing, prismatic monohull');
disp(' ');

dis=2.20459*input('Weight of boat [Kg]:');
b=3.2808*input('Av. Beam [m]: ');
B=(3.14159265/180)*input('Av. Dedrise [deg]:');
LCG=3.2808*input('LCG from aft [m]: ');
VCG=3.2808*input('VCG from keel line [m]: ');
V=0.911333*input('Speed [Km/h]: ');
E=(3.14159265/180)*input('Thrust Inclination to keel line [deg]:');
f=3.2808*input('Distance between line of thrust & CG [m]: ');
Cap=0;%0.7;%input('Drag coefficient of prop and other apendages');
Aap=0;%0.02*10.76364864;%10.76364864*input('profile Area of apendages [m^2]');
a = VCG - (b/4)*tan(B);
DCF=0.0004;
ro=1.94;
Da = Cap*Aap*ro*(V^2)/2;;
CLB = dis/(0.5*ro*V^2*b^2);
Cv = V/(32.2*b)^0.5;

% solving CLo from fig
CLoding = -1;
CLo = 0;
while CLoding<0;
    CLo = CLo + 0.01;
    CLoding = CLo-0.0065*B*CLo^0.6-CLB;
end
CLo = CLo - 0.02;
CLoding = -1;
while CLoding<0;
    CLo = CLo + 0.0001;
    CLoding = CLo-0.0065*B*CLo^0.6-CLB;
end
CLo = CLo - 0.0002;
CLoding = -1;
while CLoding<0;
    CLo = CLo + 0.0000001;
    CLoding = CLo-0.0065*B*CLo^0.6-CLB;
end
```



```

%-----
%   TAU's INFLUENCE STARTS HERE!!!
%-----
TAU = 0.0001;

stop = 0;
ouMOMding=0;
while stop == 0;

% solving LAM from fig 10
dingg = -1;
LAM = 0;
while dingg < 0;
    LAM = LAM + 0.01;
    dingg = ((TAU/(3.14159265/180))^1.1)*(0.012*LAM^0.5+(0.0055*LAM^(5/2))/Cv^2)-CLo;
end
LAM = LAM - 0.01;
dingg = -1;
while dingg < 0;
    LAM = LAM + 0.0001;
    dingg = ((TAU/(3.14159265/180))^1.1)*(0.012*LAM^0.5+(0.0055*LAM^(5/2))/Cv^2)-CLo;
end
LAM = LAM - 0.0001;
dingg = -1;
while dingg < 0;
    LAM = LAM + 0.0000001;
    dingg = ((TAU/(3.14159265/180))^1.1)*(0.012*LAM^0.5+(0.0055*LAM^(5/2))/Cv^2)-CLo;
end
Cp = 0.75 - 1/(5.21*(Cv^2)/(LAM^2)+2.39);
c = LCG - Cp*LAM*b;

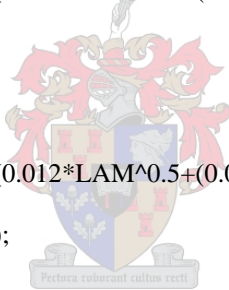
CF=9e-5*TAU+0.0016;

V1 = (1-0.012*TAU^1.1*((-45/30)*B+95)/(LAM^0.5*cos(TAU)))^0.5;
Vm = V1*V;
Df = ro*Vm^2*LAM*b^2*(CF+DCF)/(2*cos(B));

%-----
%   SOLVING THE 3 EQUILIB EQUATIONS
%-----
N = dis*cos(TAU)-Da*sin(TAU)-sin(E)*(dis*sin(TAU)+Df+Da*cos(TAU))/cos(E);
T = (dis*sin(TAU)+Df+Da*cos(TAU))/cos(E);
MOMding = N*c+Df*a-T*f+Da*sin(TAU)*LCG+Da*cos(TAU)*(f/cos(E)+LCG*tan(E));
% disp([num2str(MOMding),' ',num2str(TAU)])

kyk = MOMding*ouMOMding;
if kyk < 0;
    stop = 1;

```



```

else
    ouMOMding = MOMding;
end

```

```

TAU = TAU + 0.0001;
%stop=1;
end

```

```

% _____
% REITERATE WITH SMALLER INTERVALS!!!

```

```

TAU = TAU-0.0002;

```

```

stop = 0;
ouMOMding=0;
while stop == 0;

```

```

% solving LAM from fig 10

```

```

dingg = -1;

```

```

LAM = 0;

```

```

while dingg<0;

```

```

    LAM = LAM + 0.01;

```

```

    dingg = ((TAU/(3.14159265/180))^1.1)*(0.012*LAM^0.5+(0.0055*LAM^(5/2))/Cv^2)-CLo;

```

```

end

```

```

LAM = LAM - 0.01;

```

```

dingg = -1;

```

```

while dingg<0;

```

```

    LAM = LAM + 0.0001;

```

```

    dingg = ((TAU/(3.14159265/180))^1.1)*(0.012*LAM^0.5+(0.0055*LAM^(5/2))/Cv^2)-CLo;

```

```

end

```

```

LAM = LAM - 0.0001;

```

```

dingg = -1;

```

```

while dingg<0;

```

```

    LAM = LAM + 0.0000001;

```

```

    dingg = ((TAU/(3.14159265/180))^1.1)*(0.012*LAM^0.5+(0.0055*LAM^(5/2))/Cv^2)-CLo;

```

```

end

```

```

Cp = 0.75 - 1/(5.21*(Cv^2)/(LAM^2)+2.39);

```

```

c = LCG - Cp*LAM*b;

```

```

CF=9e-5*TAU+0.0016;

```

```

V1 = (1-0.012*TAU^1.1*((-45/30)*B+95)/(LAM^0.5*cos(TAU)))^0.5;

```

```

Vm = V1*V;

```

```

Df = ro*Vm^2*LAM*b^2*(CF+DCF)/(2*cos(B));

```



```

%-----
% SOLVING THE 3 EQUILIB EQUATIONS
%-----
N = dis*cos(TAU)-Da*sin(TAU)-sin(E)*(dis*sin(TAU)+Df+Da*cos(TAU))/cos(E);
T = (dis*sin(TAU)+Df+Da*cos(TAU))/cos(E);
MOMding = N*c+Df*a-T*f+Da*sin(TAU)*LCG+Da*cos(TAU)*(f/cos(E)+LCG*tan(E));
% disp([num2str(MOMding),' ',num2str(TAU)])

kyk = MOMding*ouMOMding;
if kyk < 0;
    stop = 1;
else
    ouMOMding = MOMding;
end

TAU = TAU + 0.0000001;
% stop=1;
end

%-----
% REITERATE WITH SMALLER INTERVALS!!!

TAU = TAU-0.0000002;

stop = 0;
ouMOMding=0;
while stop == 0;

% solving LAM from fig 10
dingg = -1;
LAM = 0;
while dingg<0;
    LAM = LAM + 0.01;
    dingg = ((TAU/(3.14159265/180))^1.1)*(0.012*LAM^0.5+(0.0055*LAM^(5/2))/Cv^2)-CLo;
end
LAM = LAM - 0.01;
dingg = -1;
while dingg<0;
    LAM = LAM + 0.0001;
    dingg = ((TAU/(3.14159265/180))^1.1)*(0.012*LAM^0.5+(0.0055*LAM^(5/2))/Cv^2)-CLo;
end
LAM = LAM - 0.0001;
dingg = -1;
while dingg<0;
    LAM = LAM + 0.0000001;
    dingg = ((TAU/(3.14159265/180))^1.1)*(0.012*LAM^0.5+(0.0055*LAM^(5/2))/Cv^2)-CLo;
end
Cp = 0.75 - 1/(5.21*(Cv^2)/(LAM^2)+2.39);

```




```
c = LCG - Cp*LAM*b;
```

```
CF=9e-5*TAU+0.0016;
```

```
V1 = (1-0.012*TAU^1.1*((-45/30)*B+95)/(LAM^0.5*cos(TAU)))^0.5;
```

```
Vm = V1*V;
```

```
Df = ro*Vm^2*LAM*b^2*(CF+DCF)/(2*cos(B));
```

```
%-----
```

```
% SOLVING THE 3 EQUILIB EQUATIONS
```

```
%-----
```

```
N = dis*cos(TAU)-Da*sin(TAU)-sin(E)*(dis*sin(TAU)+Df+Da*cos(TAU))/cos(E);
```

```
T = (dis*sin(TAU)+Df+Da*cos(TAU))/cos(E);
```

```
MOMding = N*c+Df*a-T*f+Da*sin(TAU)*LCG+Da*cos(TAU)*(f/cos(E)+LCG*tan(E));
```

```
% disp([num2str(MOMding),' ',num2str(TAU)])
```

```
kyk = MOMding*ouMOMding;
```

```
if kyk < 0;
```

```
    stop = 1;
```

```
else
```

```
    ouMOMding = MOMding;
```

```
end
```



```
TAU = TAU + 0.000000001;
```

```
% stop=1;
```

```
end
```

```
disp(' ');
```

```
disp(' ');
```

```
disp(' ');
```

```
disp(['The equilibrium planing trim angle is: TAU = ',num2str(TAU/(3.14159265/180)),' deg']);
```

```
disp(' ');
```

```
D = dis*tan(TAU)+Df/cos(TAU);
```

```
EHP=D*V/550;
```

```
disp(['Power requirement: EHP = ',num2str(EHP),' hp']);
```

```
disp(' ');
```

```
Lk = LAM*b + b*tan(B)/(2*3.14159265*tan(TAU));
```

```
disp(['The wetted keel length is: ',num2str(Lk/3.2808),' m  [' ,num2str(Lk),' ft ] ');
```

```
disp(' ');
```

```
Lc = LAM*b - b*tan(B)/(2*3.14159265*tan(TAU));
```

```
disp(['The wetted chine length is: ',num2str(Lc/3.2808),' m  [' ,num2str(Lc),' ft ] ');
```

```
disp(' ');
```

```
d=Lk*sin(TAU);
```

```
disp(['The draft to keel at transom is: ',num2str(d/3.2808),' m  [' ,num2str(d),' ft ] ');
```

The following code is similar to that shown above except that it includes a solution for the planing outriggers and then finds the equilibrium planing condition of the trimaran as discussed in chapter 3.

```

close all
clear all
clc

disp('This Program calculates:');
disp('the equilibrium planing condition of a planing trimaran');
disp(' ');

for iiii=1:11;

dis=2.20459*input('Weight of boat [Kg]:');
ddis=(iiii-1)*2.5/100;% (input('percentage displacement of outriggers @ speed: '))/100;
dis1=dis-ddis*dis;
dis2=dis-dis1;
b1=3.2808*2;% input('Av. Beam of center hull [m]: ');
b2=3.2808*0.5;% input('Av. Beam of outriggers [m]: ');
B1=(3.14159265/180)*24;% input('Av. Dedrise of center hull [deg]:');
B2=(3.14159265/180)*24;% input('Av. Dedrise outriggers [deg]:');
hig=0.2;% 3.2808*input('hight diff of keel of center hull & outrigger [m]: ');
LCG=3.2808*4.2;% input('LCG from aft [m]: ');
VCG=3.2808*0.2;% input('VCG from keel line [m]: ');
V=0.911333*120;% input('Speed [Km/h]: ');
E=0*(3.14159265/180);% *input('Thrust Inclination to keel line [deg]:');
f=0.36+VCG;% 3.2808*input('Distance between line of thrust & CG [m]: ');
Cap=0;% 0.7;% input('Drag coefficient of prop and other apendages');
Aap=0;% 0.02*10.76364864;% 10.76364864*input('profile Area of apendages [m^2]');
a1 = VCG - (b1/4)*tan(B1);
a2 = VCG - ((b1/4)*tan(B1)+hig);
DCF=0.0004;
ro=1.94;
Da = Cap*Aap*ro*(V^2)/2;
CLB1 = dis1/(0.5*ro*V^2*b1^2);
CLB2 = dis2/(0.5*ro*V^2*b2^2);
Cv1 = V/(32.2*b1)^0.5;
Cv2 = V/(32.2*b2)^0.5;

% solving CLo1 from fig
CLoding1 = -1;
CLo1 = 0;
while CLoding1<0;
    CLo1 = CLo1 + 0.01;
    CLoding1 = CLo1-0.0065*B1*CLo1^0.6-CLB1;
end
CLo1 = CLo1 - 0.02;
CLoding1 = -1;
while CLoding1<0;
    CLo1 = CLo1 + 0.0001;
    CLoding1 = CLo1-0.0065*B1*CLo1^0.6-CLB1;
end
end

```

```

CLo1 = CLo1 - 0.0002;
CLoding1 = -1;
while CLoding1<0;
    CLo1 = CLo1 + 0.0000001;
    CLoding1 = CLo1-0.0065*B1*CLo1^0.6-CLB1;
end

% solving CLo2 from fig
CLoding2 = -1;
CLo2 = 0;
while CLoding2<0;
    CLo2 = CLo2 + 0.01;
    CLoding2 = CLo2-0.0065*B2*CLo2^0.6-CLB2;
end
CLo2 = CLo2 - 0.02;
CLoding2 = -1;
while CLoding2<0;
    CLo2 = CLo2 + 0.0001;
    CLoding2 = CLo2-0.0065*B2*CLo2^0.6-CLB2;
end
CLo2 = CLo2 - 0.0002;
CLoding2 = -1;
while CLoding2<0;
    CLo2 = CLo2 + 0.0000001;
    CLoding2 = CLo2-0.0065*B2*CLo2^0.6-CLB2;
end

%-----
%   TAU's INFLUENCE STARTS HERE!!!
%-----
TAU = 0.0001;

stop = 0;
ouMOMding=0;
while stop == 0;

% solving LAM1 from fig 10
dingg1 = -1;
LAM1 = 0;
while dingg1<0;
    LAM1 = LAM1 + 0.01;
    dingg1 = ((TAU/(3.14159265/180))^1.1)*(0.012*LAM1^0.5+(0.0055*LAM1^(5/2))/Cv1^2)-CLo1;
end
LAM1 = LAM1 - 0.01;
dingg1 = -1;
while dingg1<0;
    LAM1 = LAM1 + 0.0001;
    dingg1 = ((TAU/(3.14159265/180))^1.1)*(0.012*LAM1^0.5+(0.0055*LAM1^(5/2))/Cv1^2)-CLo1;
end
LAM1 = LAM1 - 0.0001;
dingg1 = -1;
while dingg1<0;
    LAM1 = LAM1 + 0.0000001;
    dingg1 = ((TAU/(3.14159265/180))^1.1)*(0.012*LAM1^0.5+(0.0055*LAM1^(5/2))/Cv1^2)-CLo1;

```



```

end

% solving LAM2 from fig 10
dingg2 = -1;
LAM2 = 0;
while dingg2 < 0;
    LAM2 = LAM2 + 0.01;
    dingg2 = ((TAU/(3.14159265/180))^1.1)*(0.012*LAM2^0.5+(0.0055*LAM2^(5/2))/Cv2^2)-CLo2;
end
LAM2 = LAM2 - 0.01;
dingg2 = -1;
while dingg2 < 0;
    LAM2 = LAM2 + 0.0001;
    dingg2 = ((TAU/(3.14159265/180))^1.1)*(0.012*LAM2^0.5+(0.0055*LAM2^(5/2))/Cv2^2)-CLo2;
end
LAM2 = LAM2 - 0.0001;
dingg2 = -1;
while dingg2 < 0;
    LAM2 = LAM2 + 0.0000001;
    dingg2 = ((TAU/(3.14159265/180))^1.1)*(0.012*LAM2^0.5+(0.0055*LAM2^(5/2))/Cv2^2)-CLo2;
end

Cp1 = 0.75 - 1/(5.21*(Cv1^2)/(LAM1^2)+2.39);
c1 = LCG - Cp1*LAM1*b1;

Cp2 = 0.75 - 1/(5.21*(Cv2^2)/(LAM2^2)+2.39);
c2 = LCG - Cp2*LAM2*b2;

CF=9e-5*TAU+0.0016;

V11 = (1-0.012*TAU^1.1*((-45/30)*B1+95)/(LAM1^0.5*cos(TAU)))^0.5;
Vm1 = V11*V;
Df1 = ro*Vm1^2*LAM1*b1^2*(CF+DCF)/(2*cos(B1));

V12 = (1-0.012*TAU^1.1*((-45/30)*B2+95)/(LAM2^0.5*cos(TAU)))^0.5;
V12 = real(V12);
Vm2 = V12*V;
Df2 = ro*Vm2^2*LAM2*b2^2*(CF+DCF)/(2*cos(B2));

%-----
% SOLVING THE 3 EQUILIB EQUATIONS
%-----
T=(dis*sin(TAU)+Df1+2*Df2+Da*cos(TAU))/cos(E);
N=dis*cos(TAU)-Da*sin(TAU)-sin(E)*T;
N1 = N/(1+(dis2/dis1)*(b1/b2)^2);
N2 = N1*(dis2/(2*dis1))*(b1/b2)^2;
MOMding = N1*c1+2*N2*c2+Df1*a1+2*Df2*a2-
T*f+Da*sin(TAU)*LCG+Da*cos(TAU)*(f/cos(E)+LCG*tan(E));
% disp([num2str(MOMding),' ',num2str(TAU)])

kyk = MOMding*ouMOMding;
if kyk < 0;
    stop = 1;
else

```

```
ouMOMding = MOMding;
end
```

```
TAU = TAU + 0.0001;
%stop=1;
end
```

```
% _____
% REITERATE WITH SMALLER INTERVALS!!!
```

```
TAU = TAU-0.0002;
```

```
stop = 0;
ouMOMding=0;
while stop == 0;
```

```
%solving LAM1 from fig 10
```

```
dingg1 = -1;
LAM1 = 0;
while dingg1<0;
    LAM1 = LAM1 + 0.01;
    dingg1 = ((TAU/(3.14159265/180))^1.1)*(0.012*LAM1^0.5+(0.0055*LAM1^(5/2))/Cv1^2)-CLo1;
end
```

```
LAM1 = LAM1 - 0.01;
dingg1 = -1;
while dingg1<0;
    LAM1 = LAM1 + 0.0001;
    dingg1 = ((TAU/(3.14159265/180))^1.1)*(0.012*LAM1^0.5+(0.0055*LAM1^(5/2))/Cv1^2)-CLo1;
end
```

```
LAM1 = LAM1 - 0.0001;
dingg1 = -1;
while dingg1<0;
    LAM1 = LAM1 + 0.0000001;
    dingg1 = ((TAU/(3.14159265/180))^1.1)*(0.012*LAM1^0.5+(0.0055*LAM1^(5/2))/Cv1^2)-CLo1;
end
```

```
%solving LAM2 from fig 10
```

```
dingg2 = -1;
LAM2 = 0;
while dingg2<0;
    LAM2 = LAM2 + 0.01;
    dingg2 = ((TAU/(3.14159265/180))^1.1)*(0.012*LAM2^0.5+(0.0055*LAM2^(5/2))/Cv2^2)-CLo2;
end
```

```
LAM2 = LAM2 - 0.01;
dingg2 = -1;
while dingg2<0;
    LAM2 = LAM2 + 0.0001;
```



```

    dingg2 = ((TAU/(3.14159265/180))^1.1)*(0.012*LAM2^0.5+(0.0055*LAM2^(5/2))/Cv2^2)-CLo2;
end
LAM2 = LAM2 - 0.0001;
dingg2 = -1;
while dingg2<0;
    LAM2 = LAM2 + 0.0000001;
    dingg2 = ((TAU/(3.14159265/180))^1.1)*(0.012*LAM2^0.5+(0.0055*LAM2^(5/2))/Cv2^2)-CLo2;
end

Cp1 = 0.75 - 1/(5.21*(Cv1^2)/(LAM1^2)+2.39);
c1 = LCG - Cp1*LAM1*b1;

Cp2 = 0.75 - 1/(5.21*(Cv2^2)/(LAM2^2)+2.39);
c2 = LCG - Cp2*LAM2*b2;

CF=9e-5*TAU+0.0016;

V11 = (1-0.012*TAU^1.1*((-45/30)*B1+95)/(LAM1^0.5*cos(TAU)))^0.5;
Vm1 = V11*V;
Df1 = ro*Vm1^2*LAM1*b1^2*(CF+DCF)/(2*cos(B1));

V12 = (1-0.012*TAU^1.1*((-45/30)*B2+95)/(LAM2^0.5*cos(TAU)))^0.5;
V12 = real(V12);
Vm2 = V12*V;
Df2 = 2*(ro*Vm2^2*LAM2*b2^2*(CF+DCF)/(2*cos(B2)));

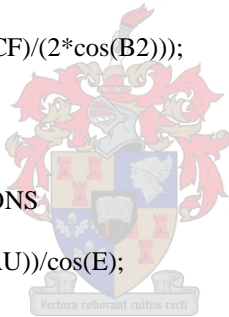
%-----
% SOLVING THE 3 EQUILIB EQUATIONS
%-----
T=(dis*sin(TAU)+Df1+2*Df2+Da*cos(TAU))/cos(E);
N =dis*cos(TAU)-Da*sin(TAU)-sin(E)*T;
N1 = N/(1+(dis2/dis1)*(b1/b2)^2);
N2 = N1*(dis2/(2*dis1))*(b1/b2)^2;
MOMding = N1*c1+2*N2*c2+Df1*a1+2*Df2*a2-
T*f+Da*sin(TAU)*LCG+Da*cos(TAU)*(f/cos(E)+LCG*tan(E));
% disp([num2str(MOMding),' ',num2str(TAU)])

kyk = MOMding*ouMOMding;
if kyk < 0;
    stop = 1;
else
    ouMOMding = MOMding;
end

TAU = TAU + 0.0000001;
% stop=1;
end

%-----
% REITERATE WITH SMALLER INTERVALS!!!

```



```

TAU = TAU-0.0000002;

stop = 0;
ouMOMding=0;
while stop == 0;

% solving LAM1 from fig 10
dingg1 = -1;
LAM1 = 0;
while dingg1<0;
    LAM1 = LAM1 + 0.01;
    dingg1 = ((TAU/(3.14159265/180))^1.1)*(0.012*LAM1^0.5+(0.0055*LAM1^(5/2))/Cv1^2)-CLo1;
end
LAM1 = LAM1 - 0.01;
dingg1 = -1;
while dingg1<0;
    LAM1 = LAM1 + 0.0001;
    dingg1 = ((TAU/(3.14159265/180))^1.1)*(0.012*LAM1^0.5+(0.0055*LAM1^(5/2))/Cv1^2)-CLo1;
end
LAM1 = LAM1 - 0.0001;
dingg1 = -1;
while dingg1<0;
    LAM1 = LAM1 + 0.0000001;
    dingg1 = ((TAU/(3.14159265/180))^1.1)*(0.012*LAM1^0.5+(0.0055*LAM1^(5/2))/Cv1^2)-CLo1;
end

% solving LAM2 from fig 10
dingg2 = -1;
LAM2 = 0;
while dingg2<0;
    LAM2 = LAM2 + 0.01;
    dingg2 = ((TAU/(3.14159265/180))^1.1)*(0.012*LAM2^0.5+(0.0055*LAM2^(5/2))/Cv2^2)-CLo2;
end
LAM2 = LAM2 - 0.01;
dingg2 = -1;
while dingg2<0;
    LAM2 = LAM2 + 0.0001;
    dingg2 = ((TAU/(3.14159265/180))^1.1)*(0.012*LAM2^0.5+(0.0055*LAM2^(5/2))/Cv2^2)-CLo2;
end
LAM2 = LAM2 - 0.0001;
dingg2 = -1;
while dingg2<0;
    LAM2 = LAM2 + 0.0000001;
    dingg2 = ((TAU/(3.14159265/180))^1.1)*(0.012*LAM2^0.5+(0.0055*LAM2^(5/2))/Cv2^2)-CLo2;
end

Cp1 = 0.75 - 1/(5.21*(Cv1^2)/(LAM1^2)+2.39);
c1 = LCG - Cp1*LAM1*b1;

Cp2 = 0.75 - 1/(5.21*(Cv2^2)/(LAM2^2)+2.39);
c2 = LCG - Cp2*LAM2*b2;

CF=9e-5*TAU+0.0016;

```

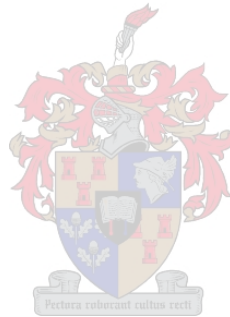


```
V11 = (1-0.012*TAU^1.1*((-45/30)*B1+95)/(LAM1^0.5*cos(TAU)))^0.5;
Vm1 = V11*V;
Df1 = ro*Vm1^2*LAM1*b1^2*(CF+DCF)/(2*cos(B1));
```

```
V12 = (1-0.012*TAU^1.1*((-45/30)*B2+95)/(LAM2^0.5*cos(TAU)))^0.5;
V12 = real(V12);
Vm2 = V12*V;
Df2 = 2*(ro*Vm2^2*LAM2*b2^2*(CF+DCF)/(2*cos(B2)));
```

```
%-----
% SOLVING THE 3 EQUILIB EQUATIONS
%-----
T=(dis*sin(TAU)+Df1+2*Df2+Da*cos(TAU))/cos(E);
N=dis*cos(TAU)-Da*sin(TAU)-sin(E)*T;
N1 = N/(1+(dis2/dis1)*(b1/b2)^2);
N2 = N1*(dis2/(2*dis1))*(b1/b2)^2;
MOMding = N1*c1+2*N2*c2+Df1*a1+2*Df2*a2-
T*f+Da*sin(TAU)*LCG+Da*cos(TAU)*(f/cos(E)+LCG*tan(E));
%disp([num2str(MOMding),' ',num2str(TAU)])
```

```
kyk = MOMding*ouMOMding;
if kyk < 0;
    stop = 1;
else
    ouMOMding = MOMding;
end
```



```
TAU = TAU + 0.000000001;
%stop=1;
end
%disp(' ');
%disp(' ');
%disp(' ');
%disp(['The equilibrium planing trim angle is: TAU = ',num2str(TAU/(3.14159265/180)), ' deg']);
%disp(' ');
D =dis*tan(TAU)+(Df1+2*Df2)/cos(TAU);
EHP=D*V/550;
%disp(['Power requirement: EHP = ',num2str(EHP),' hp']);
%disp(' ');
Lk1 = LAM1*b1 +b1*tan(B1)/(2*3.14159265*tan(TAU));
%%disp(['The wetted center keel length is: ',num2str(Lk1/3.2808),' m  [' ,num2str(Lk1),' ft ] ');
%disp(' ');
Lc1 = LAM1*b1 -b1*tan(B1)/(2*3.14159265*tan(TAU));
%disp(['The wetted center chine length is: ',num2str(Lc1/3.2808),' m  [' ,num2str(Lc1),' ft ] ');
%disp(' ');
d1=Lk1*sin(TAU);
%disp(['The draft to keel at transom is: ',num2str(d1/3.2808),' m  [' ,num2str(d1),' ft ] ');
%disp(' ');
tran = d1/cos(TAU);
Lk2 = Lk1*(tran-hig)/tran;
%disp(['The wetted outrigger keel length is: ',num2str(Lk2/3.2808),' m  [' ,num2str(Lk2),' ft ] ');
%disp(' ');
Lc2 = LAM2*b2 -b2*tan(B2)/(2*3.14159265*tan(TAU));
```



```
%disp(['The wetted outrigger chine length is: ',num2str(Lc2/3.2808),' m  [' ,num2str(Lc2),' ft ] ']);  
%disp(' ');  
d2=Lk2*sin(TAU);  
%disp(['The draft to keel at outrigger transom is: ',num2str(d2/3.2808),' m  [' ,num2str(d2),' ft ] ']);  
  
reqH(iii)=EHP;  
LK1(iii)=Lk1;  
LK2(iii)=Lk2;  
TAUUU(iii)=(TAU/(3.14159265/180));  
iii  
end
```



Below is the code used to calculate the equilibrium condition of the planing trimaran with hydrofoil support discussed in chapter 5.

```

close all
clear all
clc

for iii=1:15;
    for jjj=1:4

DIS=2.20459*5000;%input('Weight of boat [Kg]:');
LCG= 3.2808*(3.36+jjj/2.78);%input('LCG from aft [m]: ');
VCG=3.2808*0.3;%input('VCG from keel line [m]: ');
V=0.911333*iii*10;%input('Speed [Km/h]: ');
b1=3.2808*2;%input('Av. Beam of center hull [m]: ');
b2=3.2808*0.3;%input('Av. Beam of outriggers [m]: ');
E=(3.14159265/180)*0;%input('Thrust Inclination to keel line [deg]:');
%for jjjj = 1 : 10;
B1=(3.14159265/180)*24;%input('Av. Dedrise of center hull [deg]:');
B2=(3.14159265/180)*24;%input('Av. Dedrise of outriggers [deg]:');
f=0.0153+VCG;% 3.2808*input('Distance between line of thrust & CG [m]: ');
Cap=0;%0.7;%input('Drag coefficient of prop and other apendages');
Aap=0;%0.02*10.76364864;%10.76364864*input('profile Area of apendages [m^2]');
a1 = VCG - (b1/4)*tan(B1);
a2 = VCG - (b2/4)*tan(B2);
DCF=0.0004;
ro=1.94;
Da = Cap*Aap*ro*(V^2)/2;;

hig=3.2808*1;%input('Hight of outrigger keel above center keel [m]: ');

% -----
%   first find the draft for the center hull only
% -----
CLB1 = DIS/(0.5*ro*V^2*b1^2);
Cv1 = V/(32.2*b1)^0.5;

% solving CLo from fig
CLoding1 = -1;
CLo1 = 0;
while CLoding1<0;
    CLo1 = CLo1 + 0.01;
    CLoding1 = CLo1-0.0065*B1*CLo1^0.6-CLB1;
end
CLo1 = CLo1 - 0.02;
CLoding1 = -1;
while CLoding1<0;
    CLo1 = CLo1 + 0.0001;
    CLoding1 = CLo1-0.0065*B1*CLo1^0.6-CLB1;
end
CLo1 = CLo1 - 0.0002;

```

```

CLoding1 = -1;
while CLoding1<0;
    CLo1 = CLo1 + 0.0000001;
    CLoding1 = CLo1-0.0065*B1*CLo1^0.6-CLB1;
end

```

```

%-----
%   TAU's INFLUENCE STARTS HERE!!!
%-----
TAU = 0.0001;

```

```

stop = 0;
ouMOMding=0;
while stop == 0;

```

```

% solving LAM from fig 10

```

```

dingg1 = -1;
LAM1 = 0;
while dingg1<0;
    LAM1 = LAM1 + 0.01;
    dingg1 = ((TAU/(3.14159265/180))^1.1)*(0.012*LAM1^0.5+(0.0055*LAM1^(5/2))/Cv1^2)-CLo1;
end
LAM1 = LAM1 - 0.01;
dingg1 = -1;
while dingg1<0;
    LAM1 = LAM1 + 0.0001;
    dingg1 = ((TAU/(3.14159265/180))^1.1)*(0.012*LAM1^0.5+(0.0055*LAM1^(5/2))/Cv1^2)-CLo1;
end
LAM1 = LAM1 - 0.0001;
dingg1 = -1;
while dingg1<0;
    LAM1 = LAM1 + 0.0000001;
    dingg1 = ((TAU/(3.14159265/180))^1.1)*(0.012*LAM1^0.5+(0.0055*LAM1^(5/2))/Cv1^2)-CLo1;
end
Cp1 = 0.75 - 1/(5.21*(Cv1^2)/(LAM1^2)+2.39);
c1 = LCG - Cp1*LAM1*b1;

```

```

CF=9e-5*TAU+0.0016;

```

```

V11 = (1-0.012*TAU^1.1*((-45/30)*B1+95)/(LAM1^0.5*cos(TAU)))^0.5;
Vm1 = V11*V;
Df1 = ro*Vm1^2*LAM1*b1^2*(CF+DCF)/(2*cos(B1));
Df2=0;

```

```

%-----
%   SOLVING THE 3 EQUILIB EQUATIONS

```

```

%-----
N =DIS*cos(TAU)-Da*sin(TAU)-sin(E)*(DIS*sin(TAU)+Df1+Da*cos(TAU));
T =DIS*sin(TAU)+Df1+Da*cos(TAU);
MOMding = N*c1+Df1*a1-T*f+Da*sin(TAU)*LCG+Da*cos(TAU)*(f/cos(E)+LCG*tan(E));
%disp([num2str(MOMding),' ',num2str(TAU)])

kyk = MOMding*ouMOMding;
if kyk < 0;
    stop = 1;
else
    ouMOMding = MOMding;
end

TAU = TAU + 0.0001;
%stop=1;
end

Lk1 = LAM1*b1 +b1*tan(B1)/(2*3.14159265*tan(TAU));
Lc1 = LAM1*b1 -b1*tan(B1)/(2*3.14159265*tan(TAU));
d1=Lk1*sin(TAU);

%-----
%Hydrofoil input
%-----

fh1=0;%input('front foil height above keel [m]:');
f11=LCG/3.2808+0.1;%input('front foil distance from transom [m]:');
fh2=0.1;%input('stern foil height above keel [m]:');
f12=0.1;%input('stern foil distance from transom [m]:');

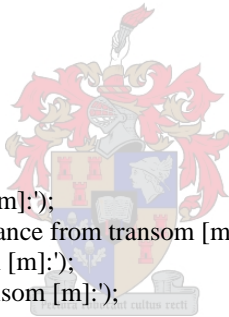
%convert to feet
f11=f11*3.2808;
fh1=fh1*3.2808;
fh2=fh2*3.2808;
f12=f12*3.2808;

%-----
% CHECK WEATHER THE hydrofoils ARE TOUCHING THE WATER

foilwet1=(Lk1-f11+fh1*tan(TAU))*sin(TAU)-fh1/cos(TAU);
foilwet2=(Lk1-f12+fh2*tan(TAU))*sin(TAU)-fh2/cos(TAU);

if foilwet1>0
    foilsarewet=1;
else
    foilsarewet=0;
end
if foilwet2>0
    foilsarewet=1;
end
end

```



```

foilloop = 0;
if foilsarewet==1;
    foiltoets=1;
    for foiltoets =1;
        foilloop = foilloop+1;

        dis = DIS-(foilloop-1)*(100*2.20459);

        ch1=0.2;%0.185+iii/500;%0.18+jjjj/100;%input('Chord [m]:');
        Sp1= 121.69*ch1^3 + 0.0597*ch1^2 - 0.0309*ch1 + 0.0049;%input('Span [m]: ');
        th1=0.07*ch1;%input('max. Thickness [m]: ');
        aoa1=0;%(3.14159265/180)*input('Angle of Attack [deg]:');
        sweep1=0;%(3.14159265/180)*input('Sweep Angle [deg]: ');
        dihe1=0;%(3.14159265/180)*input('Dihedral Angle [deg]: ');
        speed=(1000/60^2)*V/0.911333;
        temp=20;%input('Water temprature [°C]: ');

        ch2=0.1;%input('Chord [m]:');
        Sp2=20.232*ch2^3 + 0.0971*ch2^2 - 0.0514*ch2 + 0.0081;%input('Span [m]: ');
        th2=0.07*ch2;%input('max. Thickness [m]: ');
        aoa2=0;%(3.14159265/180)*input('Angle of Attack [deg]:');
        sweep2=0;%(3.14159265/180)*input('Sweep Angle [deg]: ');
        dihe2=0;%(3.14159265/180)*input('Dihedral Angle [deg]: ');

        %-----
        %Recalculate hull specs with reduced displacement carried by foils

        CLB1 = dis/(0.5*ro*V^2*b1^2);
        Cv1 = V/(32.2*b1)^0.5;

        %solving CLo from fig
        CLoding1 = -1;
        CLo1 = 0;
        while CLoding1<0;
            CLo1 = CLo1 + 0.01;
            CLoding1 = CLo1-0.0065*B1*CLo1^0.6-CLB1;
        end
        CLo1 = CLo1 - 0.02;
        CLoding1 = -1;
        while CLoding1<0;
            CLo1 = CLo1 + 0.0001;
            CLoding1 = CLo1-0.0065*B1*CLo1^0.6-CLB1;
        end
        CLo1 = CLo1 - 0.0002;
        CLoding1 = -1;
        while CLoding1<0;
            CLo1 = CLo1 + 0.0000001;
            CLoding1 = CLo1-0.0065*B1*CLo1^0.6-CLB1;
        end
end

```



```

%-----
%   TAU's INFLUENCE STARTS HERE!!!
%-----
TAU = 0.0001;

stop = 0;
ouMOMding=0;
dingding=0;
while stop == 0;

    dingding=dingding+1;

% solving LAM from fig 10
dingg1 = -1;
LAM1 = 0;
while dingg1<0;
    LAM1 = LAM1 + 0.01;
    dingg1 = ((TAU/(3.14159265/180))^1.1)*(0.012*LAM1^0.5+(0.0055*LAM1^(5/2))/Cv1^2)-CLo1;
end
LAM1 = LAM1 - 0.01;
dingg1 = -1;
while dingg1<0;
    LAM1 = LAM1 + 0.0001;
    dingg1 = ((TAU/(3.14159265/180))^1.1)*(0.012*LAM1^0.5+(0.0055*LAM1^(5/2))/Cv1^2)-CLo1;
end
LAM1 = LAM1 - 0.0001;
dingg1 = -1;
while dingg1<0;
    LAM1 = LAM1 + 0.0000001;
    dingg1 = ((TAU/(3.14159265/180))^1.1)*(0.012*LAM1^0.5+(0.0055*LAM1^(5/2))/Cv1^2)-CLo1;
end
Cp1 = 0.75 - 1/(5.21*(Cv1^2)/(LAM1^2)+2.39);
c1 = LCG - Cp1*LAM1*b1;

CF=9e-5*TAU+0.0016;

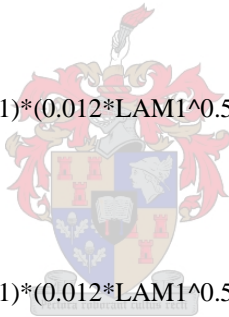
V11 = (1-0.012*TAU^1.1*((-45/30)*B1+95)/(LAM1^0.5*cos(TAU)))^0.5;
Vm1 = V11*V;
Df1 = ro*Vm1^2*LAM1*b1^2*(CF+DCF)/(2*cos(B1));
Df2=0;

%-----
% Foil CALCS

Lk1 = LAM1*b1 + b1*tan(B1)/(2*3.14159265*tan(TAU));

dep1=((Lk1-f1+f1*tan(TAU))*sin(TAU)-fh1/cos(TAU))/3.2808;
dep2=((Lk1-f2+f2*tan(TAU))*sin(TAU)-fh2/cos(TAU))/3.2808;
if dep1 <=0;
    dep1=0;

```



```

end
if dep2 <=0;
    dep2=0;
end

%front foil
%lift
dens= -0.0063*temp^2 + 0.0476*temp + 999.89;
vis= 0.0000007*temp^2 - 0.00005*temp + 0.0018;
Ren1=dens*speed*ch1/vis;
P1=(16*(dep1/ch1)^2+1)/(16*(dep1/ch1)^2+2);
AR1=Sp1/ch1;
ib1=dep1/Sp1;
sig1=1.73+0.694*ib1-2.172*(ib1)^0.5-0.514*exp(-ib1);
zet1=-0.00059+0.00847*AR1-0.000004194*AR1^2-0.000001973*AR1^3;

Cla1=(2*pi*P1*AR1*cos(sweep1)*(cos(dihe1))^2)/(AR1+2*P1*(1+sig1)*(1+zet1)*cos(sweep1)*(cos(dihe1))^2*(1
+(AR1/(2*P1*cos(sweep1)*(cos(dihe1))^2))^0.5)-(1+sig1)*(1+zet1)*AR1);
if dep1 <=0;
    Cla1=0;
end

aoa01=(-1.15*100*th1/(2*ch1))*(3.14159265/180);
aoa1real = aoa1+TAU;

Cll=Cla1*(aoa1real-aoa01);
lift1=speed^2*dens*Cll*ch1*Sp1/2;

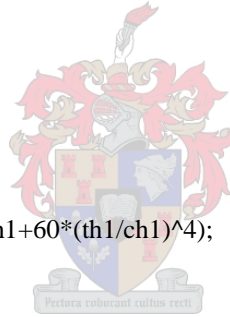
%drag

Cdp1=0.03*Ren1^(-0.1428)*(1+2*th1/ch1+60*(th1/ch1)^4);
dCdp1=0.005*Cll^2;
if dep1 <=0;
    Cdw1=0;
else
    Fi1=speed/(9.81*dep1)^0.5;
    Cdw1=0.5*Cll^2/(Fi1^2*exp(2/Fi1^2));
end
Cdi1=Cll^2*(1+sig1)*(1+zet1)/(pi*AR1*P1*cos(sweep1)*(cos(dihe1))^2);
Cds1=0;
Cd1=Cdp1+dCdp1+Cdw1+Cdi1+Cds1;
if dep1 <= 0;
    drag1 = 0;
else
    drag1=speed^2*dens*Cd1*ch1*Sp1/2;
end

%stern foil
if ch2==0
    lift2 = 0;
    drag2 = 0;
else

%lift
Ren2=dens*speed*ch2/vis;
P2=(16*(dep2/ch2)^2+1)/(16*(dep2/ch2)^2+2);

```



```

AR2=Sp2/ch2;
ib2=dep2/Sp2;
sig2=1.73+0.694*ib2-2.172*(ib2)^0.5-0.514*exp(-ib2);
zet2=-0.00059+0.00847*AR2-0.000004194*AR2^2-0.000001973*AR2^3;

```

```

Cla2=(2*pi*P2*AR2*cos(sweep2)*(cos(dihe2))^2)/(AR2+2*P2*(1+sig2)*(1+zet2)*cos(sweep2)*(cos(dihe2))^2*(1
+(1+(AR2/(2*P2*cos(sweep2)*(cos(dihe2))^2))^2)^0.5)-(1+sig2)*(1+zet2)*AR2);

```

```

if dep2 <=0;
    Cla2=0;
end

```

```

aoa02=(-1.15*100*th2/(2*ch2))*(3.14159265/180);
aoa2real = aoa2+TAU;

```

```

Cl2=Cla2*(aoa2real-aoa02);

```

```

lift2=speed^2*dens*Cl2*ch2*Sp2/2;

```

```

%drag

```

```

Cdp2=0.03*Ren2^(-0.1428)*(1+2*th2/ch2+60*(th2/ch2)^4);
dCdp2=0.005*Cl2^2;

```

```

if dep2 <=0;
    Cdw2=0;

```

```

else

```

```

    Fi2=speed/(9.81*dep2)^0.5;

```

```

    Cdw2=0.5*Cl2^2/(Fi2^2*exp(2/Fi2^2));

```

```

end

```

```

Cdi2=Cl2^2*(1+sig2)*(1+zet2)/(pi*AR2*P2*cos(sweep2)*(cos(dihe2))^2);

```

```

Cds2=0;

```

```

Cd2=Cdp2+dCdp2+Cdw2+Cdi2+Cds2;

```

```

if dep2 <= 0;

```

```

    drag2 = 0;

```

```

else

```

```

    drag2=speed^2*dens*Cd2*ch2*Sp2/2;

```

```

end

```

```

end

```

```

if lift1<=0

```

```

    lift1 = 0;

```

```

end

```

```

if lift2<=0

```

```

    lift2 = 0;

```

```

end

```

```

lift1=lift1*2.20459/9.81;

```

```

lift2=lift2*2.20459/9.81;

```

```

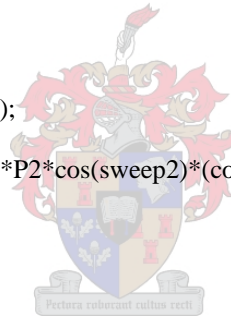
drag1=drag1*2.20459/9.81;

```

```

drag2=drag2*2.20459/9.81;

```




```

%-----
% SOLVING THE 3 EQUILIB EQUATIONS
%-----
T=(DIS*sin(TAU)+Df1+Da*cos(TAU)-2*(lift1+lift2)*sin(TAU)+2*(drag1+drag2)*cos(TAU))/cos(E);
N=DIS*cos(TAU)-Da*sin(TAU)-sin(E)*T-2*(lift1+lift2)*cos(TAU)-2*(drag1+drag2)*sin(TAU);
if N<=0
    N=0;
end
MOMding = N*c1+Df1*a1-T*f+Da*sin(TAU)*LCG+Da*cos(TAU)*(f/cos(E)+LCG*tan(E))-
2*lift1*cos(TAU)*(f1-LCG)-2*lift1*sin(TAU)*(VCG-fh1)+2*drag1*cos(TAU)*(VCG-fh1)-
2*drag1*sin(TAU)*(f1-LCG)+2*lift2*cos(TAU)*(LCG-fh2)-2*lift2*sin(TAU)*(VCG-
fh2)+2*drag2*cos(TAU)*(VCG-fh2)+2*drag2*sin(TAU)*(LCG-fh2);
%disp([num2str(MOMding), ' ',num2str(TAU)])

kyk = MOMding*ouMOMding;
if kyk < 0;
    stop = 1;
else
    ouMOMding = MOMding;
end

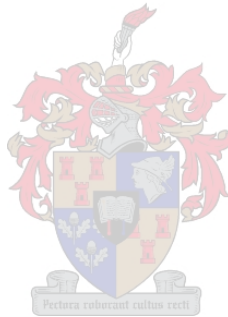
TAU = TAU + 0.0001;

%TAUDING(dingding)=TAU;
%LIFTT(dingding)=lift1;
%DIEPTE(dingding)=dep1;
%momentum(dingding)=MOMding;
%stop=1;
end

%find equilibrium specs
%-----
%    TAU's INFLUENCE STARTS HERE!!!
%-----
TAU = TAU-0.0002;

% solving LAM from fig 10
dingg1 = -1;
LAM1 = 0;
while dingg1<0;
    LAM1 = LAM1 + 0.01;
    dingg1 = ((TAU/(3.14159265/180))^1.1)*(0.012*LAM1^0.5+(0.0055*LAM1^(5/2))/Cv1^2)-CLo1;
end
LAM1 = LAM1 - 0.01;
dingg1 = -1;
while dingg1<0;
    LAM1 = LAM1 + 0.0001;

```



```

dingg1 = ((TAU/(3.14159265/180))^1.1)*(0.012*LAM1^0.5+(0.0055*LAM1^(5/2))/Cv1^2)-CLo1;
end
LAM1 = LAM1 - 0.0001;
dingg1 = -1;
while dingg1<0;
    LAM1 = LAM1 + 0.0000001;
    dingg1 = ((TAU/(3.14159265/180))^1.1)*(0.012*LAM1^0.5+(0.0055*LAM1^(5/2))/Cv1^2)-CLo1;
end
Cp1 = 0.75 - 1/(5.21*(Cv1^2)/(LAM1^2)+2.39);
c1 = LCG - Cp1*LAM1*b1;

```

```
CF=9e-5*TAU+0.0016;
```

```

V11 = (1-0.012*TAU^1.1*((-45/30)*B1+95)/(LAM1^0.5*cos(TAU)))^0.5;
Vm1 = V11*V;
Df1 = ro*Vm1^2*LAM1*b1^2*(CF+DCF)/(2*cos(B1));
Df2=0;

```

```

%-----
%Foil CALCS

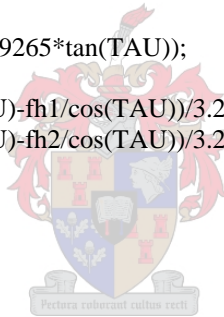
```

```
Lk1 = LAM1*b1 + b1*tan(B1)/(2*3.14159265*tan(TAU));
```

```

dep1=((Lk1-fl1+fh1*tan(TAU))*sin(TAU)-fh1/cos(TAU))/3.2808;
dep2=((Lk1-fl2+fh2*tan(TAU))*sin(TAU)-fh2/cos(TAU))/3.2808;
if dep1 <=0;
    dep1=0;
end
if dep2 <=0;
    dep2=0;
end

```



```

% front foil
% lift
dens= -0.0063*temp^2 + 0.0476*temp + 999.89;
vis= 0.0000007*temp^2 - 0.00005*temp + 0.0018;
Ren1=dens*speed*ch1/vis;
P1=(16*(dep1/ch1)^2+1)/(16*(dep1/ch1)^2+2);
AR1=Sp1/ch1;
ib1=dep1/Sp1;
sig1=1.73+0.694*ib1-2.172*(ib1)^0.5-0.514*exp(-ib1);
zet1=-0.00059+0.00847*AR1-0.000004194*AR1^2-0.000001973*AR1^3;

```

```

Cla1=(2*pi*P1*AR1*cos(sweep1)*(cos(dihe1))^2)/(AR1+2*P1*(1+sig1)*(1+zet1)*cos(sweep1)*(cos(dihe1))^2*(1
+(1+(AR1/(2*P1*cos(sweep1)*(cos(dihe1))^2))^0.5)-(1+sig1)*(1+zet1)*AR1);
if dep1 <=0;
    Cla1=0;
end

```

```

aoa01=(-1.15*100*th1/(2*ch1))*(3.14159265/180);
aoa1real = aoa1+TAU;

```

```
Cl1=Cla1*(aoa1real-aoa01);
```

```

lift1=speed^2*dens*C11*ch1*Sp1/2;

%drag

Cdp1=0.03*Ren1^(-0.1428)*(1+2*th1/ch1+60*(th1/ch1)^4);
dCdp1=0.005*C11^2;
if dep1 <=0;
    Cdw1=0;
else
    Fi1=speed/(9.81*dep1)^0.5;
    Cdw1=0.5*C11^2/(Fi1^2*exp(2/Fi1^2));
end
Cdi1=C11^2*(1+sig1)*(1+zet1)/(pi*AR1*P1*cos(sweep1)*(cos(dihe1))^2);
Cds1=0;
Cd1=Cdp1+dCdp1+Cdw1+Cdi1+Cds1;
if dep1 <= 0;
    drag1 = 0;
else
    drag1=speed^2*dens*Cd1*ch1*Sp1/2;
end

%stern foil
if ch2==0
    lift2 = 0;
    drag2 = 0;
else

%lift
Ren2=dens*speed*ch2/vis;
P2=(16*(dep2/ch2)^2+1)/(16*(dep2/ch2)^2+2);
AR2=Sp2/ch2;
ib2=dep2/Sp2;
sig2=1.73+0.694*ib2-2.172*(ib2)^0.5-0.514*exp(-ib2);
zet2=-0.00059+0.00847*AR2-0.000004194*AR2^2-0.000001973*AR2^3;

Cla2=(2*pi*P2*AR2*cos(sweep2)*(cos(dihe2))^2)/(AR2+2*P2*(1+sig2)*(1+zet2)*cos(sweep2)*(cos(dihe2))^2*(1
+(1+(AR2/(2*P2*cos(sweep2)*(cos(dihe2))^2))^2)^0.5)-(1+sig2)*(1+zet2)*AR2);
if dep2 <=0;
    Cla2=0;
end

aoa02=(-1.15*100*th2/(2*ch2))*(3.14159265/180);
aoa2real = aoa2+TAU;

C12=Cla2*(aoa2real-aoa02);

lift2=speed^2*dens*C12*ch2*Sp2/2;

%drag

Cdp2=0.03*Ren2^(-0.1428)*(1+2*th2/ch2+60*(th2/ch2)^4);
dCdp2=0.005*C12^2;
if dep2 <=0;
    Cdw2=0;
else
    Fi2=speed/(9.81*dep2)^0.5;

```



```

    Cdw2=0.5*C12^2/(Fi2^2*exp(2/Fi2^2));
end
Cdi2=C12^2*(1+sig2)*(1+zet2)/(pi*AR2*P2*cos(sweep2)*(cos(dihe2))^2);
Cds2=0;
Cd2=Cdp2+dCdp2+Cdw2+Cdi2+Cds2;
if dep2 <= 0;
    drag2 = 0;
else
    drag2=speed^2*dens*Cd2*ch2*Sp2/2;
end
end

if lift1<=0
    lift1 = 0;
end
if lift2<=0
    lift2 = 0;
end
lift1=lift1*2.20459/9.81;
lift2=lift2*2.20459/9.81;
drag1=drag1*2.20459/9.81;
drag2=drag2*2.20459/9.81;

%-----
% SOLVING THE 3 EQUILIB EQUATIONS
%-----
T=(DIS*sin(TAU)+Df1+Da*cos(TAU)-2*(lift1+lift2)*sin(TAU)+2*(drag1+drag2)*cos(TAU))/cos(E);
N=DIS*cos(TAU)-Da*sin(TAU)-sin(E)*T-2*(lift1+lift2)*cos(TAU)-2*(drag1+drag2)*sin(TAU);
if N<=0
    N=0;
end
MOMding = N*c1+Df1*a1-T*f+Da*sin(TAU)*LCG+Da*cos(TAU)*(f/cos(E)+LCG*tan(E))-
2*lift1*cos(TAU)*(f1-LCG)-2*lift1*sin(TAU)*(VCG-fh1)+2*drag1*cos(TAU)*(VCG-fh1)-
2*drag1*sin(TAU)*(f1-LCG)+2*lift2*cos(TAU)*(LCG-fl2)-2*lift2*sin(TAU)*(VCG-
fh2)+2*drag2*cos(TAU)*(VCG-fh2)+2*drag2*sin(TAU)*(LCG-fl2);
%disp([num2str(MOMding),' ',num2str(TAU)])

%displacement(foilloop)=dis;
%LIFT1(foilloop)=lift1;
%LIFT2(foilloop)=lift2;
%DEP1(foilloop)=dep1;
%DEP2(foilloop)=dep2;
%TAUUU(foilloop)=TAU*180/pi;
%foiltoets = lift1+lift2-(DIS-dis);
%LKK(foilloop)=Lk1;
%D=dis*tan(TAU)+(Df1)/cos(TAU);
%EHP=D*V/550;
%EEE(foilloop)=EHP;
%TOETS(foilloop)=foiltoets;

```

```

end %foilloop

end %foilnat

D =drag1+drag2+(dis-lift1-lift2)*tan(TAU)+(Df1)/cos(TAU);
EHP=D*V/550;

EEE(iii,jjj)=EHP;
TAUUU(iii,jjj)=TAU*180/pi;
LIFT1(iii,jjj)=lift1;
LIFT2(iii,jjj)=lift2;

end

end

disp(' ');
disp(' ');
disp(' ');
disp(['The equilibrium planing trim angle is: TAU = ',num2str(TAU/(3.14159265/180)),' deg']);
disp(' ');
D =drag1+drag2+(dis-lift1-lift2)*tan(TAU)+(Df1)/cos(TAU);
EHP=D*V/550;
disp(['Power requirement: EHP = ',num2str(EHP),' hp']);
disp(' ');
disp(['The wetted center keel length is: ',num2str(Lk1/3.2808),' m [',num2str(Lk1),' ft ] ');
disp(' ');
Lc1 = LAM1*b1 -b1*tan(B1)/(2*3.14159265*tan(TAU));
if Lc1>0
    disp(['The wetted center chine length is: ',num2str(Lc1/3.2808),' m [',num2str(Lc1),' ft ] ');
else
    disp('The center-hull-chine is out the water');
end
disp(' ');
disp(['The draft to keel at transom is: ',num2str(d1/3.2808),' m [',num2str(d1),' ft ] ');
disp(' ');

```



The following code is that which was used to calculate the stress in a circle section foil profile used in chapter 5.

```

close all
clear all
clc

disp('This program calculates the second area moment for')
disp('a constant radius foil section with a flat bottom.')
disp('Please enter the following:')
c=input('foil chord, c = ');
t=0.06*c;%input('foil thickness, t = ');

%-----
% No of elements
%-----
N=1000;

%-----
% Arc Radius
%-----
r = (c^2/4 + t^2)/(2*t);

%-----
% Defining elements
%-----

% x = [x-position of first element  x-pos.....]
x(1) = ((c/2)/N)/2;
ii = 0;
for ii = 2:N;
    x(ii) = x(ii-1) + ((c/2)/N);
end
% elements = element no.[element hight]
%      element no.[element hight]
ii = 0;
for ii = 1:N
    elements(ii,1) = (r^2 - x(ii)^2)^0.5 - (r - t);
end

%-----
% Center of Area
%-----
bo = 0;
onder = 0;
ii = 0;
for ii = 1: N
    bo = bo + elements(ii,1)*((c/2)/N)*elements(ii,1)/2;
    onder = onder + elements(ii,1)*((c/2)/N);
end
CA = bo/onder;

```



```

%-----
% Second Moment of Area
%-----

ii = 0;
for ii = 1:N
    I(ii) = (((c/2)/N)*elements(ii,1)^3)/12 + (((c/2)/N)*elements(ii,1))*(CA-elements(ii,1)/2)^2;
end

Izz = 2*sum(I);

%-----
% Output
%-----

Lift = 20000; % [N]
y=t-CA;
S = 0.1:0.1:10;
ii=0;
for ii = 1:max(size(S))
    Stress(ii) = (Lift*y*S(ii))/(12*Izz);
end

plot(S,Stress)
hold on
ylabel('Stress');xlabel('Span');title('Stress vs Span');
maxStress =690000000
plot(S,maxStress)

```



Appendix B Model Production

The model was produced by taking sections from the scaled CAD model and tracing it onto a sheet of polyurethane foam. The sections were then cut out as shown in figure B-1.

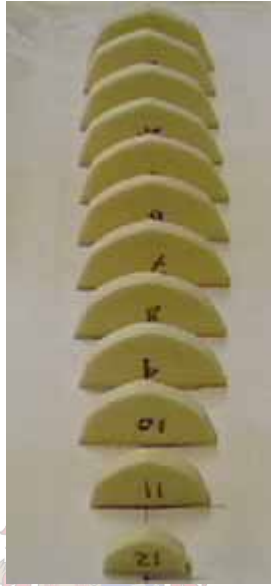


Figure B-1: Section cut-outs from polyurethane foam

The next step was to fill in between the sections and fair the hull. This was done using cement and is shown in figure B-2.



Figure B-2: Faired hull, ready for glass coating

Next the hull was covered with a layer of glass-fibre to provide a smooth and durable surface. In figure B-3, the hull is shown under vacuum together with one of the outriggers that was produced in a similar fashion.



Figure B-3: Model plug for centre hull and outrigger under vacuum

Once the glass-fibre surface had been sanded and polished to a smooth finish, the plug was used to draw a transparent vacuum moulded hull.

The spray rails were cut from a sheet of clear plastic and glued on afterward.

A frame was built to hold the centre hull and outriggers together and allow the height of the outriggers to be changed when the foils were added. A slider with an adjustable weight was also added to allow the LCG position to be changed.

Appendix C Limits of Tank Testing

Tests in a towing tank are affected by the size of the tank. The two main effects are blockage and a shallow water effect. These effects are briefly discussed below.

Blockage is the ratio of the submerged cross sectional area of the model to the cross sectional area of the tank (Bertram, 2000). It is caused by the lateral restriction of the water in the narrow channel. The effect of blockage is to increase the frictional resistance of the model. The principal factor related to this increase in resistance is (Lewis, 1988):

$$\frac{\sqrt{A_x}}{R_H} \quad (C-1)$$

where A_x is the maximum submerged cross-sectional area and R_H is the hydraulic radius of the vessel.

The hydraulic radius of the vessel can be determined as follows:

$$R_H = \frac{(b_c h_c - A_x)}{(b_c + 2h_c + p)} \quad (C-2)$$

where b_c , h_c and p are the channel width, channel depth and the vessel's wetted surface perimeter respectively. According to Migeotte (1997), the blockage effect is negligible if the value for the factor in equation C-1 is below 0.2. This was the case for the current tests.

The effect of vessels travelling in shallow water is governed by the vessels shallow water-critical speed (Dubrovsky, 2002):

$$V_{crit} = \sqrt{gd} \quad (C-3)$$

where d is the water depth. Vessels operating in shallow water will experience either an increase in wave making resistance if they are travelling below the critical speed, or a reduction in wave making resistance, if they are travelling above the critical speed. The changes in wave making resistance is presented as a function of Froude depth number in figure C-1 (Millward, 1982):

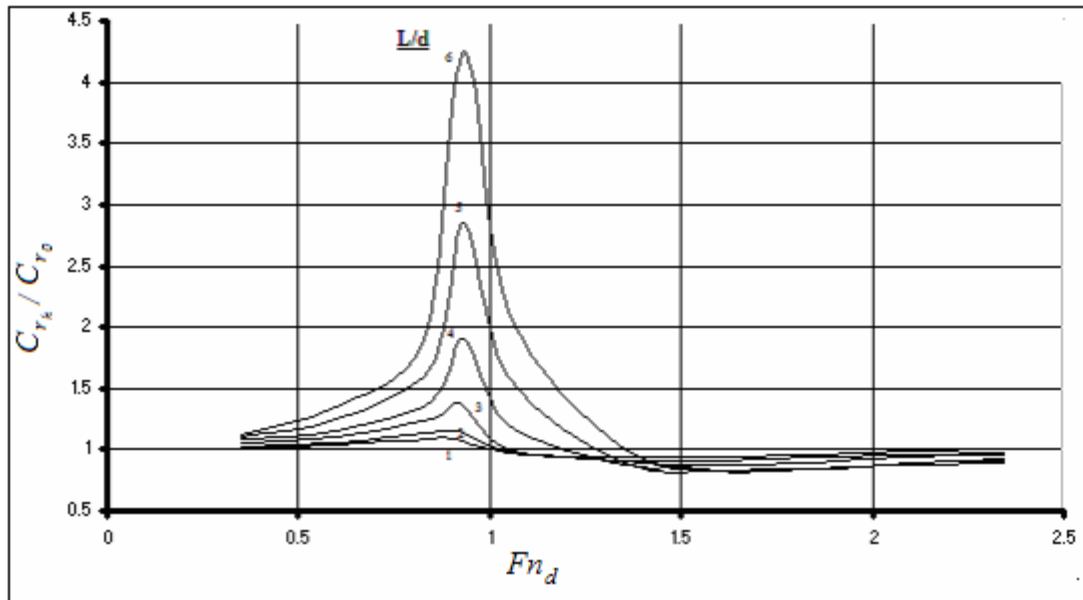


Figure C-1: Froude depth number vs. change in residuary resistance at various length to depth ratios

The Froude depth number is calculated as follows:

$$Fn_d = \frac{V}{\sqrt{gd}} \quad (C-4)$$

As the length to depth ratio for the current tests was below 0.2, the shallow water effect was negligible.

Appendix D Scaling Procedure

The following scaling method, based on Froude's scaling laws and modified for trimarans, was used by Moolman (2005) and proved to be accurate. The method is outlined for the reader's convenience in this appendix with an explanation of the core principals.

The total resistance of a model is made up of the sum of the frictional resistance and the residual resistance. The residual resistance corresponds to the wave making resistance of the prototype vessel, with some modification to account for any other resistance factors other than frictional resistance. In addition, the scaling of the frictional resistance, which is dependant on the Reynolds number, will differ for the outriggers and the centre hull. Froude's scaling law of the total resistance can therefore be modified as follows (Moolman, 2005):

$$R_T^* = (R_{F,MH}^* + 2R_{F,O}^*) + R_R^* \quad (D-1)$$

where:

R_T^* is the total resistance of the model,

$R_{F,MH}^*$ is the frictional resistance of the centre hull,

$R_{F,O}^*$ is the frictional resistance of one of the outriggers and

R_R^* is the residual resistance of the model.

The frictional resistance of each component can then be calculated as follows:

$$R_{F,i}^* = C_{F,i}^* \left(\frac{\rho^*}{2} \right) (V^*)^2 Sw_i^* \quad (D-2)$$

where Sw_i is the wetted surface area of the hull in question. C_F , the frictional coefficient of either the model or prototype, is calculated according to the ITTC 1957 correlation line which is a function of the Reynolds number of the hull in question.

$$C_{F,i}^* = \frac{0.075}{(\log_{10} Rn_i^* - 2)^2} \quad (\text{D-3})$$

Where Rn_i^* is the Reynolds number of the hull in question, which is calculated as follows,

$$Rn_i^* = \frac{V^* L_{wli}^*}{\nu^*} \quad (\text{D-4})$$

where L_{wli}^* is the waterline length of the hull in question and the ν^* is the viscosity of the water in either the towing tank or the prototype operating environment.

With the frictional resistance calculated above, equation D-1 can be rearranged and used to calculate the model residual resistance:

$$R_R^* = R_T^* - (R_{F,MH}^* + 2R_{F,O}^*) \quad (\text{D-5})$$

R_T^* is the measured resistance of the model.

The residual resistance coefficient can be calculated as follows,

$$C_R^* = \frac{R_R^*}{\left(\frac{\rho^*}{2}\right)(V^*)^2 S_{W_T}^*} \quad (\text{D-6})$$

where S_{W_T} is the total wetted surface area of the model. According to Froude's scaling laws, the residual resistance coefficient is equal for the prototype and the model:

$$C_R = C_R^* \quad (\text{D-7})$$

Equation D-6 can therefore be used again for calculating the residual resistance of the prototype vessel.

The Volumetric Froude number is used to scale the velocity because of the different lengths of the centre hull and the outriggers.

$$Fn^* = \frac{V^*}{\sqrt{g(\nabla^*)^{1/3}}} \quad (D-8)$$

Therefore, keeping the Froude number equal for the model and prototype, the prototype velocity is calculated as follows:

$$V = Fn^* \sqrt{g \nabla^{1/3}} \quad (D-9)$$

Rewriting equation D-1 for the total resistance of the prototype, including all the necessary resistance coefficients and adding a correlation coefficient leads to the following equation:

$$R_T = \left(\frac{\rho}{2} \right) V^2 \left[C_{FMH} S_{W_{MH}} + 2C_{F0} S_{W_o} + (C_R + C_A) S_{W_T} \right] \quad (D-10)$$

The correlation coefficient, C_A , includes various corrections, including roughness allowance and also particularities of the measuring device and towing tank and the method used (Bertram, 2000). The correlation coefficient generally ranges between 0.0002 and 0.0003 (Migeotte, 2005).

When foils are added to the model, the scaling procedure changes. This is due to the relatively low Reynolds number associated with the model foils. The applicable scaling method is described below.

There is a relation between the resistance displacement ratio of the model and prototype (Hoppe, 1995):

$$\varepsilon = k_{corr} \varepsilon_m \quad (D-11)$$

where $\varepsilon = R_T / \Delta$. The correlation factor, k_{corr} , for craft with multiple foils is (Migeotte, 2001):

$$k_{corr} = 1.0 - \frac{C_{Fhm} - C_{Fh} - C_A}{C_{Tm}} - \sum_i^n \frac{A_{FS_i}}{Sw} \frac{C_{Dm_i} - C_{D_i} - C_{Af_i}}{C_{Tm}} \quad (D-12)$$

where:

C_{Fhm}	frictional resistance coefficient of the model hull
C_{Fh}	frictional resistance coefficient of the prototype hull
C_A	roughness allowance for the prototype hull
C_{Tm}	total resistance coefficient of the model
A_{FS}	hydrofoil wetted area of the prototype [m ²]
Sw	hull wetted area of the prototype [m ²]
C_{Dm}	drag resistance coefficient of a foil of the model
C_D	drag resistance coefficient of a foil of the prototype
C_{Af}	roughness allowance for the model foils (Generally $C_{Af} \approx 0$)
n	the number of foils

To estimate the drag coefficient, the laminar flow and separation of the flow associated with model foils has to be taken into account. It can be calculated as a function of the Reynolds number as follows (Kirkman and Kloetzli, 1980):

For $Rn < 5 \cdot 10^4$:

$$C_{DO_0} = 1.46Rn^{-0.507}$$

$$C_{DO_{20}} = 0.466Rn^{-0.259}$$

For $5 \cdot 10^4 \leq Rn < 5 \cdot 10^5$:

$$C_{DO_0} = 0.172Rn^{-0.310}$$

$$C_{DO_{20}} = 181Rn^{-0.810}$$

For $5 \cdot 10^5 \leq Rn < 1 \cdot 10^7$:

$$C_{DO} = 2.93 \cdot 10^{-3} \left[1 + 2 \frac{t}{c} + 60 \left(\frac{t}{c} \right)^4 \right]$$

For $Rn > 1 \cdot 10^7$:

$$C_{DO} = 0.03Rn^{-0.1428} \left[1 + 2 \frac{t}{c} + 60 \left(\frac{t}{c} \right)^4 \right] \quad (\text{D-13})$$

t is the thickness and c the chord length of the foil in question. C_{DO_0} is the value of C_{DO} for $t/c = 0$, and $C_{DO_{20}}$ for $t/c = 0.20$. For other thickness to chord ratios, C_{DO} can be linearly interpolated between C_{DO_0} and $C_{DO_{20}}$ (Migeotte, 2001).